ANALYSIS OF FACTORS INFLUENCING THE PERFORMANCE OF CMS MEMBRANES FOR GAS SEPARATION

A Dissertation
Presented to
The Academic Faculty

by

Paul Jason Williams

In Partial Fulfillment
of the Requirements for the Degree
Doctor of Philosophy in the
School of Chemical and Biomolecular Engineering

Georgia Institute of Technology
August 2006

ANALYSIS OF FACTORS INFLUENCING THE PERFORMANCE OF CMS MEMBRANES FOR GAS SEPARATION

Approved by:

Dr. William Koros, Advisor
School of Chemical and Biomolecular Engineering
Georgia Institute of Technology

Dr. Christopher Jones
School of Chemical and Biomolecular Engineering
Georgia Institute of Technology

Dr. Amyn Teja
School of Chemical and Biomolecular Engineering
Georgia Institute of Technology

Dr. Satish Kumar
School of Polymer, Textile, and Fiber Engineering
Georgia Institute of Technology

Dr. Sankar Nair
School of Chemical and Biomolecular Engineering
Georgia Institute of Technology

Date Approved: April 25, 2006

This thesis is dedicated to those I love the most,
my wife Melissa and my parents.

ACKNOWLEDGEMENTS

I would first like to acknowledge my advisor, Dr. Bill Koros, for all of his guidance throughout my graduate studies at Georgia Tech. Dr. Koros is an excellent researcher, a great mentor, and great person to talk to. I could not have had a better advisor.

I would like to acknowledge all of the members of the Koros group for their help and support throughout my graduate studies. All of the group members are supportive colleagues who I am also lucky enough to call friends. In particular, I would like to thank Ted Moore, David Wallace, and Shilpa Damle-Mogri for help getting me started in my research career at Georgia Tech. I also appreciate John Perry, Bill Madden, Raymond Chafin, Preeti Chandra, and Alexis Hillock for all of their help and friendship both in and out of the lab.

I would also like to acknowledge my parents for all of their love and support throughout my life. I would not be where I am today without them and words cannot describe how much I appreciate everything they have done for me.

Finally, I would like to thank my wife Melissa. She is my strongest supporter, my thesis editor, and my best friend.

TABLE OF CONTENTS

LIST OF TABLES

LIST OF FIGURES

SUMMARY

Carbon molecular sieve (CMS) membranes represent the most attractive pure component materials to compete against polymer membranes for high performance gas separations. CMS membranes are formed from the thermal decomposition of polymer precursors and can therefore be formed into continuous defect free membranes with excellent gas separation performance. Over the last 20 years, CMS membranes have been produced in a variety of geometries and have a wide range of separation performance applicable to several important gas separations.

Though research into CMS membrane formation is quite extensive, the relationship between synthesis factors and separation performance is still not well understood. The goal of this study was to elucidate the effect of two different synthesis factors on the separation performance of CMS membranes to allow more control over separation performance. The foci of this study were to clarify (1) the effect of pyrolysis atmosphere and (2) the effect of polymer precursor composition.

Dense flat CMS membranes were synthesized from 6FDA:BPDA-DAM precursor at 550 ^{o}C using several pyrolysis atmospheres including vacuum pyrolysis (<0.05 torr), helium and argon flowing at atmospheric pressure, and helium and argon flowing at reduced pressures. The separation performance of CMS membranes produced under different pyrolysis atmospheres suggests that the amount of oxygen available during pyrolysis has a significant affect on the microstructure of membrane.

CMS membranes were produced from 6FDA:BPDA(1:1)-DAM and 6FDA:BPDA(1:1)-DAM under identical pyrolysis conditions to determine the utility of

polymer precursor composition as an engineering tool to fine-tune the performance of CMS membranes. In a second study utilizing 6FDA-6FpDA and 6FDA-6FmDA precursors, the separation performance of CMS membranes was shown to be dependent on the intrinsic precursor free volume. These studies have shown that two factors to be considered when choosing a polymer precursor are the intrinsic free volume of the polymer and the composition of the by-products evolved during pyrolysis.

CHAPTER 1

INTRODUCTION

1.1 GAS SEPARATION MEMBRANES

Gas separation membranes currently comprise a market of over 150 million U.S dollars per year. This number is expected to rise to around 750 million dollars by 2020 [1]. Figure 1.1 shows the separations that currently utilize industrial membrane technology. Currently, the separation of nitrogen from air is the largest industrial gas separation. Membranes can produce 98-99% nitrogen streams which are used to blanket food, chemicals, and most recently, fuel tanks. Natural gas purification is anticipated to be the largest commercial membrane gas separation by 2020. One of the most important separations for natural gas involves separation of carbon dioxide from methane. Carbon dioxide (CO_2) must be removed to below 2% before natural gas can be pumped through pipelines, because CO_2 can form carbonic acid and destroy the pipeline. It is expected that by 2020, membranes will begin to compete in new markets such as the separation of olefins and paraffins [1, 2]. Currently, these markets are dominated by cryogenic distillation because current membranes do not possess the separation performance necessary to compete in these markets. There are three difficulties associated with olefin/paraffin separations: 1) the large size of the molecules in comparison to traditional gas separations, 2) the similar size of the molecules, 3) the high condensability and interaction of these components with the actual membrane matrix. To compete in these new markets and to increase the performance of membranes in existing markets, new materials must be developed. In this study, a relatively new type of membrane known as carbon molecular sieves, which may be useful for such separations, will be discussed.

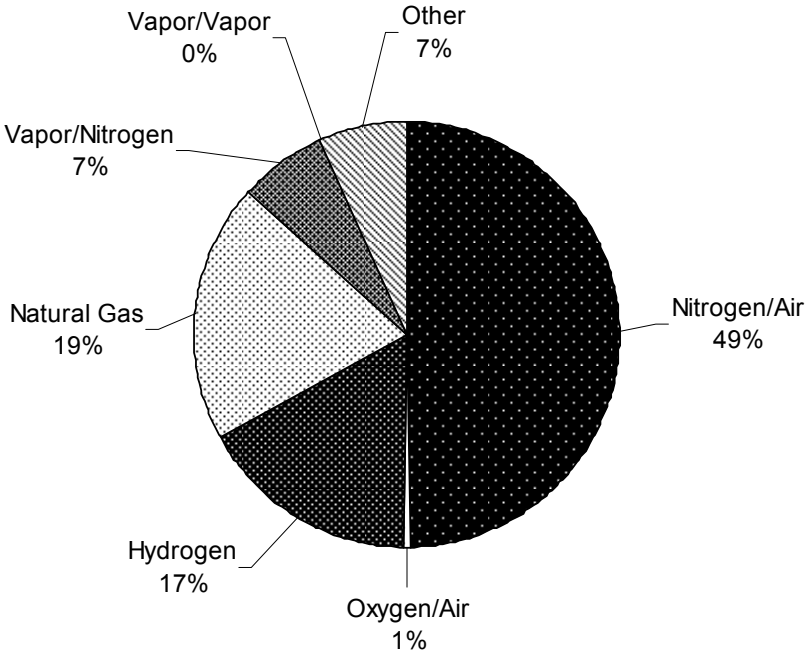

Figure 1.1 Current markets for membrane based separations, Adapted from Baker [1]

1.2 TYPES OF GAS SEPARATION MEMBRANES

1.2.1 Polymeric membranes

Currently, glassy polymer membranes are the dominant industrial membrane material for gas separations. Polymers have several advantages over other inorganic materials. These advantages include ease of processability and reasonably good separation performance. Polymers can be processed into asymmetric hollow fibers which have a very thin selective layer on the surface of a porous substructure. This geometry has several advantages industrially. Asymmetric hollow fibers have 1) very high surface/volume ratio, 2) minimal resistance to flow due to the thin surface layer, and 3) good mechanical properties due to the porous substructure.

The main disadvantage of polymer membranes is that there is a tradeoff between the productivity (permeability) and the separation efficiency (selectivity). In 1991, Robeson analyzed the separation performance of several polymer membranes that have been presented in the literature and discussed the performance in terms of the so-called "upper-bound" curves [3]. These curves show the traditional tradeoff between permeability and selectivity for solution processable polymers. Figure 1.2 contains the "upper bound" curves for the O_2/N_2 and CO_2/CH_4 separations. Burns and Koros [2] have also presented a similar upper bound for the propane/propylene separation. Unfortunately, for the olefin/paraffin separations, the separation performance necessary for membranes to compete against current separation technologies such as cryogenic distillation is above the upper bound. This has led to the development of alternative membrane materials.

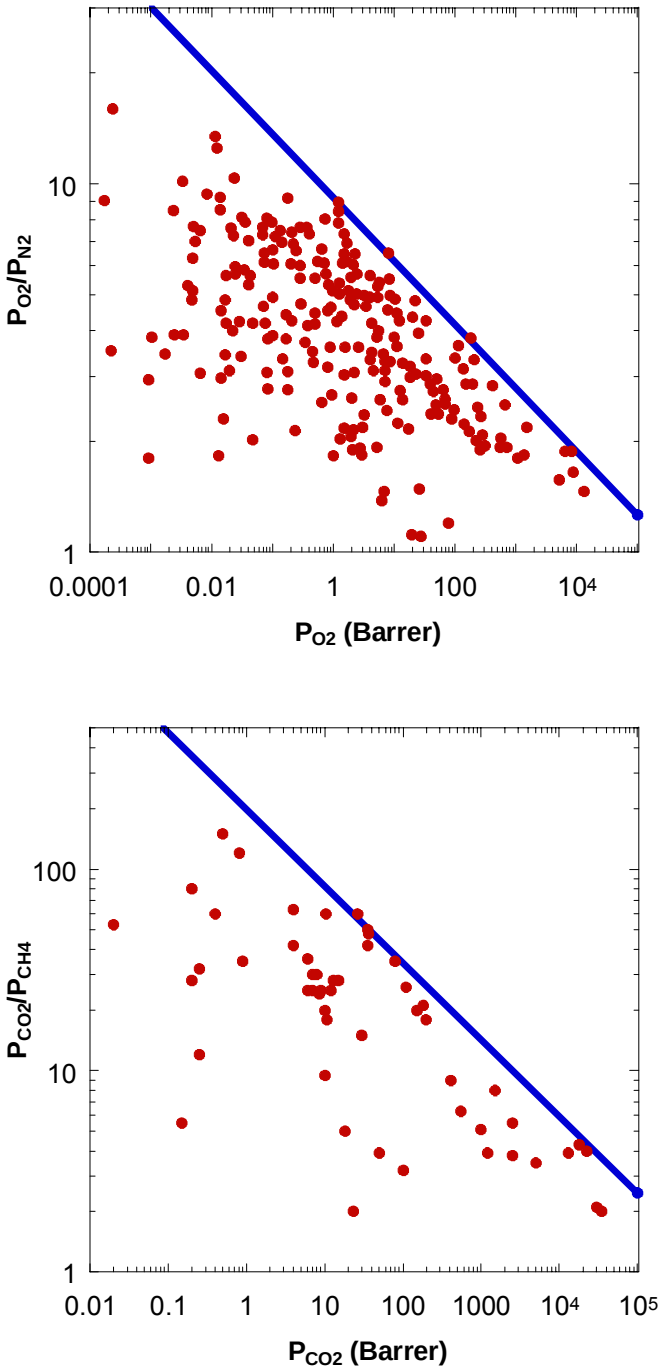

Figure 1.2 Upper bound curve for O_2/N_2 and CO_2/CH_4 separation. The data used for these plots were obtained from Robeson [3] and the plots were adapted from Moore [4].

1.2.2 Inorganic membranes

Three main types of *porous* inorganic membranes have been investigated for gas separation: zeolites, silica, and carbon molecular sieve. Silica membranes are amorphous glass membranes with a distribution of pore sizes. Silica membranes are very useful for separating hydrogen from larger gases such as hydrocarbons. Reproducible production of silica membranes has been limited, however new techniques are being developed which allow for reproducible production of membrane properties. Industrial applications of silica membranes will likely be limited to the separation of molecules of greatly dissimilar size.

Zeolites are crystalline materials primarily formed from aluminum, silicon, and oxygen. The crystal structure of zeolites results in a very rigid porous structure. For example, zeolite 4A (Figure 1.3) has been extensively investigated for air separation. The structure is composed of micropores, ~11.4 Å in diameter, connected by selective necks which are 4 Å in diameter. Therefore, diffusion of gas molecules larger than 4 Å is highly restricted through the zeolite, and the zeolite acts as a "molecular sieve." Thus, zeolites have very high selectivities and are even useful for separation of isomers. The main disadvantage of zeolite membranes is the difficulty in forming a continuous defect free structure. Intracrystalline defects hinder the properties of these materials and therefore, scale-up to industrial size membranes has been unsuccessful.

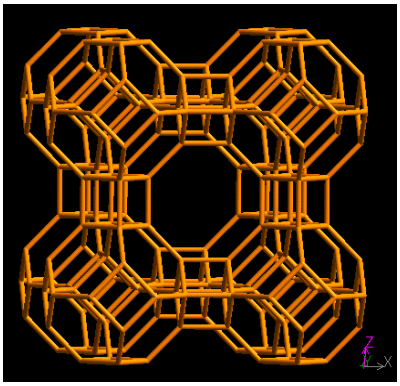

Figure 1.3 Crystal structure of zeolite 4A taken from the International Zeolite Association [5]

Carbon molecular sieve (CMS) membranes are inorganic membranes formed from the thermal decomposition of organic (polymer) precursors. These materials are formed from turbostratic carbon, which is irregularly packed sp^2 hybridized carbon. A diagram of the structure is depicted in Figure 1.4. The packing irregularities result in an amorphous material with slit shaped pores which act as molecular sieves. More detail will be provided in Chapter 2 about the structure of these materials. Carbon molecular sieves membranes have excellent separation performance in comparison to polymers and their performance rivals zeolites. The focus of this study will be the formation of CMS membranes and, more importantly, the characterization of production parameters which influence the performance of CMS membranes.

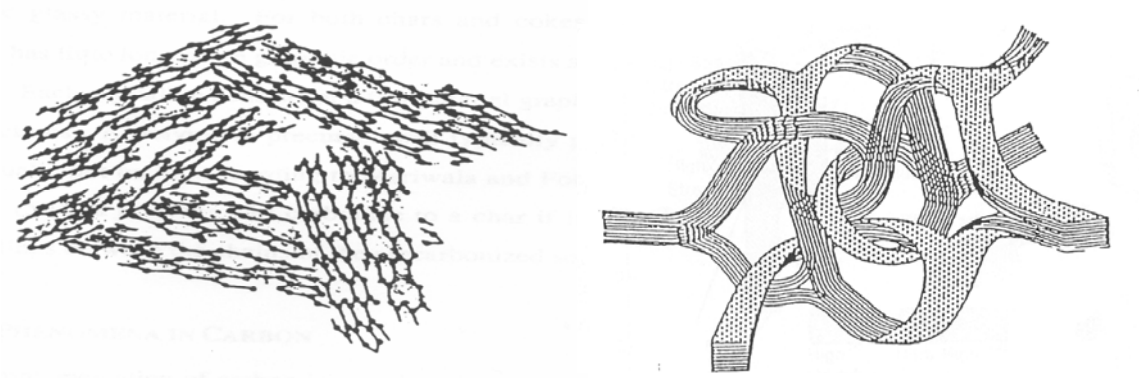

Figure 1.4 Hypothetical structure of turbostratic carbon. The pictures were taken from Pierson [6] and Jenkins and Kawamura [7].

1.3 FORMATION OF CMS MEMBRANES

Koresh and Soffer [8-12] pioneered the production of defect free hollow fiber CMS membranes from the thermal decomposition of polymer precursors. Since that time, researchers have formed relatively defect free CMS membranes in a variety of geometries. Several factors have been identified which influence the performance of CMS membranes. These factors include but are not limited to the composition of the polymer precursor, thermal decomposition temperature, "thermal soak" time, and the atmosphere under which decomposition occurs [13-16]. The effect of each of these parameters will be detailed in the following chapter.

1.4 RESEARCH OBJECTIVES

CMS membranes have been actively produced for the last 25 years. As mentioned previously, there are several factors which influence the performance of CMS membranes. Unfortunately, there have been very few systematic studies which investigate the effect of each of these parameters on the microstructure (and separation performance) of CMS membranes.

The ultimate goal of this project is to lay a foundation for systematic development of CMS membranes for a variety of gas separations. This study focused on the effects that polymer precursor composition and pyrolysis atmosphere have on the separation performance of CMS membranes. Two other factors that were examined to a lesser extent were the pyrolysis temperature and the thickness of the precursor film. In pursuit of these goals, several specific objectives were outlined:

1. Determine the utility of polymer composition as an engineering parameter for the development of CMS membranes for a variety of gas separations and identify the specific polymer structural factors that influence CMS separation performance.
2. Develop a series of polymers that can be used to analyze the effect of polymer precursor free volume on the separation performance of CMS membranes. Using this system, produce a series of CMS membranes under identical processing conditions and compare the microstructure of the CMS membranes to determine the effect of polymer free volume on resulting CMS structure.
3. Produce CMS membranes under different pyrolysis atmospheres and determine the effect of purge flow rate, purge gas composition, and purge gas pressure on the separation performance of CMS membranes.

Objective 1: Determine the utility of CMS composition as a material process development tool in the development of CMS membranes having a tunable range of separation performances

The most common method for the formation of CMS membranes is through the thermal decomposition (or pyrolysis) of polymer precursors. The conditions under which thermal decomposition occurs determine the microstructure, and thus the separation performance of CMS membranes. A variety of polymers have been used to produce

CMS membranes (more detail will be given in Chapter 2). It is well known that by varying the polymer precursor, CMS membranes with a breadth of separation performance can be produced. There are limited studies which produce CMS membranes under the same pyrolysis conditions using different precursors [14, 17]. The resulting CMS membranes have different properties, especially at low decomposition temperatures.

In this study, the composition of a copolyimide will be varied to determine the effect of polymer precursor structure on the ultimate separation performance of CMS membranes. Three polymer structure factors hypothesized to affect CMS separation performance include the polymer free volume, the composition of the decomposition products during the early stage of pyrolysis as well as the total amount of decomposition products evolved. These factors played a major role in the selection of the polyimides chosen as precursors. The goal was to elucidate the precursor structure factors which affect CMS separation performance and to determine whether or not varying the precursor structure had as significant an effect on the CMS separation performance as other factors such as thermal decomposition temperature.

Objective 2: Determine the effect of polymer precursor free volume on the resultant separation performance of CMS membranes

In objective 1, three polymer precursor structure factors were suggested to affect the separation performance of CMS membranes. Unfortunately, it is very difficult to elucidate the effect of each of these factors individually especially when using polyimide precursors. Therefore, two polyimides, 6FDA-6FmDA and 6FDA-6FpDA were used as polymer precursors. The only difference between the structure of these two polyimides is the location of a aromatic linkage in the diamine (one is para and one is meta), resulting

in a difference in free volume but not atomic composition. The decomposition of these two polymers was investigated using thermogravimetric analysis (TGA) and infrared spectroscopy (IR) to prove that the decomposition mechanism and by-products were similar. CMS membranes were produced from these precursors under identical pyrolysis conditions to elucidate the effect of intrinsic precursor free volume on the separation performance of CMS membranes. The results of this study will be useful for future selection of polymer precursor materials for a specific separation or application.

Objective 3: Determine the effect of pyrolysis atmosphere on the separation performance of CMS membranes

Scale-up of CMS membrane production is limited by several factors. Three significant limiting factors are the weak mechanical properties of CMS membranes, the difficulty in achieving reproducible formation, and the high cost of production. CMS membranes with the most attractive properties have been produced in vacuum chambers at temperatures above 550 ^{o}C on the laboratory scale. It has been estimated that the production of CMS membranes under these conditions may cost an order of magnitude more than traditional polymer membranes. One method to lower the cost would be to produce membranes in inert environments, since this might be scaled up to a continuous process. A limited number of studies have compared the performance of CMS membranes produced under inert environments and in vacuum. Geiszler and Vu [13, 16], in different studies with different polymer precursors, produced asymmetric hollow fiber CMS membranes under both vacuum atmosphere and in flowing purge gases. The authors showed a considerable effect of atmosphere on the separation performance. In another study, Suda and Haraya [18] produced flat CMS membranes using Kapton polyimide (a low free volume polymer) at high temperature using both vacuum and argon

purge gases. The change in atmospheres had little effect on separation performance. Therefore, there appeared to be some discrepancy in the literature unless the polymer precursor free volume could somehow be a factor in affecting the response to pyrolysis process environments. In the current study, the effect of pyrolysis atmosphere will be discussed in relationship to repeatable membrane formation and to the effect on separation performance. CMS membranes were produced under vacuum and in flowing argon and helium. The effect of pyrolysis atmosphere was determined for dense flat polymer membranes and compared to previous results. As noted above, this information is important for future production of CMS membranes, especially on the industrial scale.

1.5 DISSERTATION OVERVIEW

Chapter 2 contains background information pertinent to the remainder of the dissertation and presents a review of CMS membrane production. Chapter 3 discusses the materials and experimental procedures described in subsequent chapters. In Chapter 4, a copolymer series with different composition was used to make CMS membranes to investigate the relationship between precursor and CMS structure. In Chapter 5, the effect that polymer precursor free volume has on CMS separation performance will be presented. In Chapter 6, the effect of purge gas composition and flow rate during pyrolysis will be discussed. Chapter 7 contains conclusions and recommendations for future work.

1.6 REFERENCES

1. Baker, R.W., *Future Direction of Membrane Gas Separation Technology.* Industrial and Engineering Chemistry Research, 2002. **41**(6): p. 1393.

2. Burns, R.L. and Koros, W.J., *Defining the Challenges for C3H6/C3H8 Separation Using Polymeric Membranes.* Journal of Membrane Science, 2003. **211**(2): p. 299-309.

3. Robeson, L.M., *Correlation of separation factor versus permeability for polymeric membranes.* J. Membr. Sci., 1991. **62**(2): p. 165-85.

4. Moore, T., *Effects of Materials, Processing, and Operating Conditions on the Morphology and Gas Transport Properties of Mixed Matrix Membranes*, in *Chemical Engineering*. 2005, The University of Texas at Austin.

5. http://www.iza-structure.org/databases/ (Accessed March 25, 2006), International Zeolite Association.

6. Pierson, H.O., *Handbook of Carbon, Graphite, Diamond, and Fullerenes*. 1993, Park Ridge, NJ: Noyes Publication.

7. Jenkins, G.M. and Kawamura, K., *Polymeric Carbons - Carbon Fiber, Glass and Char*. 1976, London: Cambridge University Press.

8. Soffer, A., Saguee, S., Golub, D., Cohen, H., and Azariah, M., Selective clogging of failed fibers, United States Patent 5575963, 1996.

9. Soffer, A., Koresh, J.E., and Saggy, S., Separation device, United States Patent 4685940, 1987.

10. Soffer, A., Azariah, M., Amar, A., Golub, D., Saguee, S., and Tobias, H., Method of Improving the selectivity of carbon membranes by chemical vapor deposition, United States Patent 5695818, 1997.

11. Koresh, J.E. and Soffer, A., *Molecular sieve permselective membrane. Part I. Presentation of a new device for gas mixture separation.* Separation Science and Technology, 1983. **18**(8): p. 723-34.

12. Koresh, J.E. and Danon, A., *A Novel insight on the High-Temperature Helium Interaction with a Carbon Molecular Sieve.* Langmuir, 2001. **17**: p. 2739-2742.

13. Vu, D.Q., *Formation and characterization of asymmetric carbon molecular sieve and mixed matrix membranes for natural gas purification*, in *Department of Chemical Engineering*. 2001, University of Texas at Austin: Austin, TX.

14. Steel, K.M., *Carbon membranes for challenging separations*, in *Department of Chemical Engineering*. 2000, University of Texas - Austin: Austin, TX.

15. Singh, A. and Koros, W.J., *Significance of Entropic Selectivity for Advanced Gas Separation Membranes.* Industrial and Engineering Chemistry Research, 1996. **35**: p. 1231-1234.

16. Geiszler, V., *Polyimide Precursors for Carbon Molecular Sieve Membranes*. 1997, University of Texas, Austin: Austin.

17. Park, H.B., Kim, T.K., Lee, J.M., Lee, S.Y., and Lee, Y.M., *Relationship between chemical structure of aromatic polyimides and gas permeation properties of their carbon molecular sieve membranes.* Journal of Membrane Science, 2004. **229**: p. 117-127.

18. Suda, H. and Haraya, K., *Gas Permeation through Micropores of Carbon Molecular Sieve Membranes Derived from Kapton Polyimide.* Journal of Physical Chemistry B, 1997. **101**: p. 3988-3994.

CHAPTER 2

BACKGROUND AND THEORY

The first half of this chapter considers the structure of carbon membranes and models used to describe gas transport through membrane. The second half of this chapter contains a literature review of all aspects of carbon molecular sieve membrane formation.

2.1 STRUCTURE OF CARBON MEMBRANES

The most common technique used to form carbon membranes is thermal decomposition of polymer precursors. When a polymer is thermally decomposed it can either form coke or char. Coke can be heated further to form a graphitic structure while char remains in amorphous form [1]. Carbon membranes used for gas separation usually have a turbostratic structure (Pierson[1], Figure 1.2) with very little long range order and are considered essentially isotropic. The majority of carbon membranes are therefore formed from polymers which form char, but some studies have used polymers that form coke, which are only in the early stage of decomposition, before graphitization occurs. Figure 1.2 illustrates that there are lattice vacancies in the sp^2 hybridized carbon sheets, and pores are formed from packing imperfections between microcrystalline regions in the material. Therefore, the pore structure in carbon membranes is said to be slit-like and an "idealized" diagram can be seen in Figure 2.1 [2]. The pore structure in CMS membranes is a function of many parameters including the size of the microcrystalline regions and the degree of order or packing in the material. Each of these factors is related to the polymer precursor and the processing conditions.

The pore model shown in Figure 2.1 has been used to describe the pore distribution in CMS materials. The pore structure is bimodal, which contains large pores

(6-20 Å) connected by smaller pores known as "ultramicropores." It is easy to see that these small pores give the material molecular sieving ability.

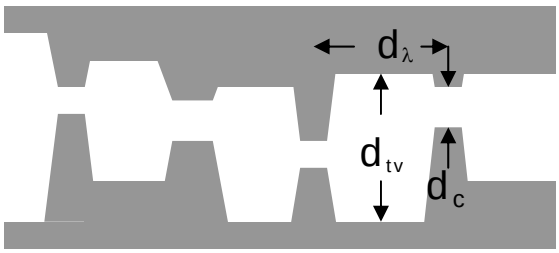

Figure 2.1 Idealized pore structure of CMS membranes adapted from Steel and Koros [2, 3]. The dimension d_c is the ultramicropore dimension, d_{tv} is the size of the adsorptive pores (otherwise know as the transverse dimension), d_λ is the jump length dimension

2.2 FUNDAMENTALS OF GAS TRANSPORT THROUGH CARBON MEMBRANES

2.2.1 Permeation in carbon membranes

Gas transport through glassy polymers and molecular sieves is commonly described by the solution-diffusion mechanism. The gas penetrant first sorbs into the membrane on the upstream (feed) side, then diffuses through the material, and finally desorbs on the downstream side of the membrane. The permeability of the membranes is described by Equation 2.1:

$$P_A = N_A \frac{\ell}{\Delta p_A} \qquad (2.1)$$

where P_A is the permeability of component A, N_A is the flux of component A, Δp_A is the partial pressure drop across the membrane and ℓ is the membrane thickness. The common unit for permeability is the Barrer:

$$1\ \text{Barrer}\ [\equiv]\ 10^{-10}\ \frac{\text{cm}^3(\text{STP})\cdot\text{cm}}{\text{s}\cdot\text{cm}^2\cdot\text{cmHg}}\ . \tag{2.2}$$

For some membrane geometries such as asymmetric hollow fibers, it is difficult to measure the thickness of the selective layer. Therefore, "permeance" is used to describe the flux through the membrane. The permeance can be written as

$$\text{permeance}_A = \frac{P_A}{\ell} = \frac{N_A}{\Delta p_A}. \tag{2.3}$$

The common unit for permeance is the Gas Permeation Unit (GPU).

$$1\ \text{GPU}\ [\equiv]\ 10^{-6}\ \frac{\text{cm}^3(\text{STP})}{\text{s}\cdot\text{cm}^2\cdot\text{cmHg}}\ . \tag{2.4}$$

Diffusion of a gas through a membrane is governed by Fick's law and therefore Equation 2.1 can be rewritten as

$$P_A = -D_A(C)\left[\frac{\partial C_A}{\partial x}\right]\frac{\ell}{p_{A2}-p_{A1}} \tag{2.5}$$

where C_A is the concentration of the component A, p_{A2} and p_{A1} are the upstream and downstream pressures respectively, and $D_A(C)$ is the concentration dependent diffusion coefficient. When pressure on the downstream is negligible, this equation can be written as

$$P_A = \overline{D}_A \cdot \overline{S}_A \tag{2.6}$$

where $\overline{D}_A$ and $\overline{S}_A$ are defined in equations (2.7) and (2.8), respectively.

$$\overline{D}_A = \frac{\int_0^{C_{A2}} D_A\, dC_A}{C_{A2}} \tag{2.7}$$

$$\overline{S}_A = \frac{C_A}{p_A} \tag{2.8}$$

The diffusion coefficient represents a kinetic, or mobility factor while the sorption coefficient represents a thermodynamic factor. For the case of molecular sieves, the sorption coefficient is determined by the condensability of the gas penetrant, detailed chemical nature of the carbon surface, and the porosity in the material.

The permselectivity for a mixture of penetrants is defined as

$$\alpha^*_{A/B} = \frac{y_A / y_B}{x_A / x_B} \tag{2.9}$$

where x_i and y_i are the mole fractions of the components at the upstream and downstream faces of the membrane, respectively. When the downstream pressure is considered to be negligible relative to the upstream, the ideal permselectivity can be used to estimate the actual permselectivty. The ideal permselectivity is the ratio of pure gas permeabilities or permeances as in Equation 2.10.

$$\alpha_{A/B} = \frac{P_A}{P_B} = \frac{\overline{D}_A}{\overline{D}_B} \cdot \frac{\overline{S}_A}{\overline{S}_B} \tag{2.10}$$

Equation 2.5 shows that the permeability can be written as the ratio of the diffusivity selectivity and the sorption selectivity.

2.2.2 Sorption in CMS membranes

Sorption isotherms in carbon molecular sieve membranes have been described by a variety of different adsorption isotherms. The most commonly used isotherm is the Langmuir isotherm:

$$C_A = \frac{C'_{AH} b_A p_A}{1 + b_A p_A} \tag{2.11}$$

where C_A is the amount of penetrant absorbed, C'_{AH} is the Langmuir hole filling capacity, b_A is the Langmuir affinity constant, and p_A is the partial pressure of A in

equilibrium with the material. The majority of penetrant is assumed to adsorb into the large pores characterized by dimensions d_{tv} and d_{λ} in Figure 2.1. These pores make up the majority of the pore volume in CMS membranes and the interaction energy of the molecule adsorbed in the large pores (see #1 below) is generally lower than the ultramicropores (see #2 below) as depicted in Figure 2.2.

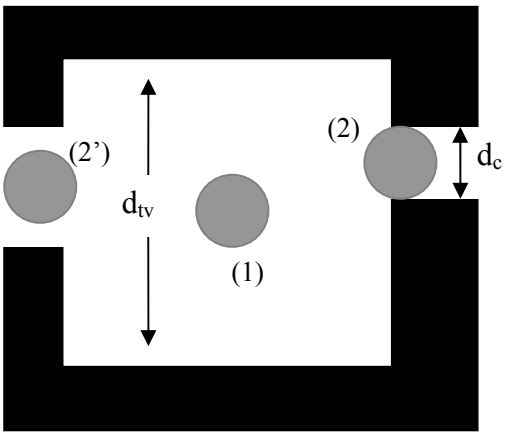

Figure 2.2. Diagram depicts the idealized equilibrium positions at various locations inside the pore structure. The diameter of d_c is smaller than the size of the molecule and therefore the interaction energy at point (2) is positive and a jump through the pore is not likely, whereas passage through the larger pore at 2' is feasible.

The sorption coefficient for CMS membranes can be defined as the secant slope of the sorption isotherm. Therefore, the sorption coefficient can be written in terms of the Langmuir constants as:

$$S_A = \frac{C_A}{p_A} = \frac{C'_{AH} b_A}{1 + b_A p_A} \tag{2.12}$$

where S_A is the sorption coefficient of A at partial pressure, p_A.

2.2.3 Diffusion in CMS membranes

2.2.3.1 Diffusion mechanisms

Diffusion in porous carbon membranes can occur via four different mechanisms: Knudsen diffusion, selective condensation, selective adsorption, and molecular sieving [4, 5]. In Knudsen diffusion, gas molecules permeate in the gas phase through pores in the membrane. If the pore size is smaller than the mean free path of the molecule, then Knudsen diffusion can occur. The Knudsen diffusion coefficient can be estimated from kinetic theory by the following equation for a single cylindrical tube of radius r [6]:

$$D_A = 97.0r\left(\frac{T}{M_A}\right)^{1/2} \tag{2.13}$$

where D_A is the diffusion coefficient (m^2/s), T is the temperature (K), r is the pore radius (m), and M_A is the molecular weight of component A. Given the complex nature of the pore structure depicted in Figures 1.4 and 2.1, it is not possible to predict D values, since the "effective" pore size is difficult to define and the "effective" pore size is not generally predictable. The selectivity from Knudsen diffusivity can be written as:

$$\alpha_{A/B} = \sqrt{\frac{M_B}{M_A}} \tag{2.14}$$

It is evident that selectivities obtained from Knudsen diffusion are not very high, especially for gases of similar molecular weight such as oxygen and nitrogen.

Selective condensation occurs when one or more of the components in the feed stream condenses in the pores of the membrane [5]. Once the pores are filled, the condensed material diffuses across the membrane. Very high selectivity can be achieved if one of the components is non-condensable [7], but the separation is limited by the condensation partial pressure of the components, which is a function of pore size and

shape. Therefore, this mechanism is difficult to control and is rarely used in carbon membranes.

Selective adsorption occurs when one or more components of the feed are preferentially adsorbed into the membrane, followed by diffusion of the adsorbed species across the membrane from sorbed site to sorbed site. The separation efficiency for this mechanism is a function of the physiochemical nature of the pore surface and the pore size. Exclusion of the rejected penetrant from sorption sites in pores is critical for successful application of such materials [5]. The driving force for mass transfer across these membranes is the difference in adsorbed phase concentration of the diffusing species. Therefore, only low partial pressure driving forces are needed for strongly adsorbing components. Rao and coworkers [4, 5, 8-10] have developed membranes which rely on this mechanism called "Selective Surface Flow (SSF^{TM}) Membranes." High selectivities can be achieved using this method for separation involving highly adsorbing species from low sorbing components. Of particular interest has been the separation of low sorbing hydrogen from highly sorbing hydrocarbon streams.

2.2.3.2 Molecular sieving

Molecular sieving occurs when the permeate molecules are separated by the molecular size using the pore structure of the membrane. In this process, the "ultramicropores" limit the diffusion of species with a similar molecular dimension. Diffusion through the ultramicropores requires penetrant molecules to overcome the repulsive interaction energy with the pore walls forming the ultramicropore. Molecules of similar size can be effectively separated because very small changes in size result in considerable differences in the activation energy of diffusion (refer to Figure 2.2).

This type of activated diffusion through the ultramicropores is often expressed by an Arrhenius relationship:

$$D_A = D_{AO} \exp\left(\frac{-E_D}{RT}\right) \tag{2.15}$$

where D_{AO} is the pre-exponential term, E_D is the activation energy of diffusion, R is the ideal gas constant, and T is the absolute temperature.

Singh and Koros [11, 12] have also discussed the importance of "entropic selectivity" in molecular sieving media, including CMS membranes. An analysis was performed comparing literature data for zeolite 4A, some CMS materials, and poly-pyrrolone polymers (which exhibit high selectivity). The results showed that the activation energy of diffusion for both O_2 and N_2 was similar for all three materials, with the substantial difference coming from the pre-exponential factor. From transition state theory, the pre-exponential factor can be defined as:

$$D_{AO} = e\lambda^2 \frac{kT}{h} \exp\left(\frac{S_D}{R}\right) \tag{2.16}$$

where λ is the average diffusive jump length, S_D is the activation entropy of diffusion, k is the Boltzmann constant, and h is Planck's constant. The jump length is a strong function of the pore structure and a weak function of penetrant size. The diffusion coefficient can also be written as:

$$D = \lambda^2 \frac{kT}{h} \frac{F}{F^+} \exp\left(\frac{-E_D}{R}\right) \tag{2.17}$$

where F is the partition function in the normal state and F^+ represents the partition function for the same gas molecule in the transition state. In the case of molecular sieves,

the normal sorbed state is in the large pores and the transition state is in the ultramicropores. The total partition function in either state can be expressed as:

$$F = F_{trans} \cdot F_{rot} \cdot F_{vib} \tag{2.18}$$

If one combines equation 2.16 and 2.17, it can be determined that:

$$\exp\left(\frac{S_{D,A} - S_{D,B}}{R}\right) = \frac{\left(F^{+}/F\right)_{A}}{\left(F^{+}/F\right)_{B}} \tag{2.19}$$

For molecules that have different dimensions, pores can inhibit rotational freedom for one molecule, while allowing it for other molecules. For example, nitrogen can be approximated as spherocylindrical with a length of 4 Å and diameter of 3 Å. Oxygen has a similar shape with diameter of ~2.8 Å and a length of 3.7 Å. Therefore, if an ultramicropore has a dimension of 3.8 Å, oxygen is allowed to freely rotate, and nitrogen loses rotational freedom, leading to entropic selectivity. Singh has presented a more detailed analysis and determined the range of entropic selectivity for a 3.8 Å pore is from 3.7 to 9 for slit shaped CMS pores. Therefore, entropic selectivity plays a major role in the enhanced separation performance of CMS membranes.

2.3 FORMATION OF CARBON MEMBRANES

Carbon membranes are generally produced from thermal decomposition (pyrolysis) of polymer precursors. Like polymer membranes, a variety of different formats have been produced. The formats can be generalized into two groups, supported and unsupported. Supported membranes are formed by casting a thin polymer film on a surface or wetting a surface with an organic liquid. The supports are generally flat sheet or tubular porous inorganic materials. Unsupported membranes have been produced in

primarily three forms: (1) dense, flat sheet, (2) asymmetric hollow fiber, and (3) asymmetric film.

As mentioned previously, the gas separation performance of a carbon membrane is controlled by the pore size distribution in the material. Several factors have been identified which affect the pore size distribution:

- Polymer precursor composition
- Pyrolysis temperature and ramp rate
- Thermal soak time at maximum pyrolysis temperature
- Pyrolysis atmosphere
- Post treatment conditions

There are other minor factors that also play a role in the separation performance of carbon membranes, but the factors listed here have been identified as the most significant. In the next sections, these factors will be evaluated in more detail. The syntheses of selective surface flow and CMS membranes follow very similar procedures. This study pertains to CMS membranes and therefore, selective surface flow membranes will not be reviewed.

2.3.1 Polymer precursor composition and morphology

A variety of thermosetting polymers have been used as precursors to produce carbon molecular sieve membranes. Koresh and Soffer [13] produced the first hollow fiber CMS membranes by pyrolyzing cellulose hollow fibers. They suggest that polymers suitable as precursors for CMS membranes should not flow before they decompose. Several polymers have been used to produce CMS membranes including polyacrylonitrile [14], phenolic resin [15-17], polyfurfuryl alcohol [17-21],

poly(vinylidene) based polymers [22], cellulose derivatives [13], and polyimides [3, 23-30]. Polyimides have been the precursor of choice by many researchers likely due to their high T_g, ease of processability, and good separation performance as polymeric membranes. Jones and Koros [31, 32] have suggested that (based on separation performance and mechanical properties) the best precursors currently available for the production of carbon membranes are polyimides. Table 2.1 lists the precursor and the format of several CMS membranes that have been produced. Figure 2.3 shows the structure of most of the non-commercial polyimides listed in Table 2.1. The majority of the discussion in this review will be on polyimide based materials because of the breadth of data available in the literature, but initially, alternative precursors will be discussed. There are hundreds of studies on CMS membranes in the literature, therefore those mentioned in this review are provided to highlight some of the better CMS membranes that have been produced.

Table 2.1. Sampling of carbon membranes presented in the literature including the precursor material and morphology.

Polymer	Morphology	Reference
Matrimid	supported film	[33]
Matrimid	Film	[34]
Matrimid	Film	[2]
Kapton	supported film	[33]
Kapton	Film	[2, 35-38]
Kapton	asymmetric fiber	[39, 40]
Kapton	Film	[41]
Polyvinylidene chloride-acrylate terpolymer latex	supported film	[4]
phenolic resin	supported tube	[15, 42]
6FDA/BPDA-DAM	Film	[12, 22, 43]
poly(vinylidene-chloride-co-vinyl chloride)	supported film	[22]
phenol-formaldehyde Novolac resin	asymmetric tubular	[44]
Sulfonated phenolic resin	tubular, supported	[22, 45, 46]
BPDA/6FDA-TrMPD	asymmetric fiber	[44] [31, 32, 47, 48]
BPDA/6FDA-TrMPD	asymmetric fiber	[49, 50]
BPDA-DDBT/DABA/CF_3 containing diamine	asymmetric hollow fiber	[51]
polyfurfuryl alcohol	tubular, supported	[17, 20, 21]
polyfurfuryl alcohol	supported films	[18, 19]
polyfurfuryl alcohol	tubular, supported	[52]
polyfurfuryl alcohol	supported films	[53]
phenol-formaldehyde resin	asymmetric film	[16]
phenolic resin (Novalak type)	supported films	[54]
BPDA-ODA	tubular, supported	[55, 56]
P84 polyimide	Film	[30, 34]
6FDA-durene polyimide	Film	[28]
6FDA/PMDA(1/6)-TMMDA	Film	[29]
BTDA-mPDA/BDSA (substituted with Li, Na, or K)	Film	[57]
NTDA-BAHFDS (sulfonated PI)	Film	[58]
NTDA-BDSA (sulfonated PI)	Film	[58]
NTDA-ODADS (sulfonated PI)	film	[58]
NTDA-BAHFDS/BAPF(4/1) (sulfonated PI)	film	[58]
NTDA-BDSA/BAPF(4/1) (sulfonated PI)	film	[58]
CH_3COCH_3+CH_4 by ICPCVD	supported film	[59]
hexamethyldisiloxane by ICPCVD	supported film	[60, 61]
BTDA-ODA	film	[62]
BTDA-ODA-polyvinylpyrrolidone blends	film	[63, 64]
BTDA-ODA/m-PDA(9/1)	film	[27]
BTDA-ODA/2,4-DAT(9/1)	film	[27]
BTDA-ODA/m-TMPD(9/1)	film	[27]

Dianhydrides

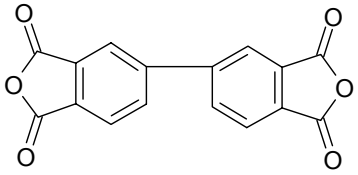

BPDA
3,3',4,4'-biphenyl tetracarboxylic acid dianhydride

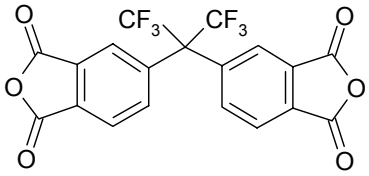

6FDA
5,5'-[2,2,2-trifluoro-1-(trifluoromethyl)ethylidene] bis-1,3-isobenzofurandione

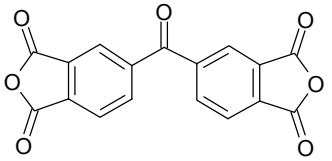

BTDA
Benzophenone tetracarboxylic dianhydride

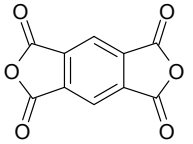

PMDA
pyromellitic dianhydride

Diamines

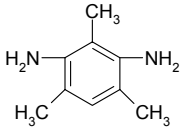

DAM, TrMPD, *m*-TMPD
2,4,6-trimethyl-1,3-phenylene diamine

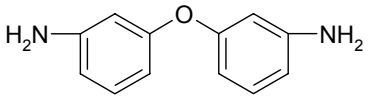

ODA
Oxydianaline

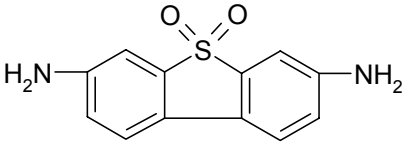

DDBT
dimethyl-3,7-diaminodiphenyl-thiophene-5,5'-dioxide

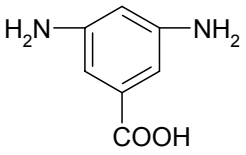

DABA
3,5-diaminobenzoic acid

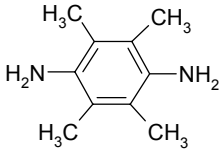

durene
2,3,5,6-tetramethyl-1,4-phenylene diamine

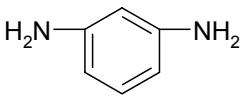

m-PDA
meta-phenylenediamine

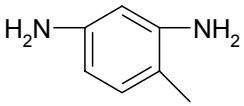

2,4-DAT
2,4-diaminotoluene

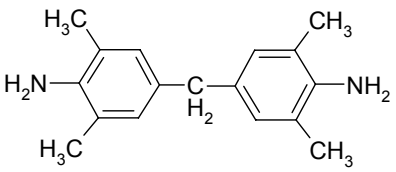

TMMDA
Tetramethylmethylenedianaline

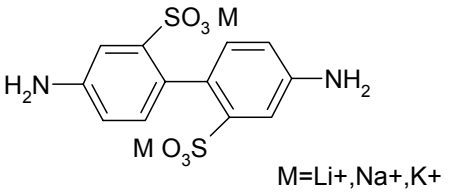

BDSA
4,4'-diamino 2,2'-biphenyl disulfonic acid

Figure 2.3. Diamines and dianhydrides used to produce polyimides in Table 2.1.

2.3.1.1 Polyfurfuryl alcohol

Polyfurfuryl alcohol (PFA) has been used extensively in the formation of supported CMS membranes. Chen and Yang [53] coated PFA onto macroporous graphite supports followed by pyrolysis at 500 ^{o}C. This process was repeated until CMS layers of 15 μm were formed. The diffusivity ratio for CH_4/C_2H_6 using this process was approximately 10.

Acharaya et al [19] have produced CMS membranes by first coating a flat stainless steel support with a solution of PFA followed by subsequent drying. CMS membranes with a selectivity of 2-3 for O_2/N_2 were produced upon subsequent pyrolysis. In another study, the same authors [18] used a spray coating technique to coat the stainless steel support. The selectivity of the spray coated membranes was considerably higher (~4 for O_2/N_2) than for the previous technique, likely due to the presence of less defects due to improved coating. Shiflett and Foley [17, 18, 20, 21] have used ultrasonic deposition to coat sintered stainless steel tubes with PFA. Selectivities of up to 30 for O_2/N_2 have been achieved by pyrolyzing the initial layer and then depositing additional PFA layers followed by additional pyrolysis. These authors have also investigated the use of additives such as TiO_2, silica zeolites, and polyethylene glycol and investigated the effects on separation performance, primarily in an attempt to increase the permeance.

Wang et al. [52] have used vapor deposition polymerization to coat furfuryl alcohol (FA) onto γ-Al_2O_3/α-Al_2O_3 and glass/α-Al_2O_3 tubes. The tubes were first impregnated with para-toluene sulfonic acid and then the inside diameter was exposed to FA vapor at 90 ^{o}C for 15 minutes, followed by heating to 200 ^{o}C to polymerize and crosslink. The tubes were then heated to carbonize the polymer precursor, and a second

polymer coating was added and subsequently carbonized. Using this technique, selectivities of 10-12 were obtained for O_2/N_2 with permeances of around $8 \cdot 10^{-10}$ (mol m^{-1} Pa^{-1} s^{-1}). All of these studies show the potential for PFA based CMS membranes, the primary limitations being that the membranes must be supported and the permeance needs to be increased to produce attractive properties. Foley and coworkers have also suggested that the formation of PFA-based CMS membranes is very sensitive to processing conditions [21]. This issue will be discussed in greater detail in subsequent sections.

2.3.1.2 Phenolic Resin

Phenolic resin has also been used to produce CMS membranes. The advantage of phenolic resin over other precursors like polyimides is low cost. Shusen et al. [16] have produced asymmetric phenol formaldehyde resin based CMS membranes. A flat film (0.05-0.10 mm) was formed by thermo-pressure molding. The membrane was subsequently heated to 850-900 ^oC in nitrogen followed by 0.5-2.0 % oxygen. One side was covered by a porous ceramic sheet during this process and therefore, the oxidation did not occur symmetrically. The resulting membrane had a reported permeability of 2300 Barrer and an O_2/N_2 selectivity of 10.65.

Fuertes and coworkers have published a series of papers using this precursor [15, 42, 54]. The authors have spin coated a small amount of a novolak type phenolic resin [54] on the surface of carbon supports. The membranes were then carbonized in a tubular furnace from 500 – 1000 ^oC in vacuum. The resulting membranes had O_2/N_2 selectivity of around 10 and CO_2/CH_4 selectivity of ~160. This work was later extended and in that case [15, 42] a novalak-type phenolic resin was deposited on the inner face of a ceramic

tubular membrane used for ultrafiltration. The membrane was subsequently pyrolyzed to 700 ^{o}C. In some cases an oxidative pretreatment was used before pyrolysis or an oxidative post-treatment after pyrolysis. The resulting membranes had O_2 permeabilities around 100 Barrer and O_2/N_2 selectivities around 12 at 25 ^{o}C. Films dip coated with resin three times had lower permeability and only slightly higher selectivities than those dipped one time. For hydrocarbon mixtures, the separation performance was improved by several treatments: air oxidation of the resin, air oxidation of the carbon, or CVD post treatment of the carbon.

Wei et al [44] have dip coated phenol-formaldehyde novolak resin containing a small amount of hexamethylene tetramine onto the surface of green tubular supports of fine phenol-formaldehyde novalak resin particles. During pyrolysis, the hexamethylamine has mobility which reduces the creation of large pores in the surface during pyrolysis. Because the selective layer and support have similar composition, there is also less stress during pyrolysis from shrinkage than from other materials. The supported membranes were pyrolyzed at 900 ^{o}C. The concentration of the solution used for the selective layer and the thickness had a considerable effect on the separation performance.

Zhou at al [45, 46] dip coated resol-type phenolic resin and a novalak-type sulfonated phenolic resin/phenolic resin mixture onto porous α-alumina tubes. The membranes were then pyrolyzed at various temperatures in a nitrogen purge. As expected, the separation performance depended on pyrolysis temperature. The sulfonated resin had much better separation performance with both high O_2 permeance (240 GPU for 500 ^{o}C CMS) and reasonably attractive selectivity (O_2/N_2 = 5.2).

2.3.1.3 Polyimides

Polyimides have become the precursor of choice for the production of CMS membranes. As mentioned previously, several factors such as thermal stability and rigidity make polyimides attractive as CMS precursors, in addition to the attractive separation performance of these materials as polymeric membranes. Of particular interest have been commercially available polyimides, which will be the focus of this review. Several non-commercial polyimides have also been used to produce CMS membranes. These are listed in Table 2.1 and the corresponding monomers used to produce these polymers can be found in Figure 2.4.

Kapton®

Kapton® is a commercially available polyimide made by Dupont. Non-commercially synthesized materials with a similar structure to Kapton® (but not the biaxial orientation present in Kapton®) are often referred to as PMDA-ODA, which denotes the monomers used to produce the polyimide (see Figure 2.4). Kapton® has been used extensively to produce CMS membranes [33, 35-37, 40, 41]. Suda and Haraya [35, 37] produced dense flat CMS membranes from Kapton® by pyrolyzing dense films between blocks of graphite at temperature between 773 and 1273 K under a 10^{-5} torr vacuum. The CMS film properties were dependent on pyrolysis temperature but had both high permeability and selectivity. He/N_2 selectivities ranged from 6-498 (P_{He} ~ 500-60 Barrer) while O_2/N_2 selectivities ranged from 3-14 (P_{O2}~ 300-1 Barrer). The authors also showed that the pore size distribution can be enlarged with treatment under the presence of water vapor at 623 K [36]. This process will be explained further in a subsequent section. In a later investigation [37], the authors performed an extensive study on the

formation of CMS membranes from commercially available Kapton® film because of the reproducibility of the precursor. The authors investigated a variety of factors such as heating rate, the pyrolysis temperature and the pyrolysis atmosphere. The results show that for membranes pyrolyzed at 1223K, permeabilities for O_2, CO_2, and He ranged from 0.92-0.15, 3.54-0.50, and 26.4-11.6 Barrer with selectivities for O_2/N_2, CO_2/N_2, and He/N_2 ranging from 21.6-36, 82.7-122, and 618-2810 respectively according to the heating rate. The authors also present activation energies for permeation, diffusion, and sorption for a variety of different gases. The results suggest that Kapton® is a very good precursor for the production of highly selective CMS membranes.

Haraya and coworkers [35, 40] have also prepared asymmetric capillary PMDA-ODA membranes by first coating a polytetrafluoroethylene (PTFE) tube with polyamic acid, then immersing the capillary in a water and/or ethanol bath, followed by drying and imidization. The PTFE capillary was removed and the asymmetric membranes pyrolyzed at 1223 K. The selectivities for these membranes approached or exceeded the dense film values when thicker selective layers were formed. In a later study, Peterson et al [40] coated the capillary membranes with a thin layer of polydimethlysiloxane, which hindered gas permeation through the defects. The selectivity for He/N_2 reached ~2800. Fuertes et al [33] have used a similar technique to produce asymmetric PMDA-ODA CMS membranes supported on a carbon disk. In that study, the authors spin coated a polyamic acid solution onto the carbon disks followed by submersion into a water coagulant bath. The films were then dried, imidized, and subsequently pyrolyzed at 550 ^oC. The resulting asymmetric membranes had an $O_2\backslash N_2$ selectivity of approximately 4 with a permeability of 45 Barrers.

Recently Hatori and coworkers [41] formed CMS membranes from Kapton® film by pyrolyzing in an argon purge from 1173-1373 K. The goal was to produce highly selective membranes to remove CO from hydrogen for fuel cell applications. The resulting membranes had selectivities from 200-5900 for H_2/CO. The study showed that CMS membranes created from Kapton® have promising results for hydrogen purification.

Matrimid 5218®

Matrimid 5218®, sometimes referred to as BTDA-DAPI, has also been used extensively to produce CMS membranes of varying formats. This polymer is available through Ciba Specialty Chemicals. Fuertes et al. [33] produced asymmetric CMS membranes from Matrimid® supported on carbon disks by a similar method to that used for their PMDA-ODA membranes. Matrimid® was dissolved in NMP or γ-butyrolactone, spin coated onto carbon disks, and then placed in a coagulant bath that was composed of water or 50/50 mixtures of water/methanol or water/propanol. The membranes were pyrolyzed at temperatures from 450 to 650 ^{o}C. The structure of the membranes was a strong function of coagulant composition, as expected. The O_2 permeability ranged from 1 to 7 Barrer while the O_2/N_2 selectivity ranged from 5.9 to 2.9.

Steel and Koros [3] produced dense freestanding CMS films from Matrimid. Dense films with thicknesses between 35 and 60 μm were cast from a 2% solution of Matrimid® in methylene chloride. The films were then pyrolyzed at 550 and 800 ^{o}C in a vacuum with a maximum pressure of 0.03 torr. The CMS membranes had an O_2 permeability ranging from ~300-10 Barrer with an O_2/N_2 selectivity of ~6-14. This study will be discussed in more detail in a later section.

Several other researchers have also produced CMS membranes from Matrimid. Vu et al [65-67] have produced asymmetric CMS fibers for CO_2/CH_4 separation. Tin et al [34, 68] have produced dense flat CMS membranes from Matrimid for a variety of separations and investigated the effect of modification of the precursor on CMS performance. These studies will be discussed in more detail later.

2.3.1.4 Relationship between polymer structure and CMS structure

Several interesting studies have recently been performed which relate the structure of the polymer precursor and the pyrolysis conditions to the final CMS properties. In most of these studies, a series of polymers are used to produce CMS membranes under the same pyrolysis conditions. These studies are important in order to develop relationships between precursor properties and CMS microstructure.

Steel [2] synthesized CMS membranes using two polyimide precursors, Matrimid and 6FDA:BPDA-DAM. The structures of these materials can be found in Table 2.2 along with important properties of the material. Both polymers were used to produce free-standing CMS membranes. As shown from the permeation data in Table 2.2, Matrimid is a more tightly packed membrane than the 6FDA based polymer.

Table 2.2 Properties of Matrimid and 6FDA:BPDA-DAM from Steel [2]. The volatile products in bold are the major products evolved. Decomposition was performed in a TGA-MS.

Polymer	P_{O2} (Barrer)	P_{O2}/P_{N2}	Possible volatile products
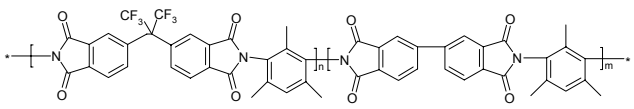 **6FDA:BPDA-DAM**	64	4.1	**CF_3-compound, CO, CO_2,** aniline, toluene, benzonitrile
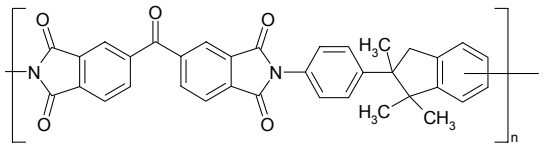 **BTDA-DAPI (Matrimid®)**	1.3	7.1	aniline, toluene, cyanotoluene, **CO_2, CO**

These polymers were carbonized using several thermal profiles. The results for two different thermal profiles can be found in Figure 2.4. The results showed that the Matrimid based membranes were more selective and less permeable than the 6FDA-based membranes produced under the same conditions. This was attributed to a difference in pore size distribution between the two molecules. It was speculated that the distribution for the Matrimid based CMS was centered at a smaller pore size and that there were generally fewer pores for diffusion.

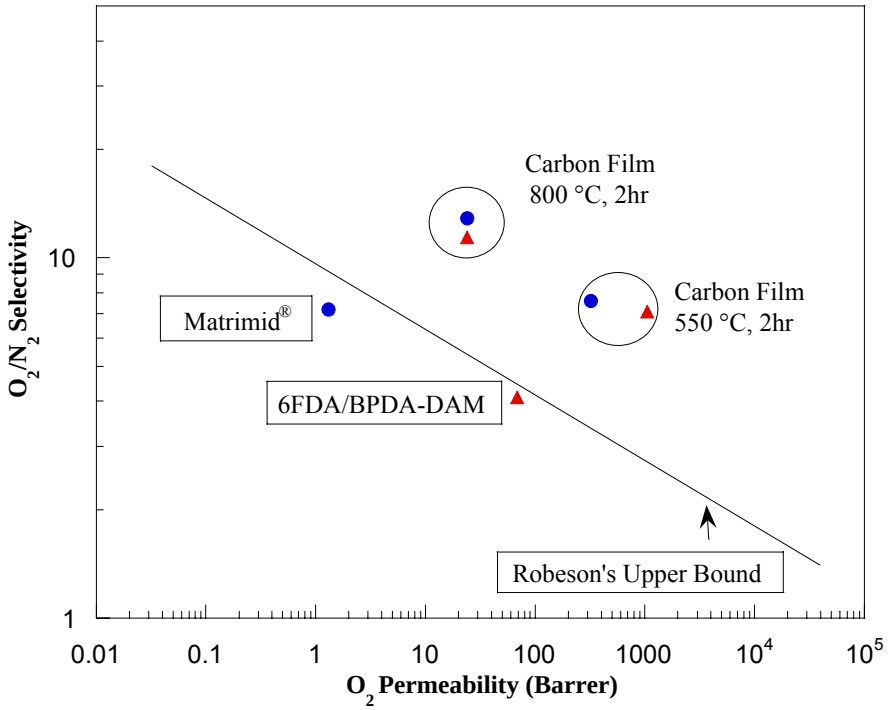

Figure 2.4 Gas separation performance of CMS membranes derived from Matrimid and 6FDA:BPDA-DAM precursors [2]

These results show that the structure of the polymer precursor plays a role in the pore size distribution of the CMS. The more packed precursor produced CMS membranes with smaller pore sizes. Unfortunately, the decomposition products of these membranes are different. It is speculated that the pore structure is also dependent on the evolved gases during decomposition. 6FDA:BPDA-DAM evolves CF_3- compounds which make up a large percentage of the products evolved. The evolution of these large molecules may also contribute to the high permeability of the CMS membranes.

Park et al. [27] have investigated the relationship between the structure of aromatic copolyimides and the resulting CMS produced from them. The three polymers are shown in Table 2.3 along with properties of the membranes. The structure of these membranes

is very similar. The only difference is the methyl substitution on one of the diamines. Increasing the amount of methyl groups increases the fractional free volume in the material because the methyl groups inhibit packing. The permeation properties of the polymer agree with the fractional free volume trends.

These three polymers were pyrolyzed at 600 and 800 ^{o}C in 150 cm^{3}/min argon to produce CMS membranes. The separation performance of the CMS membranes followed the same trends as the polymers. These results show that the structure of the CMS membrane is dependent on the composition of the polymer precursor. The authors suggest that this result was not intuitive because the decomposition process involves several mechanisms such as chain scission, stripping of side groups, and crosslinking.

This study suggests that the fractional free volume of the polymer may play a role in the CMS properties. It is possible, though, that a second factor is playing a role in the separation performance: the evolution of volatile by-products to create porosity. Analysis of the TGA spectra of each of these membranes shows that the total weight loss depends on the structure. The lowest weight loss comes from the polymer with no methyl substituant groups, PI-1 and the highest weight loss comes from PI-3. Therefore, this study shows the importance of precursor structure to separation performance, but does not definitively determine what structural factors play a role in the development of the CMS microstructure.

Table 2.3 Polymers used in study by Park et al. along with the separation performance of the polymer membranes and CMS membranes derived from these polymers [27].

Polymer	Polymer		800 °C CMS	
	P_{O2} (Barrer)	P_{O2}/P_{N2}	P_{O2} (Barrer)	P_{O2}/P_{N2}
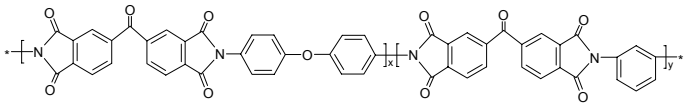 **PI-1** BTDA-(ODA:m-PDA) (9:1)	0.21	10.5	18	18
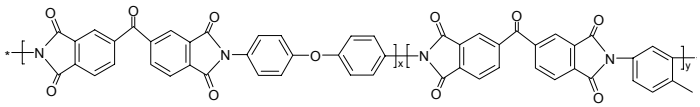 **PI-2** BTDA-(ODA:2,4-DAT) (9:1)	0.23	9.6	22	17
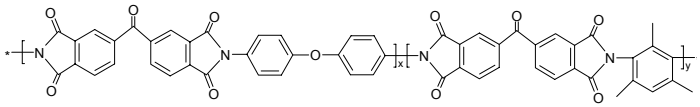 **PI-3** BTDA-(ODA:m-TMPD) (9:1)	0.38	8.3	24	16

In later studies, the same group of researchers produced CMS membranes from polyimides/polyvinylpyrollidone blends [63, 64]. The polyimide was similar to that in the previous study, BTDA-ODA. CMS membranes were produced from pure polyimide, and blends containing 5 and 10 weight % PVP (MW = 10,000) at 550 and 700 °C. TGA results show that the PVP decomposes at between 370 and 420 °C. The polyimide did not decompose until ~525 °C. Gas permeation studies showed that increasing the PVP content increases the permeability and reduces the selectivity, most likely attributed to the introduction of micropores in the CMS membranes caused by decomposition of the PVP regions in the very early stages. This, like the previous study, shows that the

microstructure of the precursor polymer has a significant effect on CMS separation performance. In a second study, PVP with different molecular weights ranging from MW = 10,000 to 55,000 were blended with polyimide. The weight fraction of PVP was constant in all films. CMS membranes produced from these blends had higher permeabilities than the pure PI. The permeability increased with increasing PVP molecular weight with a corresponding decrease in selectivity. The authors suggest this is due to an increase in the pore size due to larger PVP domains. The larger pores created increase diffusional pathways in the CMS membrane which increased permeability. There is an significant decrease in the selectivity, though, likely due to non-selective diffusion in the larger pores.

Each of the studies mentioned here suggest that the composition of the polymer precursor plays a significant role in the CMS microstructure. To date, it is difficult to elucidate the effect of individual factors such as fraction free volume or the size of decomposition products. The goal of the present study is to investigate these factors in more detail and compare the significance of the polymer composition versus other pyrolysis parameters such as pyrolysis temperature, pyrolysis atmosphere, and thermal soak time.

2.3.2 Pretreatment of polymer precursor

2.3.2.1 Oxidation

Several pretreatments have been used to condition CMS precursors before pyrolysis. The most common pretreatment is pre-oxidation. Pre-oxidation can form crosslinks in the polymer structure and therefore increase the thermal stability of the precursor. David and Ismail [14] have shown that the thermal stability of

polyacrylonitrile (PAN) hollow fiber membranes were improved when the precursors were heated to 250 ^{o}C in air or oxygen for 30 minutes. The results suggest that stabilization in an inert atmosphere can cyclize PAN, while stabilization in an oxidative environment both cyclizes and oxidizes the structure.

Kusuki and coworkers [51, 69] formed CMS membranes from asymmetric polyimide hollow fibers formed from BPDA and aromatic diamines. The authors pretreated the fibers by heating to 400 ^{o}C in atmospheric air for 30 minutes. The pretreatment was necessary to maintain the asymmetric structure of the precursors. Otherwise, the precursor softened and the carbon membranes had poor separation performance.

Centeno and Fuertes [22] analyzed the effect of oxidative pretreatment on separation performance of supported poly(vinylidene chloride-co-vinyl chloride) based CMS membranes. The films were oxidized in air at 150 or 200 ^{o}C for up to 2.5 days before carbonization. Membranes oxidized at 200 ^{o}C for 6 hours showed a decreased permeability but increase in selectivity, while those treated at 150 ^{o}C for 2.5 days had increased permeability and decreased selectivity. Therefore, the results show that oxidative pretreatment conditions must be optimized for a given precursor but may improve the CMS membrane properties.

2.3.2.2 Nonsolvent pretreatment and crosslinking

Tin et al [68] have introduced two pretreatment methods which can be used to alter the separation performance of CMS membranes. The first treatment involves crosslinking of the polymer before pyrolysis. Dense films of Matrimid 5218® were immersed in a 10% solution of *p*-xylenediamine in methanol at room temperature for 1-7

days. The films were then washed with pure methanol and dried in air at room temperature. CMS membranes were then formed by vacuum pyrolysis at 800 ^{o}C. The permeabilities of the CMS films decrease with increasing crosslinking time, which is likely attributed to a reduction in free volume and chain mobility for increased crosslink density. The selectivity of the membranes also decreased and therefore it may not generally be a good method to produce high performance CMS membranes, though different results may be obtained with different polyimide precursors.

Tin et al [34, 68] also recognized that the selectivity of one day immersed films was slightly better than those which were not pretreated. Several studies were then performed to determine the effect of nonsolvent pretreatment on separation performance. Matrimid® and polyimide P84 (from Lenzing) were soaked in solutions of methanol, ethanol, propanol, or butanol for one day and air dried. CMS membranes were subsequently pyrolyzed as before. The results show that the permeability decreased but selectivity increased for all of the CMS membranes. The largest enhancement in selectivity was attained from the ethanol soak. The effect of soak time was also tested for methanol and ethanol. The results show that the permeability decreases and selectivity increases with increasing soak time. XRD and PALS data suggests that the pretreated films have higher packing (smaller pores). The authors suggest that the function of nonsolvent treatment is "to weaken intermolecular forces and allow structural rearrangement of the carbon chains during pyrolysis." [34] These results suggest nonsolvent treatment may be a new method to produce higher performance CMS membranes.

2.3.3 Pyrolysis process

2.3.3.1 Pyrolysis temperature

The "pyrolysis temperature" is the general term used for the highest temperature that a precursor is heated to during the pyrolysis process. Several researchers have used a series of ramps and dwell times during the decomposition to form CMS membranes. Dwell times are often used at lower temperatures (<300 ^{o}C) to remove residual solvent and water. Dwell times above the glass transition temperature of the polymer are sometimes used to remove the thermal history of the polymer precursor.

The pyrolysis temperature is generally chosen to be above the decomposition point of the polymer, but below the graphitization temperature, therefore the pyrolysis temperature is strongly linked to the precursor properties. As a general rule, an increase in pyrolysis temperature (above the decomposition point) will lower the permeability of the CMS and increase the selectivity. Higher pyrolysis temperatures produce increased crystallinity, increased density, and lower average interplanar spacing in the membranes.

As an example, Shoa et al [28, 29] have produced CMS membranes from the decomposition of 6FDA-durene. This polyimide decomposed at ~496 ^{o}C under the conditions used in the study. The separation performance of membranes pyrolyzed at temperatures from 250-800 ^{o}C was evaluated. The results show that the permeability of the films generally increases from 325 to 475 ^{o}C for CO_2, O_2, N_2, and CH_4. From 475-525 ^{o}C, the permeability of the smaller gases remains fairly constant, but decreases for the larger gases. There is another increase in permeability at 550 ^{o}C and then a steady decrease to 800 ^{o}C. The authors suggest that the second increase in permeability at 550 ^{o}C may be due to the accelerated decomposition at that point because the maximum

decomposition rate occurs at 531 ^{o}C. The selectivity is also greatly affected by temperature. There is a general increase in selectivity as the pyrolysis temperature is increased, except for two local minima at 450 ^{o}C and 550 ^{o}C. Above the decomposition temperature the selectivity increases with temperature. This trend has also been observed by a variety of other researchers.

2.3.3.2 Ramp rate

CMS membranes have been produced with ramp rates up to ~13.3 ^{o}C/min. Increasing the ramp rate tends to increase the permeability and lower the selectivity of the membrane. Suda and Haraya [37] produced CMS membranes from Kapton® polyimide in an argon atmosphere. Heating rates were varied from 13.3 K/min to 1.33 K/min. The permeability of the membranes to all gases decreased with lower heating rates. The authors suggest this could be due to (1) the rate of evolution of by-products or (2) an increased pyrolysis time which allows pore sintering to occur. The first explanation agrees with the study of Hatori [26] which showed that thicker films produce different amounts of by-products due to further reaction of the by-products before they diffuse out of the membrane. Increasing the pyrolysis rate may "force out" by-products before they have a chance to re-react with the carbon membrane. As a general rule, most pyrolysis processes now reported in the literature have slow ramp rates (≤5 K/min) to increase CMS selectivity.

2.3.3.3 Thermal soak time

The "thermal soak time" is defined as the time held at the pyrolysis temperature. The thermal soak time is also used to tune the microstructure of the carbon membrane. Of course, the final properties of the material are a complex function of both the thermal

soak time and the pyrolysis temperature. Several researchers have shown that increasing the thermal soak time increases the selectivity and decreases the permeability of the CMS membrane. Steel [2] showed that increasing the soak time, when pyrolyzing at 550 ^{o}C, (~100 ^{o}C above the decomposition temperature) had a considerable effect on permeability and selectivity, which could be attributed to both pore sintering and further decomposition. At 800 ^{o}C, thermal soak time had little effect on selectivity, but permeability was decreased significantly, probably caused by sintering of the pores and narrowing of the pore size distribution. It should be noted that the thermal soak times in that study (2-8 hours) were rather long in comparison to those commonly found in the literature (≤2 hours). In a separate study, Kim et al [62] investigated shorter thermal soak times (0-60 minutes) for CMS pyrolyzed at 700 ^{o}C. The results showed that the oxygen permeability decreased by ~80% with a corresponding 66% increase in the selectivity of O_2/N_2 when the thermal soak time was increase from 0 to 60 minutes. Therefore, as mentioned previously, the effect of thermal soak time is a strong function of polymer composition and pyrolysis temperature.

2.3.3.4 Pyrolysis atmosphere

Geiszler and Koros have [50] studied the effect of pyrolysis atmosphere on the separation performance of asymmetric CMS hollow fiber membranes created from 6FDA/BPDA-DAM polyimide. The fibers were pyrolyzed under three different atmospheres including argon, helium, and vacuum (0.01-0.03 torr) with gas flow rates between 20 and 200 sccm. The results showed that inert purge pyrolysis at 200 sccm resulted in much higher permeance but lower selectivity than vacuum pyrolysis for the O_2/N_2 separation [49, 50]. A similar phenomenon was observed by Vu [67] for the

CO_2/CH_4 separation. The CMS hollow fibers in Vu's study were created from Matrimid® precursors. When Geiszler reduced the flow rate to 20 sccm [49], the permeance was reduced to below that of membranes formed in vacuum. The selectivity of these fibers remained unchanged within the error of the tests.

Geiszler gave several qualitative explanations for the above phenomena. First it was suggested that inert purge pyrolysis changes the mechanism of the carbonization reaction by increasing the gas phase heat and mass transfer over vacuum pyrolysis. Further, "by accelerating the carbonization reaction, the inert gas molecules appeared to produce a more 'open' porous matrix in the CMS membranes, resulting in a higher permeability and less selective pore structure." Geiszler also suggested that at high flow rates (200 sccm), convective mass transport might enhance decomposition, at least to the point where the inert gases enhance the transfer of large by-products of decomposition away from the carbon membrane. At low flow rates (20 sccm), by-products may have further decomposed and deposited in the pores or on the surface of the membrane, resulting in lower permeate flux.

Suda and Haraya [37] have formed flat CMS films from Kapton® polyimide by pyrolysis at 1000 ^{o}C in argon and in vacuum. The results from this study have shown that there was little difference in the permeation properties between membranes formed in argon purge and vacuum. Therefore, it is likely that the effect of pyrolysis atmosphere may be related to the properties of the precursor and the temperature profile used during pyrolysis. Considerable more detail about the studies that have investigated pyrolysis atmosphere will be described in Chapter 6.

2.3.4 Post treatment

Most post treatment processes are used to alter the pore size distribution in the CMS membrane. The most common method used to increase the pore size in CMS membranes is low temperature oxidation. Researchers have used several different techniques. Soffer et al [70] treated hollow fiber CMS membranes derived from cellulose precursors using 400 ^{o}C air for 15 minutes to increase the permeance. Kusakabe et al. [71] produced supported CMS membranes from BPDA-ODA polyimide. The membranes were then post treated with a nitrogen-oxygen mixture with varying N_2/O_2 ratios. The oxidation temperatures ranged from 100 to 300 ^{o}C and the oxidation time was up to 3 hours. The post treatment increased the permeance by an order of magnitude, but had little effect on the selectivity. The authors attributed this to an increase in pore volume without broadening the pore size distribution.

Fuertes [72] has used post oxidation to increase the pore size in CMS membranes derived from phenolic resin. The results show that oxidation at temperature from 100-450 ^{o}C can increase the pore distribution to such an extent that the diffusion mechanism changes from molecular sieving to adsorption selective. Therefore, when the correct oxidation pretreatment is used, heavier hydrocarbons such as n-butane diffuse faster than non-adsorbing materials such as hydrogen and very good selectivities are obtained. The results also show that the selectivity of adsorbables/nonadsorbables decreases with high temperatures (>450 ^{o}C) and oxidation times longer than a few hours. These results show the magnitude by which post oxidation can be used to affect the pore size distribution in CMS membranes.

2.3.5 Current separation performance

As noted earlier, polymeric membranes currently dominate the commercial market for gas separations since they are inexpensive, can be produced as asymmetric fibers (which have high surface to volume ratio), and have very good mechanical properties. The drawback to polymer membranes are that they lack good separation performance at high temperatures and are strongly affected by highly aggressive components, especially for molecules with similar sizes. The cost to produce carbon membranes is estimated to be one to two orders or magnitude higher than polymeric membranes due to the difficulty of scaling up to rapid production rates for modules, so they will presumably be used only in applications where polymer membranes have some serious difficulty. One method commonly used to compare membrane performance is to plot permeability versus selectivity, the so called "upper bound plot", to enable comparing performance of different materials. These studies are only a sample of the CMS membranes that have been produced and were chosen for the following reasons:

1. Most are formed from commercially available precursors and have shown promise for CMS formation.
2. Most of the studies detail several membranes produced under different conditions and the effect of those conditions on separation performance.
3. Permeability and selectivity data are either given or can be determined using the information in the publications, especially for the O_2 and N_2.

The precursors selected were Kapton®, Matrimid®, a phenolic resin, PVD-PVDC, PFA, polyimide P84. Two laboratory-synthesized polyimides were also chosen for comparison, BTDA-ODA and 6FDA:BPDA-DAM. Figure 2.5 compares the

performances of some of these CMS membranes to that of polymer membranes listed in the literature for O_2/N_2 separation. The polymer data and the "upper bound" were obtained from Robeson [73]. The results show that almost all of the CMS membranes discussed here have properties above the polymeric upper bound. The "best" separation performance, in comparison to the polymer upper bound were from the CMS membranes produced from PFA and the polyimides Kapton®, BTDA-ODA, and 6FDA:BPDA-DAM.

The PFA membranes presented here were presented by Foley and coworkers [17, 20, 21]. These membranes were synthesized by ultrasonically depositing a layer of PFA on a stainless steel support followed by drying and subsequent pyrolysis. This process was then repeated several times to form the resulting supported membranes. This process may result in an asymmetric membrane and authors have also shown that producing reproducible properties for this type of membrane is difficult [21]. The permeabilities listed here are based on the entire thickness of the membrane, and therefore may be overestimated. Equation 2.1 shows that the permeability is normalized by the thickness and therefore overestimation of the membrane thickness exaggerates the permeability. This is a problem sometimes encountered in the membrane literature when a thin selective layer in membranes performs the separation such as in an asymmetric membrane and therefore accurate knowledge of the selective layer thickness is necessary for accurate determination of intrinsic properties such as permeability. Nevertheless, the selectivity for the membranes mentioned here is very high and thus, these membranes are interesting. Also, the results from the PFA study show that the processing conditions have a drastic effect on the separation performance. The separation performance ranges

from P_{O2}=850 Barrer (O_2/N_2=2.1) to P_{O2}=1.9 Barrer (O_2/N_2=30.4) with fairly similar pyrolysis procedures. The remainder of the "high performance" CMS membranes from Figure 2.5 were produced from polyimides. Polyimides still appear to be the most attractive polymer for the production of CMS membranes, as mentioned by Jones and Koros in 1994 [32]. One advantage of polyimide precursors is that they can be used unsupported and several studies have shown that they can be used to produce asymmetric hollow fiber CMS membranes [50, 51, 67]. Also, each of the polyimide based CMS membranes listed shown here have a range of separation properties. Therefore, for commercial application, producing high performance CMS membranes for multiple applications may only require altering the pyrolysis process, without changing the polymer precursor. This is a major advantage of CMS membranes over other materials.

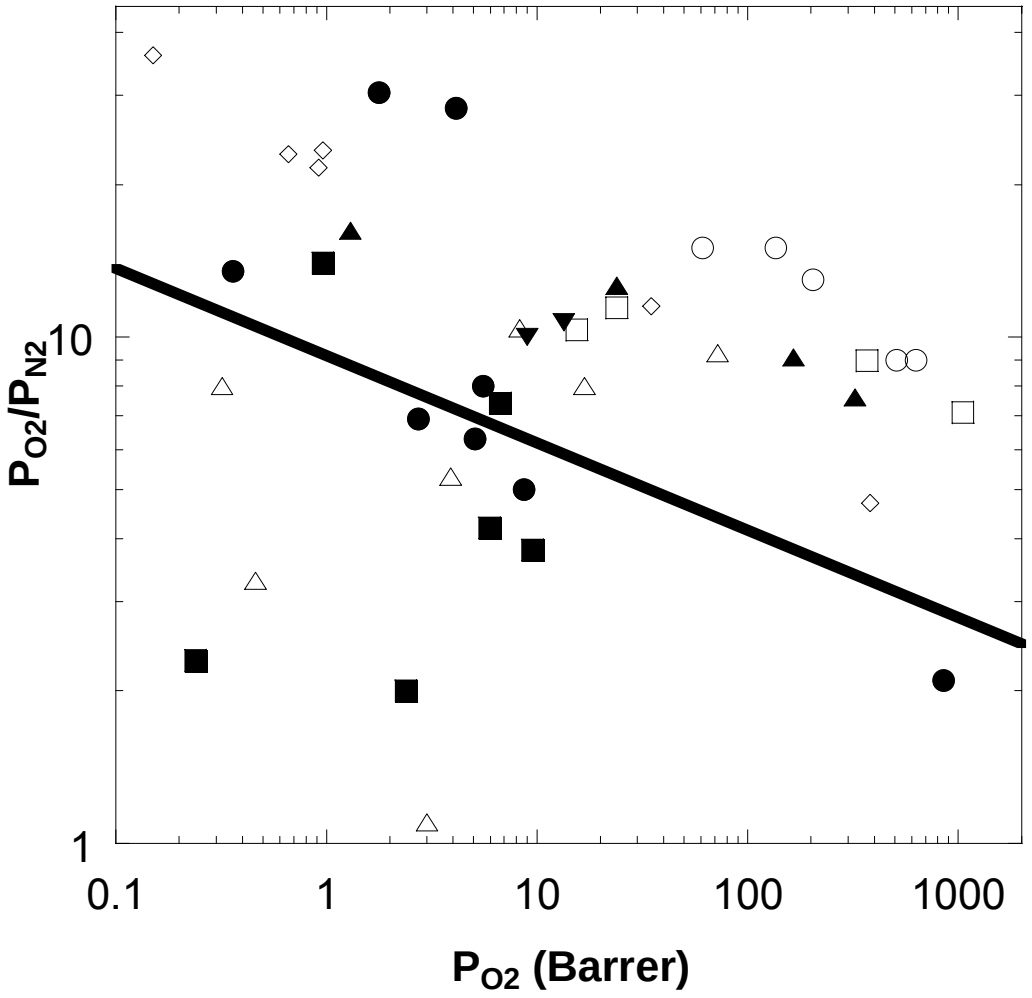

Figure 2.5. Comparison of various CMS membranes with polymeric membrane upper bound (Upper bound [73], ● are supported tubular PFA CMS [21], □ are dense flat 6FDA-BPDA-DAM CMS [2], ■ are PVDC-PDV CMS [22], ○ are dense flat BTDA-ODA CMS [62], ▲ are dense flat CMS from Matrimid [2], ◊ are dense Kapton CMS [37], ▼are flat phenolic resin based CMS supported on carbon disks [54], Δ are dense flat P84 [74]

2.3.6 Reproducibility of CMS membranes

One of the major problems that must be overcome when producing CMS membranes is to be able to easily produce membranes with reproducible separation properties. Several groups have shown that CMS membranes produced under what appear to be the same pyrolysis conditions tend to have a range of separation performance. Singh-Ghosal and Koros [43] produced membranes at three different temperatures (535. 550, and 800 ^{o}C). As expected, temperature had a major effect on separation performance. Interestingly, the O_2/N_2 selectivity of films produced at the same temperature varied by as much as 5. Similar results were obtained by Steel [2]. Foley and coworkers [75] have studied the variability in separation performance in great detail. As mentioned previously, this group has produced supported CMS membranes from PFA by a variety of different techniques including brush coating of a PFA solution onto the support, spray coating the supports, and ultrasonic deposition [17-21, 75, 76]. Though fairly similar pyrolysis techniques have been used to produce all of the membranes, the permeance and selectivity have varied considerably. Strano and Foley [75] have attributed the variations in separation performance to defect pores formed during the pyrolysis process.

Strano and Foley [75] discussed the following observations from permeance data for supported CMS membranes. 1) The flux versus pressure for weakly adsorbing species is linear for ideal selectivity ratios significantly above Knudsen values while those with selectivity ratios near Knudsen values show a non-linear dependence. The authors attribute the first effect to adsorption within the nanopores in the carbon in the Henry's law regime while the latter is attributed to viscous and Knudsen flow in large

pores. 2) The separation performance of CMS adsorbents are fairly repeatable and almost directly related to carbon synthesis conditions while the performance of CMS membranes sometimes varies when similar synthesis conditions are used. 3) Increasing the selectivity with respect to one gas pair parallels increasing selectivity for all weakly adsorbing gas pairs. 4) The activation energy for permeation for CMS membranes varies from author to author, even when similar synthesis conditions are used. The heats of adsorption for bulk carbon samples are sometimes much lower than for CMS membranes formed under similar conditions. The authors suggest that these observations are consistent with defective nanopores in the membrane which could be created during synthesis by complications such as polymer contamination, crack formation during cooling, or thermal property mismatch between carbon and support.

In support of these observations, the authors have suggested the following parallel resistance model to represent the permeability of a weakly adsorbing gas in a CMS membrane.

$$\pi_i = (1-f)\pi_{np,i} + f\pi_{d,i} \tag{2.20}$$

where π_i is the permeability of component i, $\pi_{np,i}$ is the pressure independent intrinsic permeability of the carbon membrane, $\pi_{d,i}$ is the permeability through the defects and f is the surface area fraction of defective pores (the authors originally used α). The authors suggest the following model to represent the flow through the defective pores which takes into account Knudsen diffusion and viscous flow.

$$\pi_{d,i} = \frac{\varepsilon}{\tau RT}\left(\frac{4}{3}\beta d_m\sqrt{\frac{8RT}{M_i}} + \frac{d_m^2\bar{p}}{\gamma\eta_i}\right) \tag{2.21}$$

where β and γ are 0.8 and 2.5 respectively for membranes. The combined porosity and tortuosity factor (ε/τ) is a function of membrane structure but is equal to one for a theoretical bundle of straight pores. Therefore, in this simplistic vision, the pore size, d_m, completely describes the separation performance of the defective nanopores. The authors also modeled the flux versus pressure at various pore sizes and have shown that as the pore size increases from 1-200 nm, there is a much more pronounced quadratic dependence of flux versus pressure, which is consistent with observation (1) above. The authors have assumed that the permeability in the bulk carbon is constant and independent of synthesis conditions. This may not be a very valid assumption, since several authors have shown considerable differences in performance with pyrolysis temperature, which cannot be entirely attributed to nanopores. Nonetheless, the authors suggest that any variation in bulk carbon permeability is insignificant in comparison to variations due to nanopores.

Using this model, the authors have determined the best fit volume fraction of defects, intrinsic carbon permeability, and film thickness (which is determined by the actual thickness and the area fraction of defects) for all membranes using a regression technique for pores of 1, 50, and 200 nm. The authors have shown that a single 200 nm pore in a 10 cm^2 film could have a significant effect on separation performance, but be too small to detect by adsorption or microscopic techniques. Using the model parameters, and a 50 nm pore size, the authors show that their data fits experimental data well and accurately predicts pressure dependent flux in several membranes. The model was also used to examine the variability in the data of Singh-Ghosal and Koros [43], though different intrinsic permeabilies were estimated at each pyrolysis temperature. The

model is useful and estimates intrinsic permeabilities of the carbon without any defects. This model stresses the importance of the production of defect free membranes. The presence of defects is a possible factor which leads to irreproducible membrane performance, especially supported carbon membranes which can easily develop stresses during the pyrolysis process. It is also possible that a variety of other factors also contribute to irreproducibility issues.

2.4 REFERENCES

1. Pierson, H.O., *Handbook of Carbon, Graphite, Diamond, and Fullerenes*. 1993, Park Ridge, NJ: Noyes Publication.

2. Steel, K.M., *Carbon membranes for challenging separations*, in *Department of Chemical Engineering*. 2000, University of Texas - Austin: Austin, TX.

3. Steel, K.M. and Koros, W.J., *Investigation of porosity of carbon materials and related effects on gas separation properties.* Carbon, 2003. **41**: p. 253-266.

4. Rao, M.B. and Sircar, S., *Nanoporous carbon membrane for gas separation.* Gas Separation and Purification, 1993. **7**(4): p. 279-284.

5. Rao, M.B. and Sircar, S., *Nanoporous carbon membranes for separation of gas mixtures by selective surface flow.* Journal of Membrane Science, 1993. **85**: p. 253-264.

6. Hines, A.L. and Maddox, R.N., *Mass Transfer Fundamentals and Applications*. 1985, Englewood Cliffs, New Jersey: Prentice-Hall.

7. Sakata, J. and Yamamoto, M., Apparatus for separating condensable gas, UNited States Patent 4583996, 1986.

8. Golden, C.M.A.T., Rao, M.B., and Sircar, S. *Selective surface flow carbon membranes for gas separation*. in *Fundamentals of Adsorption [6th Conference on Fundamentals of Adsorption]*. 1998.

9. Naheiri, T., Ludwig, K.A., Anand, M., Rao, M.B., and Sircar, S., *Scale-up of selective surface flow membrane for gas separation.* Separation Science and Technology, 1997. **32**(9): p. 1589-1602.

10. Sircar, S., Rao, M.B., and Thaeron, C.M.A., *Selective surface flow membrane for gas separation.* Separation Science and Technology, 1999. **34**(10): p. 2081-2093.

11. Singh, A. and Koros, W.J., *Significance of Entropic Selectivity for Advanced Gas Separation Membranes.* Industrial and Engineering Chemistry Research, 1996. **35**: p. 1231-1234.

12. Singh, A., *Membrane materials with enhanced selectivity; an entropic interpretation.* Ph. D. Dissertation, The University of Texas at Austin, 1997.

13. Koresh, J.E. and Soffer, A., *Molecular sieve permselective membrane. Part I. Presentation of a new device for gas mixture separation.* Separation Science and Technology, 1983. **18**(8): p. 723-34.

14. David, L.I.B. and Ismail, A.F., *Influence of the thermastabilization process and soak time during pyrolysis on the polyacrylonitrile carbon membranes for O_2/N_2 separation.* Journal of Membrane Science, 2003. **213**: p. 285-291.

15. Fuertes, A.B. and Menendez, I., *Separation of hydrocarbon gas mixtures using phenolic resin-based carbon membranes.* Separation and Purification Technology, 2002. **28**: p. 29-41.

16. Shusen, W., Meiyun, Z., and Zhizhong, W., *Asymmetric molecular sieve carbon membranes.* Journal of Membrane Science, 1996. **109**: p. 267-270.

17. Shiflett, M.B. and Foley, H.C., *Ultrasonic Deposition of High-Selectivity Nanoporous Carbon Membranes.* Science, 1999. **285**(5435): p. 1902-1905.

18. Acharya, M. and Foley, H.C., *Spray-coating of nanoporous carbon membranes for air separation.* Journal of Membrane Science, 1999. **161**: p. 1-5.

19. Acharya, M., Raich, B.A., Foley, H.C., Harold, M.P., and Lerou, J.J., *Metal-Supported Carbogenic Molecular Sieve Membranes: Synthesis and Applications.* Industrial and Engineering Chemistry Research, 1997. **36**: p. 2924-2930.

20. Shiflett, M.B. and Foley, H.C., *On the preparation of supported nanoporous carbon membranes.* Journal of Membrane Science, 2000. **179**: p. 275-282.

21. Shiflett, M.B. and Foley, H.C., *Reproducible production of nanoporous carbon membranes.* Carbon, 2001. **39**: p. 1421-1446.

22. Centeno, T.A. and Fuertes, A.B., *Carbon molecular sieve gas separation membranes based on poly(vinylidene chloride-co-vinyl chloride).* Carbon, 2000. **38**: p. 1067-1073.

23. Barsema, J.N., Klijnstra, S.D., van der Vegt, N.F.A., Koops, G.H., and Wessling, M., *Intermediate polymer to carbon gas separation membranes based on Matrimid PI.* Journal of Membrane Science, 2004. **328**: p. 93-102.

24. Hatori, H., Yamada, Y., and Shiraishi, M., *Preparation of macroporous carbon films from polyimide by phase inversion method.* Carbon, 1992. **30**: p. 303-304.

25. Hatori, H., Yamada, Y., Shiraishi, M., Nakata, H., and Yoshitomi, S., *Carbon molecular sieve films from polyimide.* Carbon, 1992. **30**: p. 305-306.

26. Hatori, H., Yamada, Y., Shiraishi, M., Yoshihara, M., and Kimura, T., *The mechanism of polyimide pyrolysis in the early stage.* Carbon, 1996. **34**(2): p. 201-208.

27. Park, H.B., Kim, T.K., Lee, J.M., Lee, S.Y., and Lee, Y.M., *Relationship between chemical structure of aromatic polyimides and gas permeation properties of their carbon molecular sieve membranes.* Journal of Membrane Science, 2004. **229**: p. 117-127.

28. Shao, L., Chung, T.-S., and Pramoda, K.P., *The evolution of physiochemical and transport properties of 6FDA-durene toward carbon membranes; from polymer, intermediate to carbon.* Microporous and Mesoporous Materials, 2005. **84**: p. 59-68.

29. Shao, L., Chung, T.-S., Wensley, G., Goh, S.H., and Pramoda, K.P., *Casting solvent effects on morphologies, gas transport properties of a novel 6FDA/PMDA-TMMDA copolyimide membrane and its derived carbon membranes.* Journal of Membrane Science, 2004. **244**: p. 77-87.

30. Tin, P.S., Chung, T.-S., Liu, Y., and Wang, R., *Separation of CO2/CH4 through carbon molecular sieve membranes derived from P84 polyimide.* Carbon, 2004. **42**: p. 3123-3131.

31. Jones, C.W. and Koros, W.J., *Carbon molecular sieve gas separation membranes-II. Regeneration following organic exposure.* Carbon, 1994. **32**(8): p. 1427-1432.

32. Jones, C.W. and Koros, W.J., *Carbon molecular sieve gas separation membranes-I. Preparation and characterizaton based on polyimide precursors.* Carbon, 1994. **32**(8): p. 1419-1425.

33. Fuertes, A.B., Nevskaia, D.M., and Centeno, T.A., *Carbon composite membranes from Matrimid(r) and Kapton(r) polyimides for gas separation.* Microporous and Mesoporous Materials, 1999. **33**: p. 115-125.

34. Tin, P.S., Chung, T.-S., and Hill, A.J., *Advanced Fabrication of Carbon Molecular Sieve Membranes by Nonsolvent Pretreatment of Precursor Polymers.* Industrial and Engineering Chemistry Research, 2004. **43**: p. 6476-6483.

35. Suda, H. and Haraya, K., *Molecular Sieving Effect of Carbonized Polyimide Membrane.* Journal of the Chemical Society, Chemical Communications, 1995: p. 1179-1180.

36. Suda, H. and Haraya, K., *Alkane/Alkene permselectivities of a carbon molecular sieve membrane.* Chemical Communications, 1997: p. 93-94.

37. Suda, H. and Haraya, K., *Gas Permeation through Micropores of Carbon Molecular Sieve Membranes Derived from Kapton Polyimide.* Journal of Physical Chemistry B, 1997. **101**: p. 3988-3994.

38. Wang, K., Suda, H., and Haraya, K., *The characterization of CO2 permeation in a CMSM derived from polyimide.* Separation and Purification Technology, 2003. **21**: p. 61-69.

39. Haraya, K., Suda, H., Yanagishita, H., and Matsuda, S., *Asymmetric Capillary Membrane of a Carbon Molecular Sieve.* Journal of the Chemical Society, Chemical Communications, 1995: p. 1781-1782.

40. Peterson, J., Matsuda, M., and Haraya, K., *Capillary carbon molecular sieve membranes derived from Kapton for high temperature gas separation.* Journal of Membrane Science, 1997. **131**: p. 85-94.

41. Hatori, H., Takagi, H., and Yamada, Y., *Gas separation properties of molecular sieving carbon membranes with nanopore channels.* Carbon, 2004. **42**: p. 1169-1173.

42. Centeno, T.A. and Fuertes, A.B., *Carbon molecular sieve membranes derived from a phenolic resin supported on porous ceramic tubes.* Separation and Purification Technology, 2001. **25**: p. 379-384.

43. Singh-Ghosal, A. and Koros, W.J., *Air separation of flat sheet homogeneous pyrolytic carbon membranes.* Journal of Membrane Science, 2000. **174**: p. 177-188.

44. Wei, W., Hu, H., You, L., and Chen, G., *Preparation of carbon molecular sieve membrane from phenol-formaldehyde Novolac resin.* Carbon, 2002. **40**: p. 445-467.

45. Zhou, W., Yoshino, M., Kita, H., and Okamoto, K.-i., *Carbon Molecular Sieve Membranes Derived from Phenolic Resin with a Pendant Sulfonic Acid Group.* Industrial and Engineering Chemistry Research, 2001. **40**: p. 4801-4807.

46. Zhou, W., Yoshino, M., Kita, H., and Okamoto, K.-i., *Preparation and gas permeation properties of carbon molecular sieve membranes based on sulfonated phenolic resin.* Journal of Membrane Science, 2003. **217**: p. 55-67.

47. Jones, C.W. and Koros, W.J., *Characterization of Ultramicroporous Carbon Membranes with Humidified Feeds.* Industrial and Engineering Chemistry Research, 1995. **34**: p. 158-163.

48. Jones, C.W. and Koros, W.J., *Carbon Composite Membranes: A Solution to Adverse Humidity Effects.* Industrial and Engineering Chemistry Research, 1995. **34**: p. 164-167.

49. Geiszler, V., *Polyimide Precursors for Carbon Molecular Sieve Membranes.* 1997, University of Texas, Austin: Austin.

50. Geiszler, V.C. and Koros, W.J., *Effects of Polyimide Pyrolysis Conditions on Carbon Molecular Sieve Membrane Properties.* Industrial and Engineering Chemistry Research, 1996. **35**: p. 2999-3003.

51. Okamoto, K.-i., Kawamura, S., Yoshino, M., Kita, H., Hirayama, Y., Tanihara, N., and Kusuki, Y., *Olefin/Paraffin Separation through Carbonized Membranes Derived from an Asymmetric Polyimide Hollow Fiber Membrane.* Industrial and Engineering Chemistry Research, 1999. **38**: p. 4424-4432.

52. Wang, H., Zhang, L., and Gavalas, G.R., *Preparation of supported carbon membrane from furfuryl alcohol by vapor deposition polymerization.* Journal of Membrane Science, 2000. **177**: p. 25-31.

53. Chen, Y.D. and Yang, R.T., *Preparation of Carbon Molecular Sieve Membrane and Diffusion of Binary Mixtures in the Membrane.* Industrial and Engineering Chemistry Research, 1994. **33**: p. 3146-3153.

54. Centeno, T.A. and Fuertes, A.B., *Supported carbon molecular sieve membranes based on a phenolic resin.* Journal of Membrane Science, 1999. **160**: p. 201-211.

55. Hayashi, J.-i., Mizuta, H., Yamamoto, M., Kusuki, K., Morooka, S., and Suh, S.-H., *Separation of Ethane/Ethylene and Propane/Propylene Systems with a Carbonized BPDA-pp'ODA Polyimide Membrane.* Industrial and Engineering Chemistry Research, 1996. **35**: p. 4167-4181.

56. Hayashi, J.-i., Yamamoto, M., Kusakabe, K., and Morooka, S., *Simultaneous Improvement of Permeance and Permselectivity of 3,3'-4,4'-Biphenyltetracarboxylic Dianhydride-4,4'-Oxydianiline Polyimide Membrane by Carbonization.* Industrial and Engineering Chemistry Research, 1995. **34**: p. 4364-4370.

57. Kim, Y.K., Park, H.B., and Lee, Y.M., *Carbon molecular sieve membranes derived from metal-substituted sulfonated polyimide and their gas separation properties.* Journal of Membrane Science, 2003. **226**: p. 145-158.

58. Islam, M.N., Zhou, W., Honda, T., Tanaka, K., Kita, H., and Okamoto, K.-i., *Preparation and gas separation performance of flexible pyrolytic membranes by low-temperature pyrolysis of sulfonated polyimides.* Journal of Membrane Science, 2005. **261**: p. 14-26.

59. Wang, L.-J. and Hong, F.C.-N., *Surface structure modification on the gas separation performance of carbon molecular sieve membranes.* Vacuum, 2005. **78**: p. 1-12.

60. Wang, L.-J. and Hong, F.C.-N., *Effects of surface treatments and annealing on carbon-based molecular sieve membranes for gas separation.* Applied Surface Science, 2005. **240**: p. 161-174.

61. Wang, L.-J. and Hong, F.C.-N., *Carbon-based molecular sieve membranes for gas separation by inductively-coupled-plasma chemical vapor deposition.* Microporous and Mesoporous Materials, 2005. **77**: p. 167-174.

62. Kim, Y.K., Park, H.B., and Lee, Y.M., *Preparation and characterization of carbon molecular sieve membranes derived from BTDA-ODA polyimide and their separation properties.* Journal of Membrane Science, 2005. **255**: p. 365-273.

63. Kim, T.K., Park, H.B., and Lee, Y.M., *Gas separation properties of carbon molecular sieve membranes derived from polyimide/polyvinylpyrrolidone blends: effect of the molecular weight of polyvinylpyrrolidone.* Journal of Membrane Science, 2005. **251**: p. 159-167.

64. Kim, Y.K., Park, H.B., and Lee, Y.M., *Carbon Molecular sieve membranes derived from thermally labile polymer containing blend polymers and their separation properties.* Journal of Membrane Science, 2004. **243**: p. 9-17.

65. Vu, D.Q., Koros, W.J., and Miller, S.J., *Effect of Condensable Impurities in CO2/CH4 Gas Feeds on Carbon Molecular Sieve Hollow-Fiber Membranes.* Industrial and Engineering Chemistry Research, 2003. **42**: p. 1064-1075.

66. Vu, D.Q., Koros, W.J., and Miller, S.J., *High Pressure CO2/CH4 Separation Using Carbon Molecular Sieve Hollow Fiber Membranes.* Industrial and Engineering Chemistry Research, 2002. **41**: p. 367-380.

67. Vu, D.Q., *Formation and characterization of asymmetric carbon molecular sieve and mixed matrix membranes for natural gas purification*, in *Department of Chemical Engineering*. 2001, University of Texas at Austin: Austin, TX.

68. Tin, P.S., Chung, T.-S., Kawi, S., and Guiver, M.D., *Novel approaches to fabricate carbon molecular sieve membranes based on chemical modified and solvent treated polyimides.* Microporous and Mesoporous Materials, 2004. **73**: p. 151-160.

69. Kusuki, Y., Shimazaki, H., Tanihara, N., Nakanishi, S., and Yoshinaga, T., *Gas permeation properties and characterization of asymmetric carbon membranes by pyrolyzing asymmetric polyimide hollow fiber membrane.* Journal of Membrane Science, 1997. **134**: p. 245-253.

70. Soffer, A., Koresh, J.E., and Saggy, S., Separation device, United States Patent 4685940, 1987.

71. Kusakabe, K., Yamamoto, M., and Morooka, S., *Gas permeation and micropore structure of carbon molecular sieving membranes modified by oxidation.* Journal of Membrane Science, 1998. **149**: p. 59-67.

72. Fuertes, A.B., *Effect of air oxidation on gas separation performance of adsorption-selective carbon membranes.* Carbon, 2001. **39**: p. 697-706.

73. Robeson, L.M., *Correlation of separation factor versus permeability for polymeric membranes.* J. Membr. Sci., 1991. **62**(2): p. 165-85.

74. Barsema, J., *Carbon Membranes: Precursor, preparation, and functionalization*. 2004, University of Twente: Twente.

75. Strano, M.S. and Foley, H.C., *Modeling ideal selectivity variation in nanoporous membranes.* Chemical Engineering Science, 2003. **58**: p. 2745-2758.

76. Strano, M.S. and Foley, H.C., *Temperature- and pressure-dependent transient analysis of single component permeation through nanoporous carbon membranes.* Carbon, 2002. **40**: p. 1029-1041.

CHAPTER 3

MATERIALS AND EXPERIMENTAL PROCEDURES

3.1 INTRODUCTION AND OVERVIEW

This chapter discusses the materials and procedure used to synthesize carbon molecular sieve membranes. It also describes the experimental procedures used to characterize the membranes. Section 3.2 discusses the polymers used as precursors and section 3.3 discusses the procedure used to synthesize CMS membranes. Section 3.4 and 3.5 present the equipment and procedure used for permeation and sorption experiments. Section 3.6 discusses additional material characterization techniques.

3.2 MATERIALS

3.2.1 Polymers

CMS membranes were formed via the high-temperature decomposition of polyimide precursors. Polyimides are high T_g polymers formed from the condensation reaction between dianhydrides and diamines. Four different polyimides were used in this study. The structures of these materials are shown in Table 3.1. The polyimides were formed by mixing a 1:1 ratio of diamine to diandydride in solution to form a polyamic acid followed by thermal imidization. The first two polymers are formed from the condensation reaction between three monomers: 4,4'-(hexafluoroisopropylidene) diphthalic anhydride (6FDA), 3,3'-4,4' biphenyl tetracarboxilic acid dianhydride (BPDA) and 2,4,6-trimethyl-1,3-phenylene diamine (DAM). As shown in Table 1, the ratio of 6FDA:BPDA was varied to produce copolymers with random chain structure. The third polymer was formed from 4,4'-(hexafluoroisopropylidene) dianiline (6FpDA) and 6FDA.

The fourth polymer was formed using 3,3'-(hexafluoroisopropylidene) dianiline (6FmDA) and 6FDA. 6FDA:BPDA(1:1)-DAM and 6FDA:BPDA(1:2)-DAM were previously synthesized by the Koros research group or by Dupont. 6FDA:6FpDA was synthesized by John Perry in the Koros Group. 6FDA-6FmDA was obtained from Hoescht-Celanese.

Each of the polymers in this study contains the 6FDA dianhydride. The bulky CF_3-groups on this monomer inhibit chain packing in polymer membranes, leading to high free volume. The series of 6FDA:BPDA-DAM polymers were chosen because the 6FDA:BPDA ratio could be varied, thereby affecting the physical properties of the initial polymer membranes. This will be discussed in detail in later chapters. The second set of polymers, 6FDA-6FpDA and 6FDA-6FmDA, have very similar structures, the only difference being the location of the $-C(CF_3)_2-$ linkage between aromatic rings. Because the diamines in these polymers contain packing inhibiting CF_3- groups, the small differences in structure of the two polymers lead to significantly different properties, as will be discussed in subsequent chapters.

Table 3.1 Chemical structure of polymers used to form CMS membranes

Polymer	Chemical Structure
6FDA:BPDA(m:n)-DAM	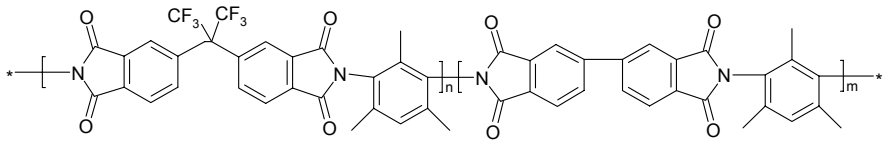
6FDA-6FpDA	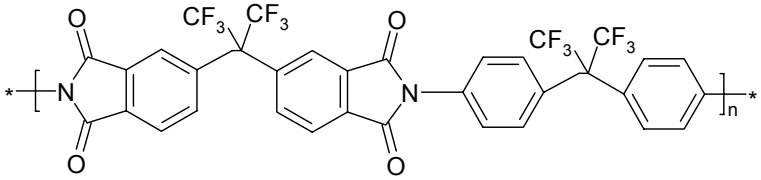
6FDA-6FmDA	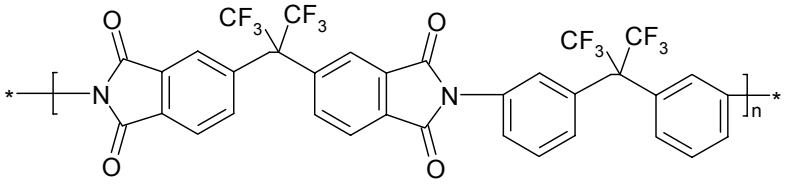

3.2.2 Gases

The gases used in this study were obtained from either Air Products or Airgas. All gases had purities greater than 99.999%.

3.3 CMS MEMBRANE FORMATION

3.3.1 Precursor membrane formation

Polymer membranes were produced by a solution casting technique. Polymer powder was dried overnight in vacuum at 115 ^{o}C to remove any adsorbed water. After drying, polymer was mixed with dichloromethane (CH_2Cl_2, 99.9% from Sigma-Aldrich) to form 2-5 wt% polymer solutions. The resulting polymer solutions were stored in 20 or 40 ml ICHEM vials (Fisher Scientific) and placed in a Burrell Model 75 Wrist Action

Shaker or a roller system designed in the Koros lab for at least one hour. The casting surface was a glass mirror with a 13 mm stainless steel ring sitting on top. The solution was then placed in a glass syringe, filtered with pressure through a Millex®-RH 0.45 μm PTFE filter (Millipore Corporation), and slowly dripped onto the glass surface inside of the steel ring. An inverted glass funnel was placed over the solution to minimize the evaporation rate of the solvent. The open end of the funnel was covered with a Kimwipe. This method also prevented any dust from landing on the polymer solution. The solution was allowed to evaporate for several hours until completely vitrified.

The resulting polymer film was removed from the surface by one of several techniques. One method was to simply take a razorblade to lift the edge of the film and ease the film off of the surface. Some films were removed by first lifting the edge with razor and then squirting a few drops of deionized water under the exposed edge. This caused the film to lift off of the plate. The polymer films were dried in air at room temperature for several hours (if they were removed with water) and then in vacuum at 115 ^{o}C to remove residual solvent and any water in the membrane. Occasionally, visible stress points were formed in the film during removal from the glass plate. Any areas that had visible stresses were not used for further CMS production.

3.3.2 Formation of CMS membranes

To produce films for pyrolysis, one inch diameter circles were cut from the large polymer films produced in the previous section. A one inch diameter steel die was used to punch out seven small films. Occasionally, the punch did not completely cut out the films. In these cases, scissors were used to cut out the areas of the film that were still attached. Each individual film was then weighed and placed on a ribbed quartz plate as

shown in Figure 3.1. The quartz plate has ¼" wide and 1/8" deep grooves which allow decomposition products to evolve from both sides of the film equally. The films were then placed inside a quartz tube as shown in Figure 3.2. The quartz tube was 50 mm ID x 54 mm OD x 115 cm long. One end of the quartz tube was sealed with glass while the other end was open and allowed the transfer of the quartz plate. Once the quartz plate was inserted, a Pyrex® glass cap, sealed against an o-ring, was placed over the open end of the furnace.

Two operating methods were used for polymer pyrolysis. The first method utilized a vacuum atmosphere during pyrolysis. For the first method, the right side of the quartz tube was connected to an Edwards Model 3 high vacuum pump. A liquid nitrogen trap was placed in line with the pump and quartz tube to prevent any pump oil from entering the quartz tube and to catch any heavy by-products evolved during decomposition. The pressure in the system was monitored by a MKS 628B Capacitance Manometer attached to a MKS PRD2000 readout. The pressure used for vacuum pyrolysis varied from 0.05 to 0.005 torr and will be discussed in more detail in subsequent chapters. The second operating mode utilized an inert purge. For those experiments, a compressed air tank was attached to the left side of the quartz tube instead of the pressure transducer. The flow was regulated with a needle valve and/or a MKS mass flow controller. Once the membranes were placed in the quartz tube and the open end was capped, the purge valve was opened and inert gas was allowed to flow through the chamber. The flow rate of gas was measured at the outlet of the quartz tube using a Hewlett Packard 0101-0113 Soap Film flowmeter and a stopwatch. Before beginning the heating cycle, inert gas equivalent to 20 quartz tube volumes was allowed to flow through

the apparatus. The flow rate was measured before and after the pyrolysis process to ensure that the flow rate had not changed during the experiment.

The furnace used to heat the quartz tube was a Thermacraft Model 23-24-1ZH three zone tubular furnace. The heating cycle was controlled by an Omega Engineering Model CN-2010 temperature controller. The pyrolysis protocols used in this study can be found in Figure 3.3. The protocols consist of slow ramps to 550 or 800 ^{o}C followed by a constant temperature soak for two hours at the ultimate temperature These protocols are similar to the ones used by several researchers [1-7]. After pyrolysis, all films were allowed to cool to below 50 ^{o}C before removal from the quartz tube.

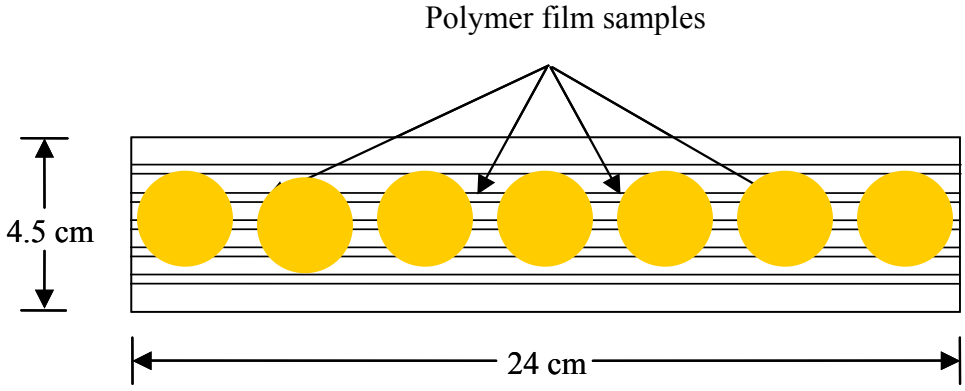

Figure 3.1 Schematic of quartz plate with polymer precursor films used during pyrolysis, adapted from Vu [1].

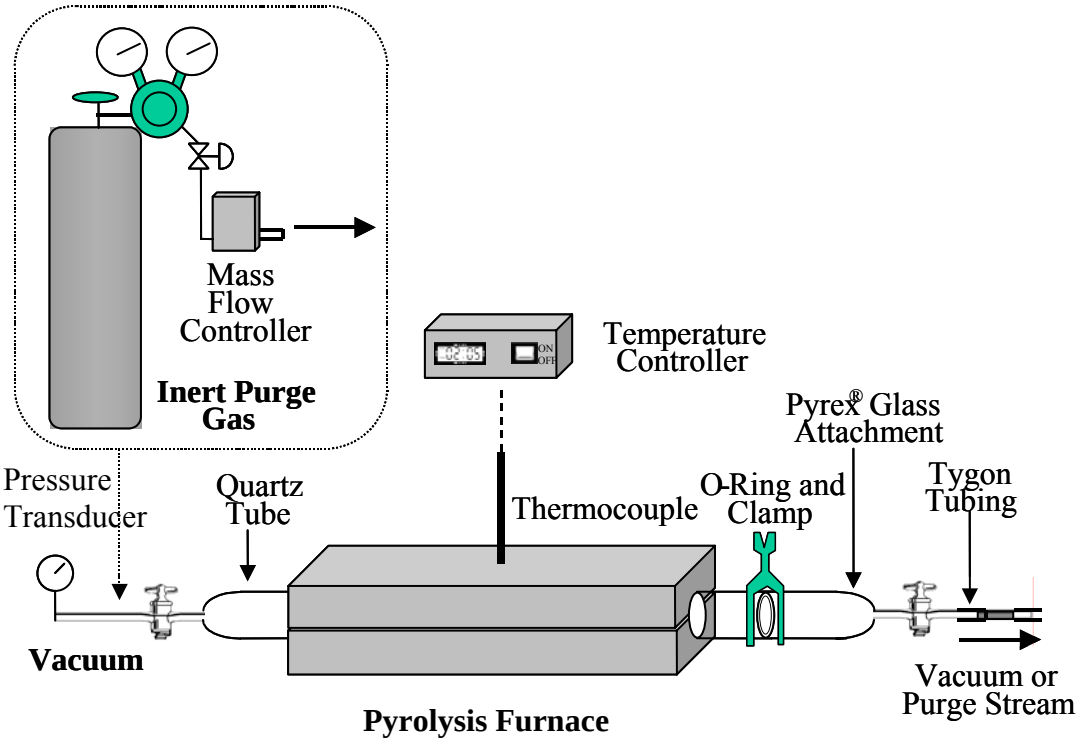

Figure 3.2 Pyrolysis furnace used to produce CMS membranes (adapted from Vu [1]). The furnace can be operated as shown in vacuum mode or with an inert purge.

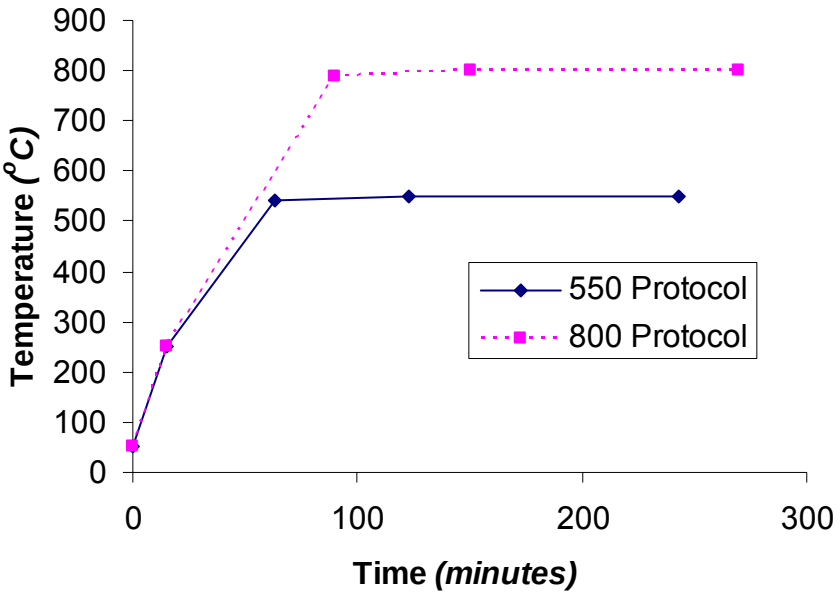

Figure 3.3 Pyrolysis protocols used to form CMS membranes

3.4 PERMEATION

3.4.1 Permeation Measurements

The permeability and selectivity of CMS membranes was measured using a standard isochoric technique (constant volume, variable pressure). Using this method, the permeability of a membranes is directly proportional to the steady state increase in the permeate pressure. The permeability of a given gas can be calculated from Equation 3.1

$$P = \frac{\left(2.94x10^{4}\right)(V)(l)(\frac{dp}{dt})}{(T)(A)(\Delta p)} \qquad (3.1)$$

P = $\frac{10^{-10}\,cm^{3}(STP)\cdot cm}{cm^{2}\cdot s\cdot cmHg}$, (Barrer)

$\frac{dp}{dt}$ = rate of pressure rise (torr/min)

V = downstream volume (cm3)

l = film thickness (mil)

T = reservoir temperature (K)

A = film area (cm^2)

Δp = pressure drop across sample (psia)

The time lag, θ_A, is the time at which the initial permeate pressure (essentially zero) intersects the line formed by extrapolating dp/dt to p=0. The time lag is related to the thickness of the membrane, and the diffusion coefficient of penetrant "A", D_A, through the membrane (cm^2/s) via the following expression:

$$\theta_A = \frac{\ell^2}{6D_A} \qquad (3.2)$$

Steady state permeation data (typically $t > 10\theta$) was used to calculate dp/dt. The time lag was sometimes used to determine the diffusion coefficient of the membrane. It is often difficult to accurately determine the diffusion coefficient for CMS membranes because the time lag is extremely short (<1 min).

3.4.2 Masking of CMS membranes into the permeation cell

To test membranes for permeation, the membranes must first be masked into a permeation cell. A schematic of a permeation cell can be found in Figure 3.4. The cell is made of stainless steel and designed to 'sandwich' a membrane between a high pressure upstream and a vacuum downstream. The cell used in this study was machined from stainless steel and has two o-ring seals as shown in Figure 3.4.

First, the CMS membranes were sandwiched in between two pieces of aluminum tape with a ½" opening which was used to define the membrane test area. The aluminum tape was obtained from Avery Dennison and had an adhesive backing. The openings in the tape were cut using a stainless steel die. A third piece of tape with a 5/8" opening and larger overall area than the mask was then used to tape the mask onto the bottom face of the permeation cell. CMS membranes are very brittle, and therefore minimal pressure is used when bonding the CMS membranes to the aluminum tape. Using minimal pressure can lead to areas which are weakly bonded to the mask and sometimes act as a leak point. To minimize leaks around the edge of the CMS film, Devcon five minute epoxy was used to bond the CMS membrane to the aluminum tape, as shown in Figure 3.4. The permeability of the epoxy was negligible in comparison to that of the membrane and therefore acted as a barrier to permeation and minimized leaks across the membrane.

Once the epoxy was dried, the top face of the permeation cell was connected using six bolts and the entire cell placed into the permeation apparatus.

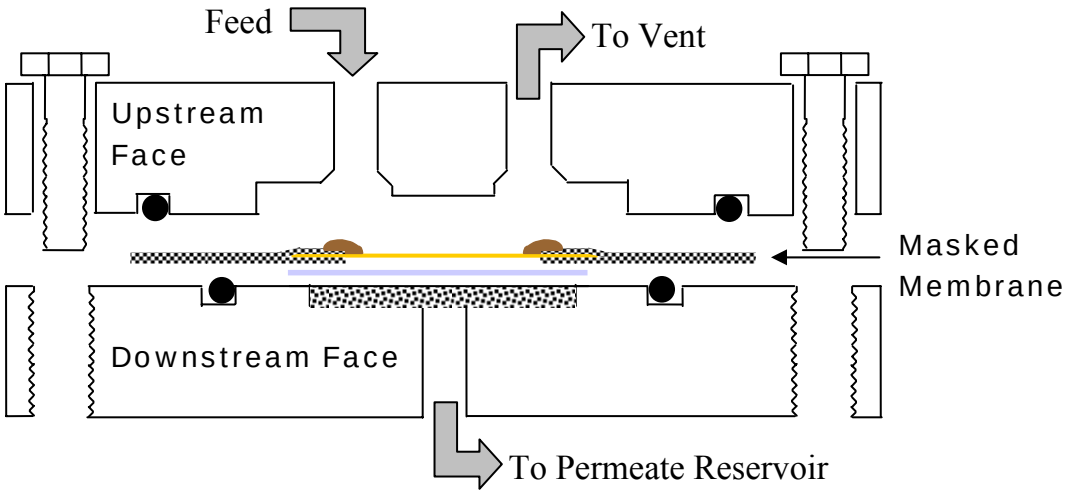

Figure 3.4 Schematic of the permeation cell. A cross section through the cell is shown with a "sandwich" type masked membrane. The membrane assembly is composed of: membrane, yellow; filter paper, light gray; epoxy, brown; adhesive backed aluminum, checkered. Bolts, shown at left and right, and o-rings, solid black circles, assure a leak tight seal. Adapted from Moore et al [8, 9].

3.4.3 Permeation system

A schematic of the permeation system can be found in Figure 3.5. The system is enclosed in a temperature regulated box. For the systems used in this study, the temperature was controlled with a Cole-Parmer Thermoworks temperature controller and a Cole Parmer air/gas RTD. The heat source was heating tape from Barnstead/Thermolyne. The metal box was insulated with Rmax R+3 insulation obtained from Home Depot. A small computer fan was used to maintain thermal uniformity throughout the box. All of the fittings in the permeation system were either stainless steel Swagelok® or Swagelok® VCR® fittings. All of the valves in the permeation system are either Swagelok SS-4H-V13 or SS-4UW-V13.

The upstream pressure was measured with a Sensotec Model Z/0713-22ZA-02 0-1000 psia transducer attached to a Sensotec model GM digital readout. The downstream transducer (#1 in Figure 3.5) was a 10 Torr Baratron® 622A or 121AA capacitance manometer supplied by MKS instruments. These transducers were connected to a PDR-5-B, also from MKS, which provides power and a digital readout of the voltage output, which was easily converted to pressure. This voltage is recorded with a Keithley KCPI-3107 data acquisition board installed in a computer running Labview® software from National Instruments. Some data were recorded with a model 1242 strip chart recorder from Soltec.

3.4.4 Permeation Experiments

After masking the CMS and placing the permeation cell in the permeation apparatus, the downstream of the permeation cell (valve C) was opened to vacuum for ~15 minutes. The downstream was then closed off and the upstream of the apparatus was opened to vacuum (valves E and G). Once the downstream and upstream pressures were fairly similar, both the downstream and upstream were opened to vacuum for ~ 24 hours to completely degas the membrane and mask. It was important to maintain the downstream pressure lower than or equal to the upstream or the mask could be pushed away from the cell, leading to leaks.

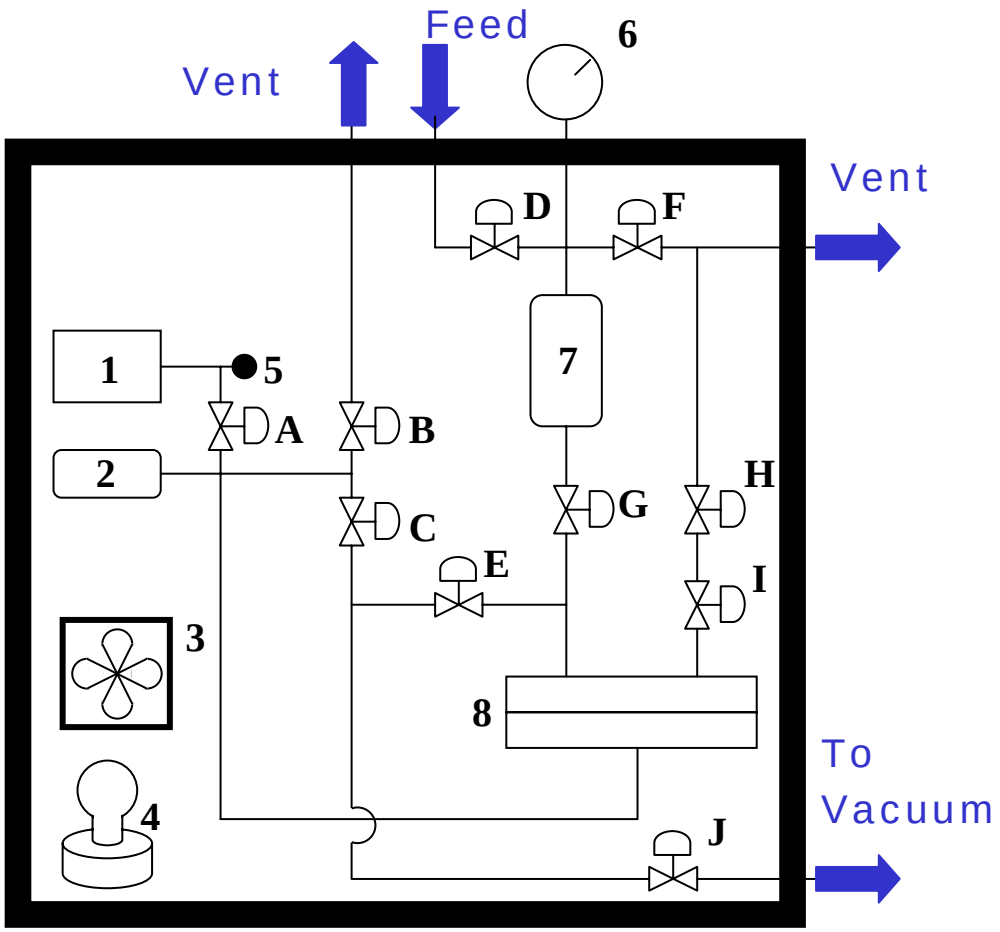

Figure 3.5 Schematic of the permeation system. (1) Downstream Pressure Transducer (2), Permeate Reservoir (3) Fan, (4) Heater, (5) Rupture Device, (6) Upstream Pressure Transducer, (7) Feed Reservoir, (8) Permeation Cell, (A) Downstream Pressure Transducer Isolation Valve, (B) GC Valve, (C) Downstream Vacuum Valve, (D) Feed Valve, (E) "Middle" Valve, (F) Vent Valve, (G) Cell Isolation Valve, (H) Retentate (Metering) Valve, (I) Retentate Shutoff Valve, and (J) Vacuum Shutoff Valve. Adapted from Moore [8, 9].

After the membranes were degassed, the leak rate of atmospheric gases into the permeate reservoir was measured by closing valves B, C, E, G, and I to isolate the cell. The leak rate was quantified for further analyses. To begin an experiment, gas was first introduced into the feed side with the cell isolation valve closed. After that, the system

was allowed to reach thermal equilibrium. After the temperature was allowed to equilibrate, the middle valve and downstream valves were closed and the cell isolation valve was opened to allow the feed gas to contact the membrane. The pressure rise in the permeate reservoir due to permeation through the membrane was initiated. After the first gas had been tested, the system was again evacuated for at least 10 time lags before testing the second gas. To make sure permeation measurements were repeatable, one of the gases was retested after all of the other gases.

After all gases were tested, the permeation cell was opened and the mask removed from the permeation cell. The permeate area of the membrane was then determed by placing the mask, epoxy side down, on a flatbed scanner. A .tif uncompressed image file of the area was then created as shown in Figure 3.6. The digital image was then analyzed using the Scion Image program from Scion Corporation. This is a downloadable image editing program. The actual permeate area was selected using the program and the area was calculated based on the number of pixels encompassed in the selected area. Often, small drops of impermeable epoxy were placed on areas of the film that looked defective. The use of the digital image program made it much easier to determine the actual permeate area of the film when it was not a simple round area.

Figure 3.6 Digital image of masked CMS film used for determining the permeate area

3.5 GAS SORPTION

Gas sorption was used to obtain the equilibrium concentration of a gas in a membrane at a given pressure. This data was used to obtain the sorption coefficient of a membrane. Gas sorption can also be used to obtain the diffusion coefficient of a membrane, if the thickness is known, by using the appropriate model. In this study, pressure decay sorption was used to obtain sorption isotherms and diffusion coefficients.

3.5.1 Pressure decay sorption system

A diagram of the pressure decay sorption apparatus can be found in Figure 3.7. The reservoirs were placed in a water bath to control the temperature. The pressure transducers were very sensitive to temperature, and therefore the temperature in the headspace above the water bath was also controlled using a Cole Parmer Thermowork temperature controller and a piece of heating tape. The main components of the system

were the feed reservoir and sample reservoir. These two reservoirs were made of stainless steel by the machine shop at Georgia Tech. Each of these reservoirs were connected to a pressure transducer from Ametek Aerospace. Each reservoir had an open end where the sample was placed, which was then sealed using a Swagelok® VCR fitting. Each transducer was connected to a Keithley Instruments 2700 Multimeter Data interfaced with a PC running Labview® data acquisition software.

3.5.2 Pressure decay sorption experiment

Sorption experiments began by placing a sample in the sample reservoir. The entire system was then opened to vacuum to degas the membrane and the reservoirs. After ~24 hours, the sample reservoir and feed reservoir were closed to vacuum and the leak rate out of each of the reservoirs was determined. Gas was then introduced into the feed reservoir and allowed to equilibrate for approximately 30 minutes. The valve between the sample and feed reservoirs was then opened for about 3 seconds and then closed. The pressure in the feed reservoir quickly reached equilibrium but the pressure in the sample reservoir decayed over time and then reached an equilibrium point. The amount of material sorbed was calculated from a mole balance.

The initial amount of gas in the system is equal to the sum of gas in the feed and sample reservoirs and the membrane.

$$n_{tot} = n_{res} + n_{sam} + n_{membrane} \tag{3.3}$$

The variables are: the total moles of gas (n_{tot}), the moles of gas in the feed reservoir (n_{res}), the moles of gas in the sample reservoir (n_{sam}), and the moles of gas in the membrane ($n_{membrane}$). Before the initial expansion, there was no gas in the sample or membrane,

therefore these values are zero. After expansion, a mole balance was used to determine the amount of moles of gas sorbed in the membrane.

$$n_{tot} = n^{i}_{res} + n^{i}_{sam} + n^{i}_{membrane} = n^{f}_{res} + n^{f}_{sam} + n^{f}_{membrane} \qquad (3.4)$$

Since each of the reservoir volumes are known and the whole system was maintained at constant temperature, this calculation was directly obtained from the pressures in each reservoir.

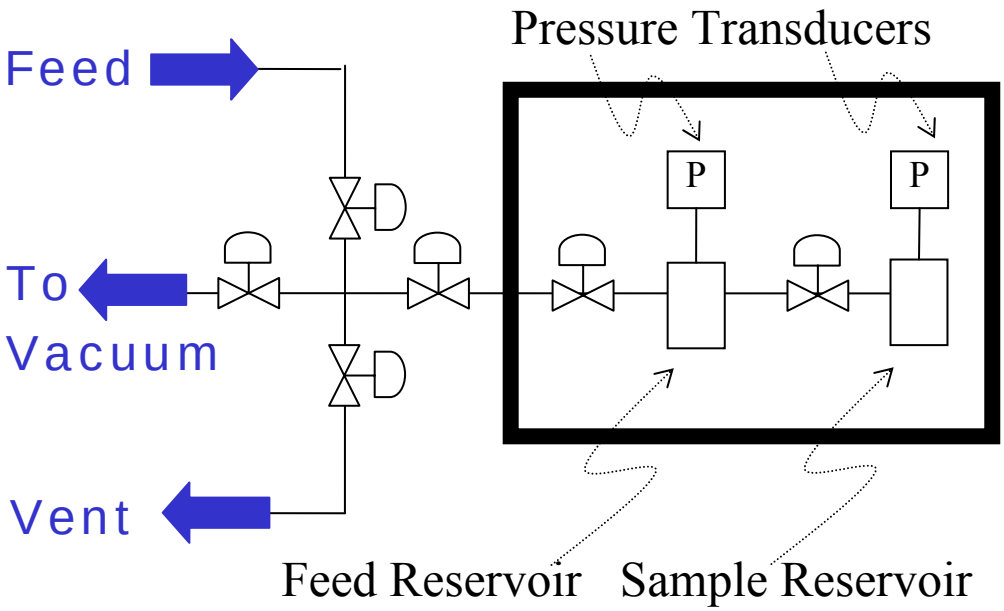

Figure 3.7 Diagram of the pressure decay sorption apparatus [9].

3.6 OTHER CHARACTERIZATION METHODS

3.6.1 TGA-IR

Thermal gravimetric analysis combined with Fourier transform infrared spectroscopy was used to characterize the decomposition process of the polymers used in this study. The next sections are used to describe the instrumentation and the experimental procedure used for analysis.

3.6.1.1 TGA-IR apparatus

Thermal gravimetric analysis (TGA) was performed using a Netzsch STA 409 PC Luxx TGA/DSC. The instrument was equipped with a silicon carbine furnace. Several operating modes were used during this study. For high temperature (>700 ^{o}C) pyrolysis, an aluminum oxide sample carrier equipped with a type S thermocouple was used. When combined DSC/TGA analysis was required, a DSC carrier equipped with type K thermocouple was used but the maximum operating temperature in inert environments was 800 ^{o}C.

To analyze the gaseous by-products evolved during decomposition, the vent from the TGA was connected to a Bruker Tensor 27 FTIR with external TGA cell. The cell had a heated transfer line that ran to a heated gas cell. The TGA cell also had an external liquid nitrogen cooled MCT detector. The flow rate of gas through the system was controlled by metering valves and the flow rate was measured using rotameters.

3.6.1.2 TGA-IR experimental procedure

All experiments used to decompose polymer precursor films were performed as follows. The inert purge gas was set to 30 ml/min through both the furnace and the balance instrumentation. Flow through the instrumentation was required to eliminate the

buildup of by-products around the balance. Purge gas was allowed to flow for a significant time to allow the balance to come to equilibrium. Once at equilibrium, the balance was zeroed and the furnace chamber was opened to allow sample to be placed in the sample holder. Polymer films with weights ranging from 10-100 mg were used in each analysis. Each film was carefully placed in the sample pan to avoid jarring the pan and sample carrier. Sudden contact with the sample carrier sometimes caused the balance to lose its zero point. Once the samples were inside, the furnace was sealed and the system was allowed to purge for approximately one hour to remove any oxygen in the furnace. The samples were then heated according to a variety of thermal profiles which will be discussed in subsequent chapters.

For experiments which required IR analysis, additional steps were performed. First, a nitrogen purge was opened which purged the area around the external detector. After about an hour, liquid nitrogen was added to the dewar to cool the detector. It was important to make sure (1) that the system was purged before liquid nitrogen was added and (2) that the dessicant in the TGA cell was new or regenerated. If not, ice formed near the detector which caused a variety of problems with the IR spectrum including major baseline shifts over a period of time. The software for the TGA and IR are integrated so data collection was similar for both TGA and TGA-IR experiments.

3.6.2 FTIR/ATR

FTIR of polymer and CMS films was performed using the Bruker Tensor 27 spectrometer mentioned above. The CMS films produced in this study were approximately 50 microns thick and therefore it was difficult to perform IR analysis in transmission mode. Thus, IR was obtained using a Harrick MVP_2 micro ATR. The ATR

has a slip wrench attachment so that constant pressure was used to press the film against a SiO_2 crystal. All experiment were performed using at least 256 scans.

3.6.3 Wide angle x-ray diffraction (WAXD)

X-ray diffraction analysis was performed using a Phillips Panalytical X-ray diffractometer in the Nair research group at Georgia Tech. All analyses were performed using either an X'pert Pro detector or a Miniprop detector with parallel plate collimator.

3.6.4 Density gradient column

The densities of polymer membranes were determined using a Techne density gradient column. The column was produced from two solutions of calcium nitrate in water, which had differing densities. The column was 70 cm long, placed in a water bath, and temperature controlled using a temperature controller/circulator. The density gradient in the column was calibrated using glass balls calibrated to ± 0.0001 g/cm^3, also from Techne. The polymer films had a tendency to float in the column due to gas bubbles attached to the surface. Therefore, films were soaked in the low density solution for several minutes before placing in the column. The density of samples were measured after at least 5 hours and again after 24 hours to determine repeatability.

3.7 REFERENCES

1. Vu, D.Q., *Formation and characterization of asymmetric carbon molecular sieve and mixed matrix membranes for natural gas purification*, in *Department of Chemical Engineering*. 2001, University of Texas at Austin: Austin, TX.

2. Steel, K.M., *Carbon membranes for challenging separations*, in *Department of Chemical Engineering*. 2000, University of Texas - Austin: Austin, TX.

3. Jones, C.W. and Koros, W.J., *Characterization of Ultramicroporous Carbon Membranes with Humidified Feeds.* Industrial and Engineering Chemistry Research, 1995. **34**: p. 158-163.

4. Jones, C.W. and Koros, W.J., *Carbon Composite Membranes: A Solution to Adverse Humidity Effects.* Industrial and Engineering Chemistry Research, 1995. **34**: p. 164-167.

5. Jones, C.W. and Koros, W.J., *Carbon molecular sieve gas separation membranes-II. Regeneration following organic exposure.* Carbon, 1994. **32**(8): p. 1427-1432.

6. Jones, C.W. and Koros, W.J., *Carbon molecular sieve gas separation membranes-I. Preparation and characterization based on polyimide precursors.* Carbon, 1994. **32**(8): p. 1419-1425.

7. Geiszler, V., *Polyimide Precursors for Carbon Molecular Sieve Membranes*. 1997, University of Texas, Austin: Austin.

8. Moore, T., Damle, S., Williams, P.J., and Koros, W., *Characterization of low permeability gas separation membranes and barrier material; design and operation considerations.* Journal of Membrane Science, 2004. **245**: p. 227-231.

9. Moore, T., *Effects of Materials, Processing, and Operating Conditions on the Morphology and Gas Transport Properties of Mixed Matrix Membranes*, in *Chemical Engineering*. 2005, The University of Texas at Austin.

CHAPTER 4

FORMATION AND CHARACTERIZATION OF CMS MEMBRANES FROM 6FDA:BPDA(1:1)-DAM AND 6FDA:BPDA(1:2)-DAM

This chapter investigates the utility of polymer precursor composition as a synthesis parameter in the development of "tunable" CMS membranes for gas separation. Section 4.1 will discuss the choice of polymer precursors as well as the properties of the polymer precursors. Section 4.2 will discuss characterization techniques used to monitor the decomposition of the polyimide precursors and propose a scheme by which the molecules decompose to form CMS membranes. Section 4.3 will discuss the separation performance of the CMS membranes produced in terms of gas permeability and selectivity for membranes formed at different temperatures.

4.1 6FDA:BPDA(1:1)-DAM and 6FDA:BPDA(1:2)-DAM precursors

4.1.1 Selection of precursors

6FDA:BPDA(1:1)-DAM has been used extensively in the Koros research group as a precursor to CMS membranes [1-13]. CMS membranes produced from this precursor have now been characterized in term of pyrolysis atmosphere, temperature, thermal soak time, and even membrane geometry. This precursor is very useful for producing CMS membranes with high permeabilities, while still having good selectivities for gas pairs such as CO_2/CH_4 and O_2/N_2. Steel [4] has shown that attractive CMS membrane performance can also be obtained for the propane/propylene separation using 6FDA:BPDA(1:1)-DAM. In the current study, a polyimide precursor in the same 'family', 6FDA:BPDA(1:2)-DAM will be compared to 6FDA:BPDA(1:1)-DAM to determine how changes in the microstructure of polymer precursors affect the separation

performance of the resulting CMS membranes. Of particular importance will be to determine whether the composition of the precursors is a particularly important factor for CMS membrane formation when compared to factors such as pyrolysis temperature and whether this factor may be used in future studies as a tool to "tune" the separation properties of CMS membranes for a particular separation.

Lee and coworkers [14] have recently performed a similar study using BTDA-ODA:aromatic diamine (9:1) copolymers with different quantities of methyl groups on the diamine, as highlighted in Chapter 2. The study has shown that the CMS separation performance is dependent on the precursor structure, even though differences in the composition were very subtle. The O_2 permeabities range from 18-24 Barrers at 800 ^oC with a corresponding decrease in the O_2/N_2 selectivity from 18-16. In the current study, the goal was to expand on this and other studies and begin to derive the relationships between the separation performance and the composition of the polymer precursor.

4.1.2 Precursor structures

The general structure of the polyimides used in this study was given in Table 3.1. The exact structure of each polymer is therefore given in Table 4.1. The polymers are formed from 6FDA and BPDA dianhydrides, along with the DAM diamine. Structurally, the only difference between the polyimide monomers comes from the ratio of 6FDA to BPDA dianhydrides. Of particular importance to the properties of these two monomers is the $-C(CF_3)_2-$ moiety in 6FDA. This bulky pendant group is known to inhibit the packing of polyimide chains while maintaining rigidity in the polymer backbone.

Table 4.1 6FDA:BPDA(1:1)-DAM and 6FDA:BPDA(1:2)-DAM polymer repeat units

Polymer Name and Structure
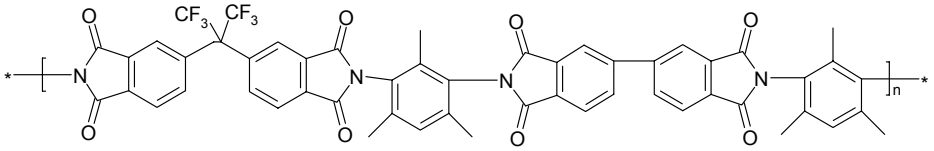 **6FDA:BPDA(1:1)-DAM**
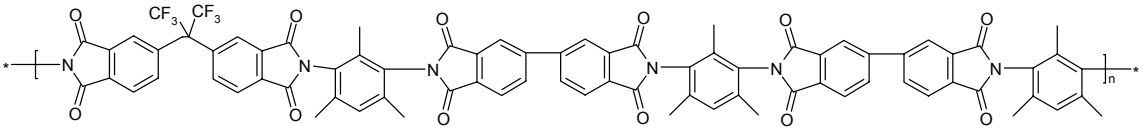 **6FDA:BPDA(1:2)-DAM**

4.1.3 Wide angle x-ray diffraction of polymers

Wide angle x-ray diffraction was used to compare the structure of the two polyimides, Figure 4.1. The two polyimides are amorphous and therefore the x-ray pattern only shows the expected amorphous peak. The peak location is related to the average distance between polymer chains and therefore, gives an idea of the level of polymer chain packing. The average d-spacing in 6FDA:BPDA(1:1)-DAM is approximately 6.0 Å while the d-spacing for 6FDA:BPDA(1:2)-DAM is only 5.9 Å. These results suggest that that the presence of the 6FDA monomer inhibits the packing between polymer chains, most likely due to the bulky $–CF_3$ groups.

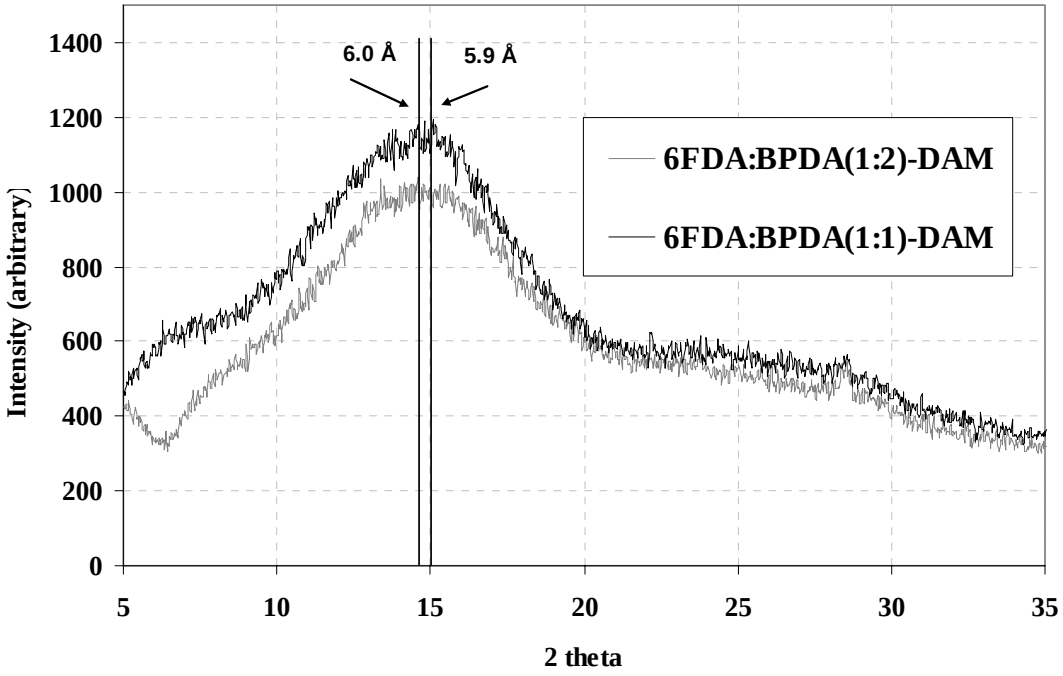

Figure 4.1 WAXD pattern of 6FDA:BPDA(1:1)-DAM and 6FDA:BPDA(1:2)-DAM precursor polymers

4.1.4 Precursor densities and FFV

The fractional free volume of glassy polymer membranes is the amount of volume in the membrane which is not occupied by polymer chains. There have been extensive studies relating the fractional free volume of glassy polymers to the permeation properties. In the current study, the fraction free volume of the polymer precursors was estimated using group contribution theory. This method, first presented by Bondi [15] and further developed by van Krevlen [16], and Park and Paul [17] utilizes the experimental specific volume of a polymer and compares it to the van der Waals volume to determine the unrelaxed free volume using Equations 4.1 and 4.2.

$$FFV = \frac{(V - V_o)}{V} \qquad (4.1)$$

$$V_o = 1.3\sum_{k=1}^{K}(V_w)_k \qquad (4.2)$$

where V is the specific volume of the polymer, V_o is the volume occupied by polymer chains, V_w is the van der Waals volume of a "group" comprising the monomer, and K is the total number of "groups" in a monomer. Park and Paul [17] have refined previous studies to include larger "groups" which can be used to more accurately determine the Van der Walls volume, especially for polyimides. The density of the polymer precursors was determined using a density gradient column. Table 4.2 lists the densities and fractional free volumes of the polymer precursors. The free volume of 6FDA:BPDA(1:1)-DAM is higher than that of 6FDA:BPDA(1:2)-DAM. It should be noted that there is considerable error associated with the numerical calculation of free volume due to the need for estimation of the Van der Waals volume. However, if a consistent method is used, the calculated free volume of 6FDA:BPDA(1:1)-DAM is always higher than that of 6FDA:BPDA(1:2)-DAM. This result was expected in relation to the polymer structure and to the WAXD patterns. These results agree with WAXD results which show that the average d-spacing in 6FDA:BPDA(1:1)-DAM is larger than 6FDA:BPDA(1:2)-DAM. The (1:1) ratio polymer has a higher concentration of $-CF_3$ groups which inhibit polymer packing. This leads to higher free volume content and a larger average d-spacing in the polymer precursor.

Table 4.2 Density and fractional free volume of polymer precursors. Densities were determined using a density gradient column and free volumes were calculated using [16, 17].

Polymer	Density (g/cm^3)	FFV	WAXD d-spacing
6FDA:BPDA(1:1)-DAM	1.300 ± 0.001	0.145	6.0 Å
6FDA:BPDA(1:2)-DAM	1.281 ± 0.001	0.140	5.9 Å

4.2 CHARACTERIZATION OF CMS MEMBRANES AND THE TRANSITION FROM POLYMER TO CMS

4.2.1 TGA-IR of membrane during pyrolysis

TGA analyses were performed to monitor the weight loss of polymer films as they are heated during the pyrolysis process. In each experiment, a polymer film sample with a thickness of ~2 mil and a mass of ~10 mg was placed in an alumina sample cup inside the TGA. Nitrogen was purged through the TGA furnace at 30 ml/min. The thermal profiles used were similar to the 550 ^{o}C and 800 ^{o}C profiles used in subsequent experiments to form CMS membranes. Therefore, this test was designed to simulate the conditions used during pyrolysis and determine the temperatures at which thermal decomposition occurs, as well as the weight loss throughout pyrolysis. Figures 4.2 and 4.3 contain the TGA curves for 6FDA:BPDA(1:1)-DAM and 6FDA:BPDA(1:2)-DAM. For further discussion, the thermal profiles will be named by the final pyrolysis temperature (ie. 550 and 800).

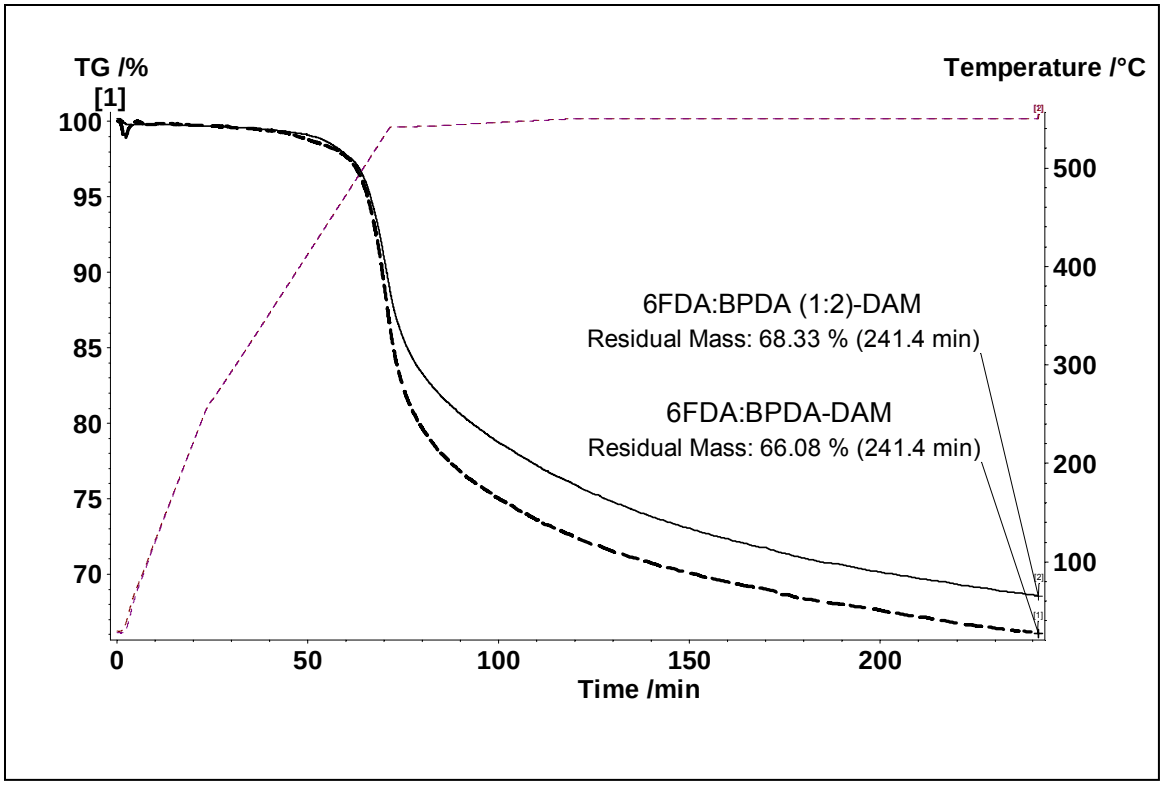

Figure 4.2 TGA profiles for pyrolysis using the 550 °C thermal profile.

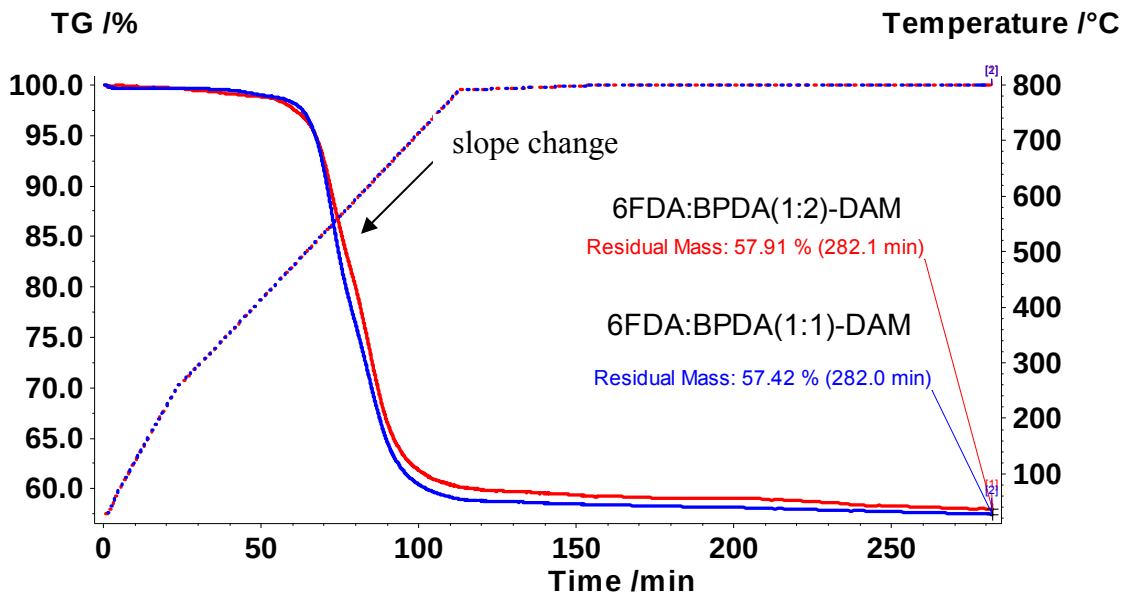

Figure 4.3 TGA profiles for pyrolysis using the 800 °C thermal profile.

The thermal profiles for the two precursors are fairly similar. Thermal decomposition of these polymers can be divided into four stages. Below ~450 ^{o}C, there is a very small weight loss that may be attributed to desorption of residual solvent and water, or possibly further imidization (or crosslinking) of the polyimide, which would result in water formation. The second (~450-525 ^{o}C) and third (~525-650 ^{o}C) stages of decomposition involve rapid weight loss. The second stage mainly involves the degradation of pendant groups from the polymer backbone. This will be detailed further below using FTIR analysis. The third stage likely involves cleavage of the polymer backbone and the formation of the residual carbon structure. The fourth stage involves the removal of non-elementary carbon components [18, 19]. There is very little weight loss during the fourth stage. It is speculated that in the fourth stage of decomposition, the molecular structure changes more significantly by rearrangement of the char than by further decomposition and removal of atoms.

Figures 4.2 and 4.3 show that throughout the 550 ^{o}C pyrolysis process, there is significant weight loss. Even after the two hour thermal soak at 550 ^{o}C, mass is removed at a rate of approximately -0.04%/min. Also, during the major weight loss peak between 500 and 550 ^{o}C, there is not the change in slope that occurs using the 800 ^{o}C profile. Therefore, the 550 ^{o}C material is still likely in the "third stage" of decomposition at the end of the pyrolysis process. The rate of weight loss at the end of the 800 ^{o}C protocol is nearly an order of magnitude slower because the material is almost fully decomposed into carbon.

To further elucidate the decomposition reaction occurring during pyrolysis, the decomposition products were analyzed using FTIR. In these experiments, samples were

heated to 800 ^{o}C at 10 ^{o}C/min to maximize the concentration of decomposition products transferred to the IR cell. The infrared spectra of the decomposition products for both of the polymer precursors are very similar. The overall spectra for 6FDA:BPDA(1:1)-DAM along with the TGA spectrum can be found in Figure 4.4. Figure 4.5 contains TGA and IR traces for several key compounds evolved during pyrolysis.

The first by-product evolved is CO_2 (broad peak at 2360 cm^{-1}) and possibly some water. Both of these materials are difficult to accurately detect using the system in this study because the laser used for analysis travels through air before the gas cell, and therefore local changes in atmospheric CO_2 and water can cause problems. Nevertheless, these peaks also appear before the major decomposition peak in several other polyimides, such as Matrimid. This peak may be attributed to cleavage of unreacted acid groups (CO_2 evolved) or possibly from a crosslinking reaction (water evolved). Currently, the exact nature of this reaction is unknown. During the onset of decomposition, the initial by-products are CF_3H (1150, 1178 cm^{-1}) and HF (multiplet 4250-4500 cm^{-1}) and CH_4 (3017 cm^{-1}). The by-products evolve from the cleavage of the C-C bonds in the -$C(CF_3)_2$- moiety and cleavage of the –CH_3 groups from DAM. The fluorinated molecules evolve over a short time period during the first stage of decomposition. The other major by-products to evolve are CO_2, and CO (broad doublet at 2110 and 2190 cm^{-1}), which likely come from the cleavage of the imide bonds. These molecules exhibit two major peaks, one during stage two and one during stage three of decomposition. These peaks may arise from the cleavage of the two types of imides (from 6FDA and BPDA), but further investigation was beyond the scope of this study. In the later stages of decomposition, small amounts of an unidentified by-product evolves

which has IR peaks associated with an aromatic ring and an -N=C=O group. This is also likely from the cleavage of the imide bonds. Since this is a larger by-product, it is likely that the majority of this product further decomposes before it diffuses out of the CMS membrane and evolves as CO or CO_2, with the aromatic remaining to form the carbon structure.

The decompositional analysis of these polyimides was not performed to determine the exact mechanism by which the polymers decompose, as this was not directly relevant to the study. The goal was to identify by-products that evolve, which may attribute to the formation of the porous microstructure of the resulting CMS membrane. The results show that the major light decomposition by-products are CF_3H, HF, CO_2, CO, and CH_4. In the next section, a discussion of the CMS formation factors will stress the importance of these light by-products in terms of the microstructure of the CMS membrane.

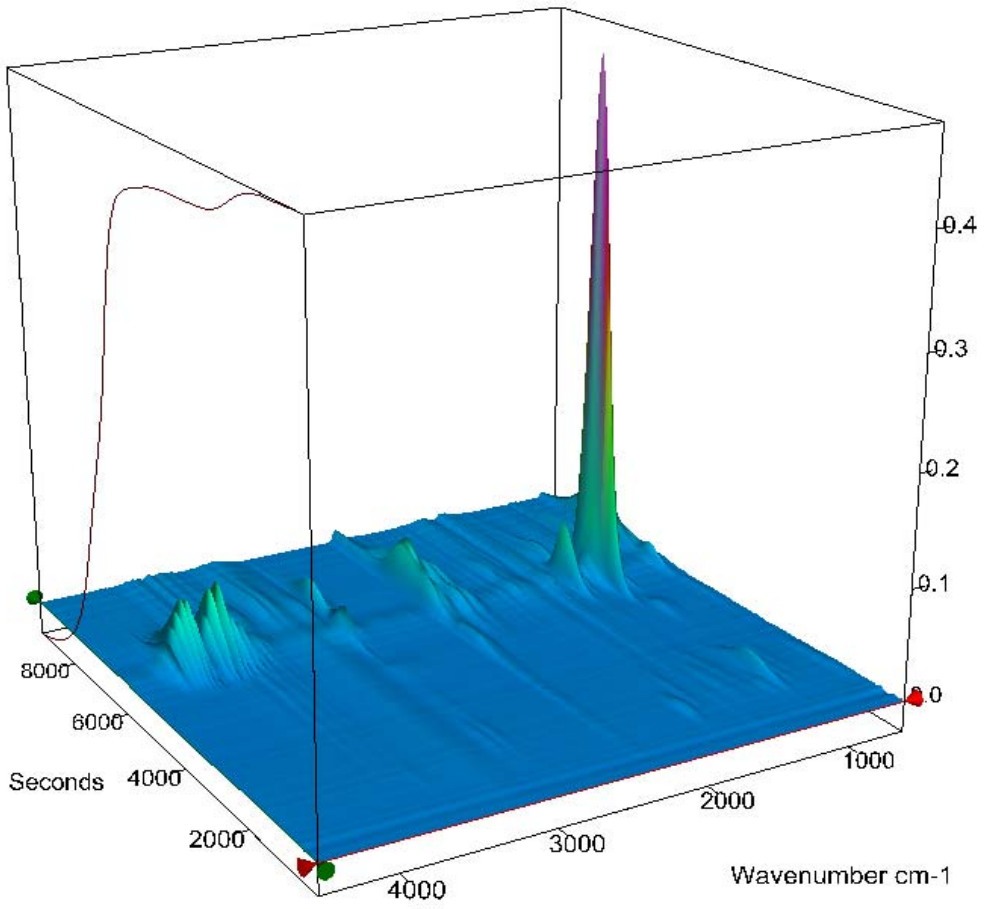

Figure 4.4 FTIR spectra of decomposition products evolved during pyrolysis along with the general shape of the TGA spectrum (on left side).

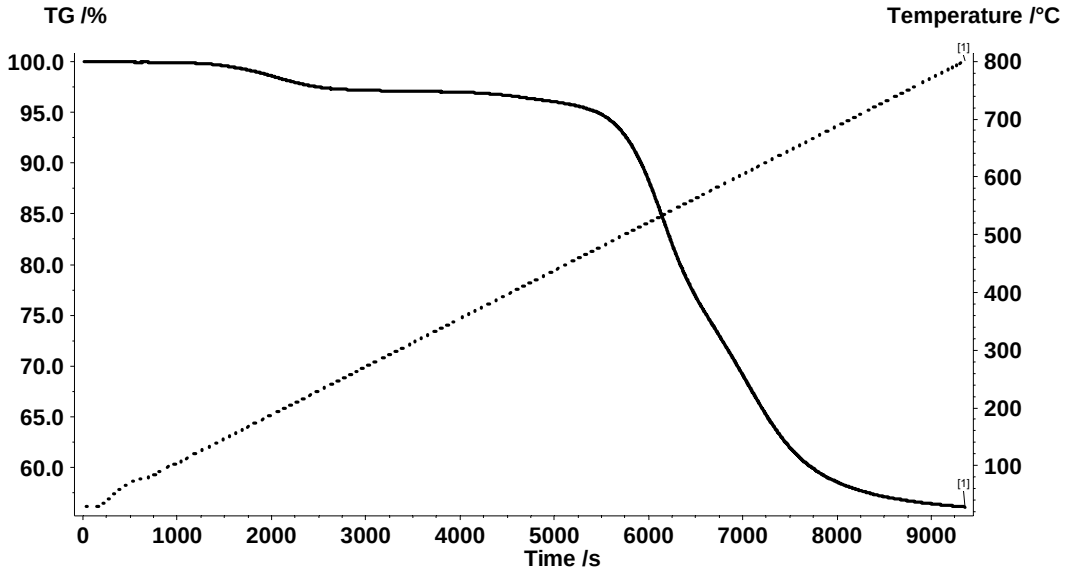

(a)

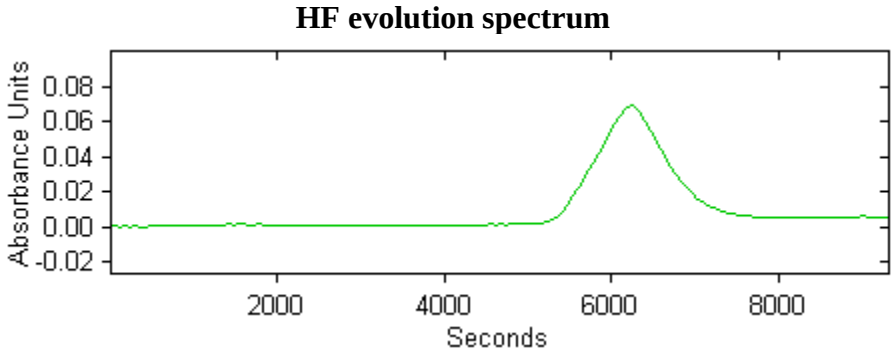

(b)

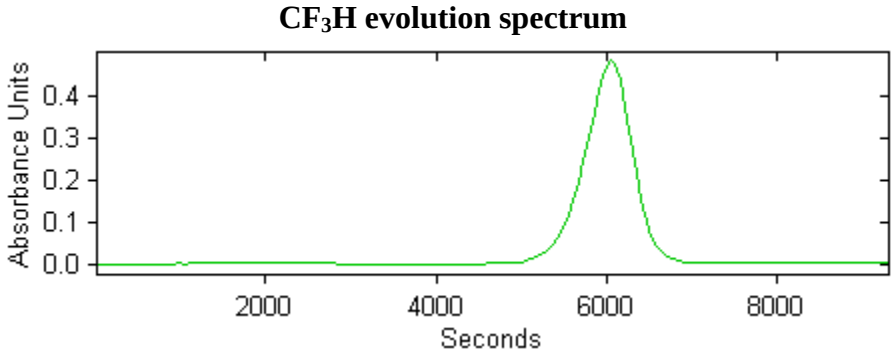

(c)

Figure 4.5 Intensity of by-products evolved during decomposition of 6FDA:BPDA(1:1)-DAM at 10 ^{o}C min to 800 ^{o}C. (a) TGA (b) HF (c) CF_3H (d) CO (e) CO_2 (f) CH_4

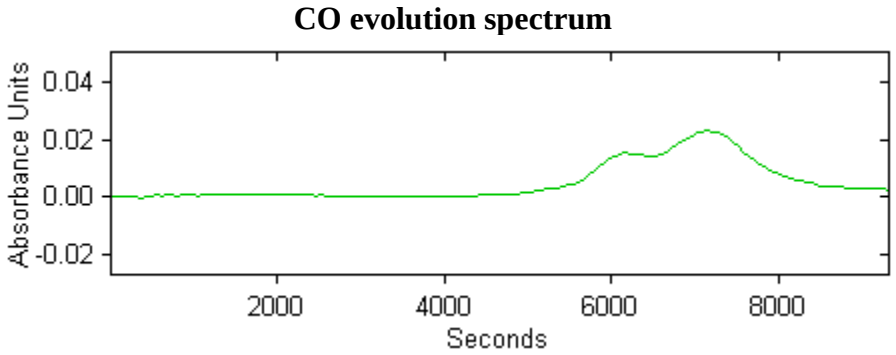

(d)

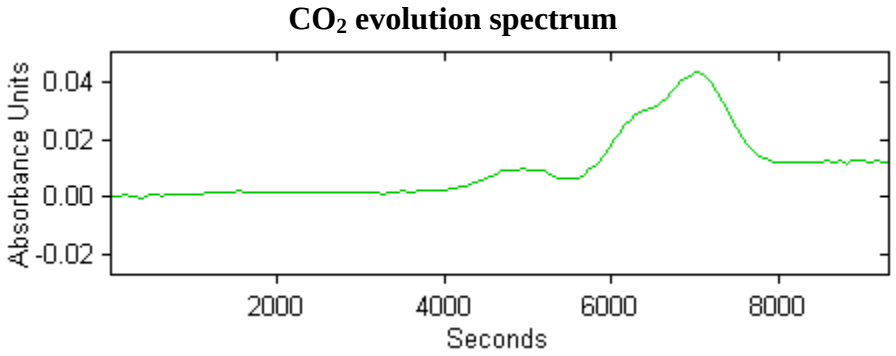

(e)

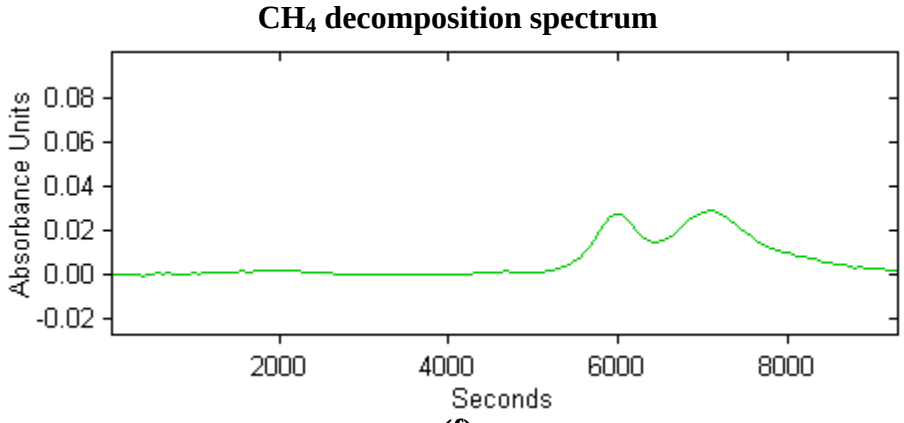

(f)

Figure 4.5 Intensity of by-products evolved during decomposition of 6FDA:BPDA(1:1)-DAM at 10 ^{o}C min to 800 ^{o}C. (a) TGA (b) HF (c) CF_3H (d) CO (e) CO_2 (f) CH_4 (continued)

4.2.2 IR spectroscopy of polymers and CMS membranes

ATR spectroscopy was used to characterize the CMS membranes formed using the 550 ^{o}C and 800 ^{o}C pyrolysis protocol. The goal was to characterize the transformation of polymer to membranes and determine whether any identifiable functional groups remain in the CMS membranes. Figure 4.6 contains the IR spectra of polymer and carbon membrane for both precursors. The results show that as the polymer is pyrolyzed, the strength of the IR peaks decrease considerably, because the material has decomposed and comprises almost entirely carbon. The only peaks that are even discernable are in the "fingerprint" region and a peak at ~600 cm^{-1} which is likely attributed to adsorbed CO_2. The strength of the fingerprint peaks is much lower than in the polymer at 550 ^{o}C. At 800 ^{o}C, there are no discernable peaks, most likely due to the nearly complete carbonization of the membranes at this temperature.

.

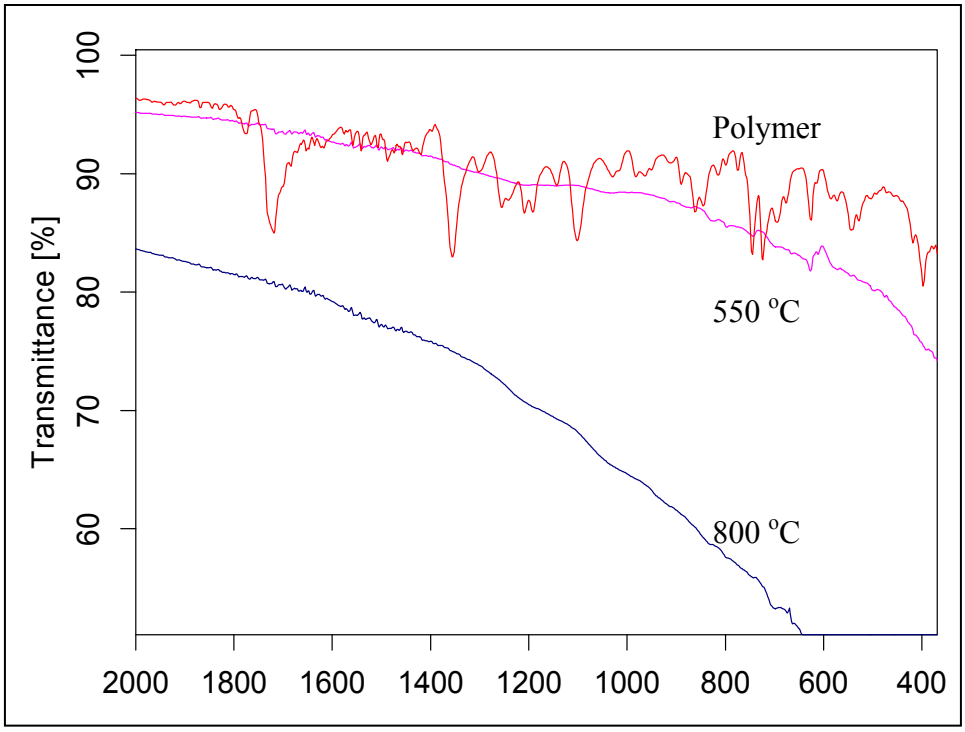

(a)

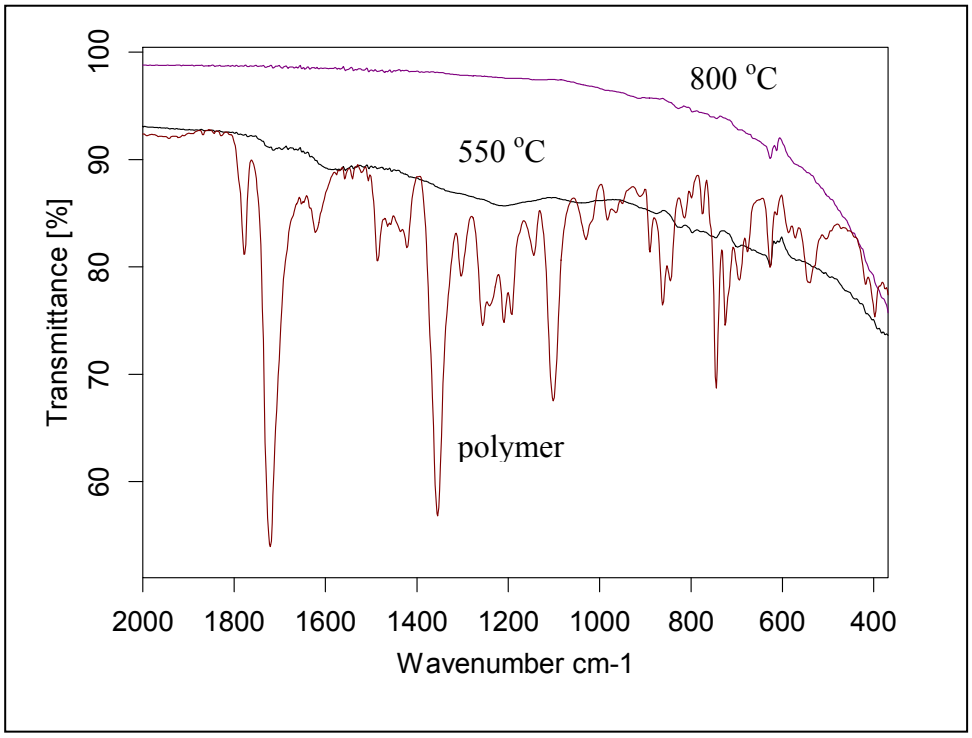

(b)

Figure 4.6 FTIR spectra of polymer and CMS membranes from (a) 6FDA:BPDA(1:1)-DAM and (b) 6FDA:BPDA(1:2)-DAM

4.2.3 WAXD of CMS membranes

WAXD was used to investigate the average interplanar distance between carbon planes in the CMS membranes as well as investigate the degree of graphitization. Figures 4.7 and 4.8 contains the WAXD patterns for membranes produced at 550 ^{o}C and 800 ^{o}C respectively. The 550 ^{o}C patterns are characterized by a large amorphous region with little or no order. There is also a very weak amorphous peak at ~42 degrees (2 theta) which is similar to the (100) peak in graphitic carbon. More importantly, there is little difference between the patterns for the two membranes at 550 ^{o}C. It has been previously discussed that the porosity in carbon membranes comes from defects in the packing of carbon planes in the amorphous carbon regions. Therefore, the interplanar spacing can be used to qualitatively compare the size of the pores in the CMS membranes. The 550 ^{o}C membranes are characterized by a large amorphous hump between 10 and 30 degrees (2 theta), therefore it is likely that these membranes have little order and a large distribution of pores. Conversely, the membranes produced at 800 ^{o}C are characterized be a much narrower amorphous peak. The 6FDA:BPDA(1:2)-DAM based CMS has a peak centered at 25.1 degrees (2 theta) which corresponds to a distance of ~3.54 Å, while the peak from the 6FDA:BPDA(1:1)-DAM based membrane has a peak centered at 24.2 degrees (2 theta) which corresponds to a distance of ~3.67 Å. The peak near 42 degrees (2 theta) which reflects the (100) graphite peak at around 43.5 degrees (2 theta) is much stronger in these membranes than in the 550 ^{o}C material. This peak represents the distance between carbon atoms in the same plane. Therefore increases in the intensity of this peak suggest that at 800 ^{o}C, the material is more ordered and similar to graphite.

The WAXD results suggest several important characteristics of these carbon membranes. First, there appears to be little difference between the pore structures of the membranes produced at 550 ^{o}C from different precursors. It is difficult to discern trends from the 550 ^{o}C membranes because the WAXD peak is broad, which is attributed to a broad pore size distribution and a highly disordered structure. Second, membranes produced at 800 ^{o}C have much more order, as expected, and the average pore size has shifted to a much smaller size than the 550 ^{o}C membranes. Finally, membranes produced at 800 ^{o}C with (1:2) have a smaller average d-spacing spacing than (1:1) membranes, which suggests a smaller average pore size. In the following sections, these material properties will be discussed in terms of gas permeation and sorption.

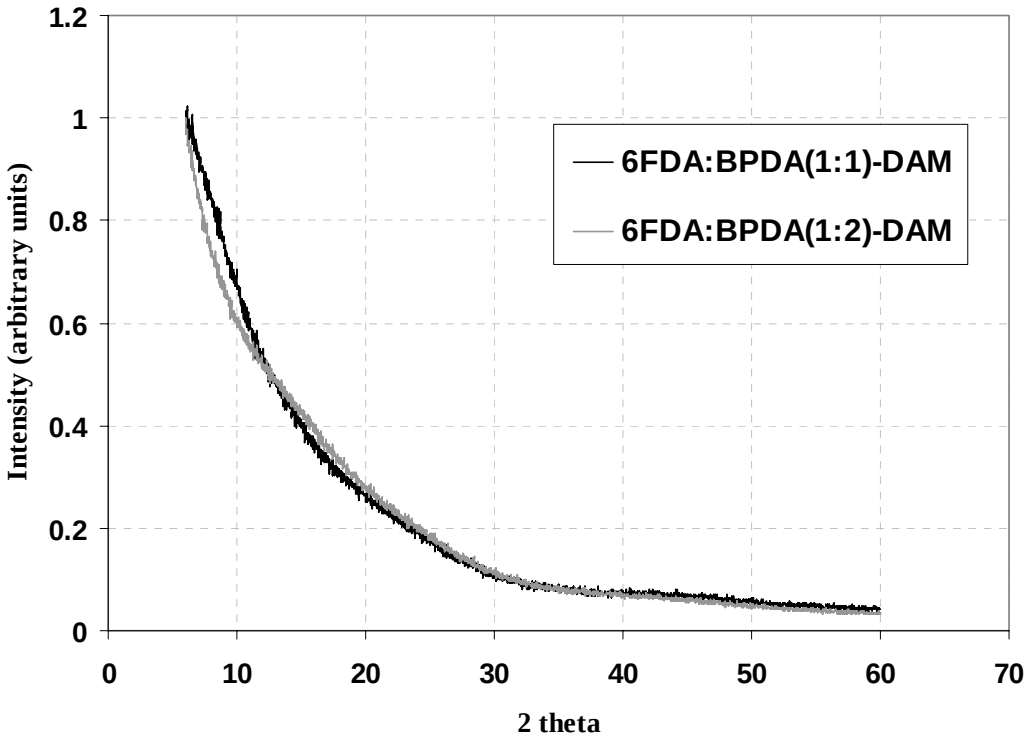

Figure 4.7 WAXD pattern of CMS membranes produced from 6FDA:BPDA(1:1)-DAM and 6FDA:BPDA(1:2)-DAM at 550 ^{o}C

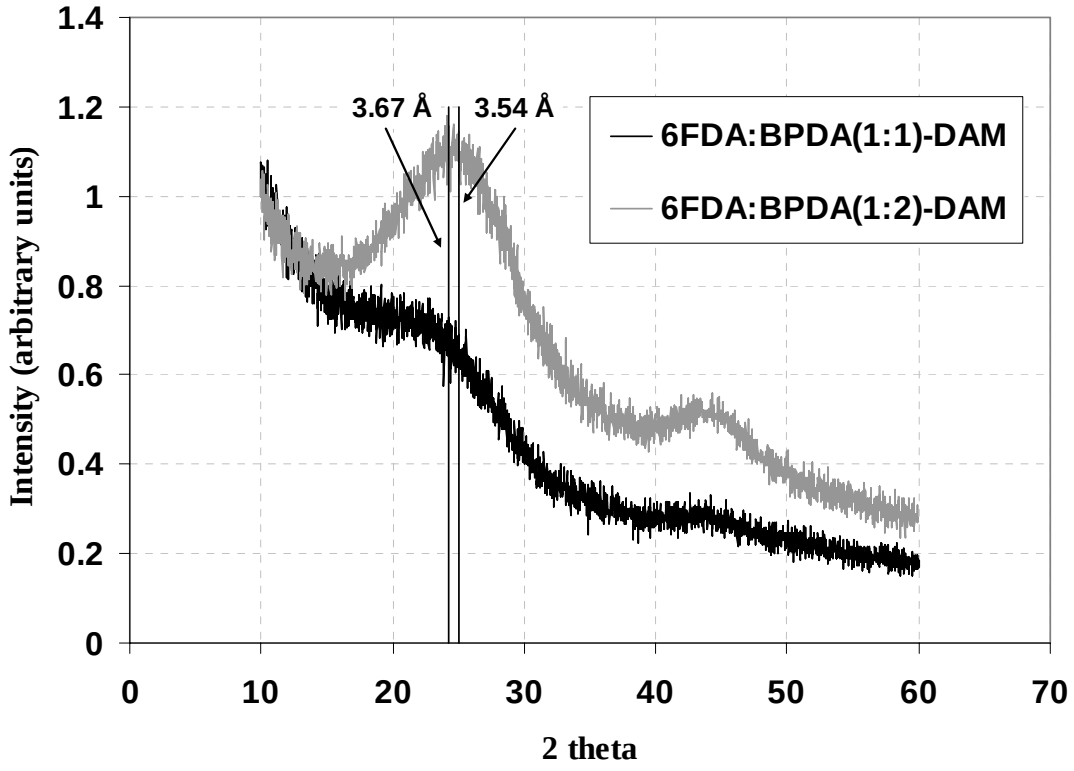

Figure 4.8 WAXD pattern of CMS membranes produced from 6FDA:BPDA(1:1)-DAM and 6FDA:BPDA(1:2)-DAM at 800 ^{o}C

4.3 TRANSPORT PROPERTIES OF CMS MEMBRANES DERIVED FROM 6FDA:BPDA(1:1)-DAM AND 6FDA:BPDA(1:2)-DAM

4.3.1 Influence of oxygen and effect on the current study

After the current study was almost completed, a significant parameter, the pyrolysis pressure during vacuum pyrolysis, was determined to have a significant impact on CMS membrane separation performance. Appendix A discusses the importance of this parameter, the impact it has on separation performance, and the proposed model describing the effect of pyrolysis pressure. More detail is also given in Chapter 6 when analyzing pyrolysis in different environments. A second parameter, the polymer precursor thickness was also determined to affect the separation performance and this is also discussed in relation to the pyrolysis pressure in Appendix A. This discovery is very

important in relation to repeatable membrane formation and gives insight into difficulties obtained by previous researchers. Appendix A also shows that when the synthesis conditions are strictly controlled, CMS membranes with repeatable separation performances can be obtained.

Without considering the effect of thickness or vacuum pressure, many membranes for the current study were synthesized and therefore, comparison of these membranes is not possible, without a great deal of uncertainty. The ultimate goal of the study in this chapter was *to analyze the relationship between polymer precursor composition and CMS separation performance* so control of all other pyrolysis parameters is important. Therefore, in this section, only membranes produced under identical pyrolysis conditions will be discussed and the effects of precursor thickness and pyrolysis pressure do not have an impact on the data presented.

For one set of films, the permeability, sorption coefficients, and diffusion coefficients were determined to analyze the effect of polymer precursor composition on all of these transport parameters. For two other sets of films, only the permeability was determined. These films are used to prove that different synthesis conditions can be used to obtain the same trends in permeability obtained from the first set of films and that the results are not anomalous. All of the films discussed here have a thickness of approximately 2 mils.

One of the conditions presented in this chapter is a different pyrolysis temperature, 675 ^{o}C, which was not previously discussed. The ramp rate and thermal soak time for the 675 ^{o}C pyrolysis temperature is the same as the other two pyrolysis protocols. Currently, membranes are being synthesized in <0.005 torr vacuum using the

800 ^{o}C protocol. Fortunately, the issues faced in this chapter were not a problem with the results obtained in Chapter 5. In that study, the measurements were taken over a fairly short time range and there was little change in the pyrolsis protocols throughout the experiments.

4.3.2 Permeation properties of CMS membranes

The permeabilities of CMS membranes were obtained using the isochoric method described in Chapter 3. Table 4.3 lists the separation performance of CMS membranes produced using the 550 ^{o}C pyrolysis protocol at 0.005 torr. This set of films was synthesized after the importance of oxygen concentration was identified. In subsequent discussions, 6FDA:BPDA(1:1)-DAM will be referred to as 1:1 and 6FDA:BPDA(1:2) will be referred to as 1:2. The results show that for both the O_2/N_2 and CO_2/CH_4 separations the permeability for the 1:1 membranes is higher but accompanied by a decrease in membrane selectivity. For example, the permeability of oxygen increases from 436 to 633 Barrers when the 1:1 precursor in used instead of the 1:2 precursor, while the O_2/N_2 selectivity decreases from 9.6 to 8.8.

Table 4.4 lists the separation performance of two more sets of films produced under different synthesis conditions which were produced before the importance of pressure was discovered. Since both the pressure and the temperature are different in these systems, no comparisons between the ACTUAL permeability and selectivity data can be made between sets. The data are presented to analyze *internal* trends in the data sets. The second synthesis condition investigated utilized the 800 ^{o}C pyrolysis. The two membranes for comparison were synthesized in ~0.030 torr of air. The permeability of these membranes is approximately an order of magnitude lower than those synthesized at

550 ^{o}C, 0.005 torr. This result was entirely expected due to two factors. First, the membranes are synthesized at a higher temperature, and second, the membranes are synthesized under a higher oxygen concentration. More importantly, the trend in separation performance is the same as the series at 550 ^{o}C. The O_2 permeability of the 1:1 membranes is 17.9 Barrers while the permeability of the 1:2 membranes is only 7.6 Barrers. The O_2/N_2 selectivity of the 1:1 membrane is 9.8 while the selectivity for the 1:2 membrane is 10.8. Similar results were also obtained for the CO_2/CH_4 separation.

The third series of membranes were produced using the 675 ^{o}C profile as described above. The pyrolysis atmosphere was ~0.041 torr of air. This atmosphere had the highest concentration of oxygen of any of the membranes tested. These membranes had excellent separation performance, especially for the CO_2/CH_4 separation. The trends in separation performance were again similar to the other studies. The O_2 permeability for the 1:1 membrane was 16 Barrers with an O_2/N_2 selectivity of 11.7 while the O_2 permeability for the 1:2 series was 6 Barrers with an O_2N_2 selectivity of 13.8. The CO_2 permeability for the 1:1 membranes was 62 Barrers with a CO_2/CH_4 selectivity of 152 while the permeability for the 1:2 membranes was 21 Barrers with a selectivity of 202. Though the actual separation performance of this series of membranes is much different than the other two series, the same trends are observed. For *all conditions*, the permeability of the 1:1 membranes is higher than the 1:2 membranes, with a lower selectivity.

Table 4.3 Permeability of CMS membranes synthesized from 6FDA:BPDA(1:1)-DAM and 6FDA-BPDA(1:2)-DAM at 550 ^{o}C in 0.005 torr. The film thicknesses are approximately 2 mil.

Polymer	Environment	P_{N2}	P_{O2}	P_{CH4}	P_{CO2}	O_2/N_2	CO_2/CH_4
1:1	550 ^{o}C (<0.005 torr air)	72	633	36	2579	8.8	71
1:2	550 ^{o}C (<0.005 torr air)	46	436	22	1653	9.6	76

Table 4.4 Permeability of CMS membranes synthesized from 6FDA:BPDA(1:1)-DAM and 6FDA-BPDA(1:2)-DAM under different pyrolysis conditions. The film thicknesses are approximately 2 mil. The data is not intended to compare the synthesis conditions but to compare the trends under each condition.

Polymer	Environment	P_{N2}	P_{O2}	P_{CH4}	P_{CO2}	O_2/N_2	CO_2/CH_4
1:1	800 ^{o}C (0.030±0.003 torr air)	1.8	17.9	0.8	58.9	9.8	71
1:2	800 ^{o}C (0.030±0.003 torr air)	0.7	7.6	0.2	21.4	10.8	87
1:1	675 ^{o}C (0.041±0.003 torr air)	1.36	16	0.41	62	11.7	152
1:2	675 ^{o}C (0.041±0.003 torr air)	0.42	6	0.10	21	13.8	202

4.3.3 Equilibrium sorption analysis in CMS membranes

Permeation in CMS membranes is affected by both the gas sorption capacity and the diffusion coefficient. While diffusion is controlled by the size of the ultramicropores, the sorption capacity is controlled by the larger micropores which are connected by the ultramicropores. The adsorption capacity of ultramicropores is small in comparison to the large adsorptive pores. To determine the effect of precursor composition on the large adsorptive pores, sorption isotherms were obtained. The sorption isotherms presented are for both 1:1 and 1:2 produced under 0.03 torr of air at 550 ^{o}C. The conditions are not identical to the conditions for the permeation data obtained in the previous section. The

results in Appendix A, though, have shown that the sorption isotherm is not as strongly affected by pyrolysis pressure as permeation. The sorption isotherms for the 1:1 membranes can be found in Figure 4.9 while the isotherms for the 1:2 membranes can be found in Figure 4.10. The sorption coefficients were obtained by fitting each of the isotherms using a Langmuir isotherm. The sorption coefficients can be found in Table 4.4.

The isotherms for both sets of membranes are very similar. The sorption coefficients show that the 1:1 film has a slightly higher sorption coefficient than the 1:2 film for methane and CO_2, but is lower for nitrogen. Therefore, there is likely very little difference in the sorption isotherms of the two membranes. This result was unexpected because it was assumed that the pore volume in 1:1 based membranes would be higher than 1:2 based membranes due to the higher weight loss during decomposition. There is no difference in the sorption selectivity for the 6FDA:BPDA(1:1)-DAM and the 6FDA:BPDA(1:2)-DAM CMS membranes. The sorption affinity for all CMS membranes is similar and therefore, from membrane to membrane, there is very little difference in the sorption selectivity. The results suggest that the high selectivities in these CMS membranes are due to diffusion selectivity and not sorption selectivity: this was, in fact, expected.

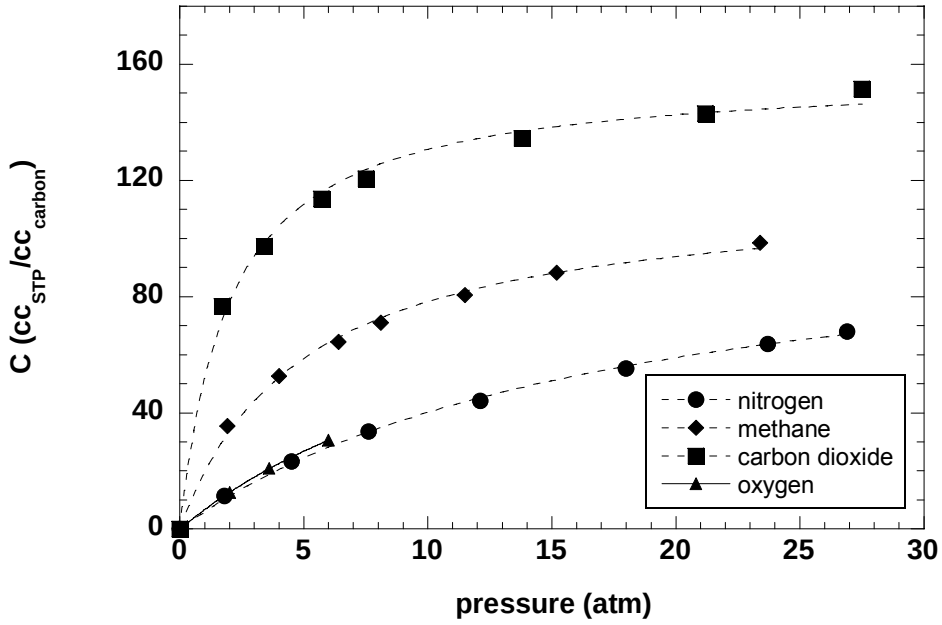

Figure 4.9 Sorption isotherms for CMS membranes from 6FDA:BPDA(1:1)-DAM at 550 ^{o}C

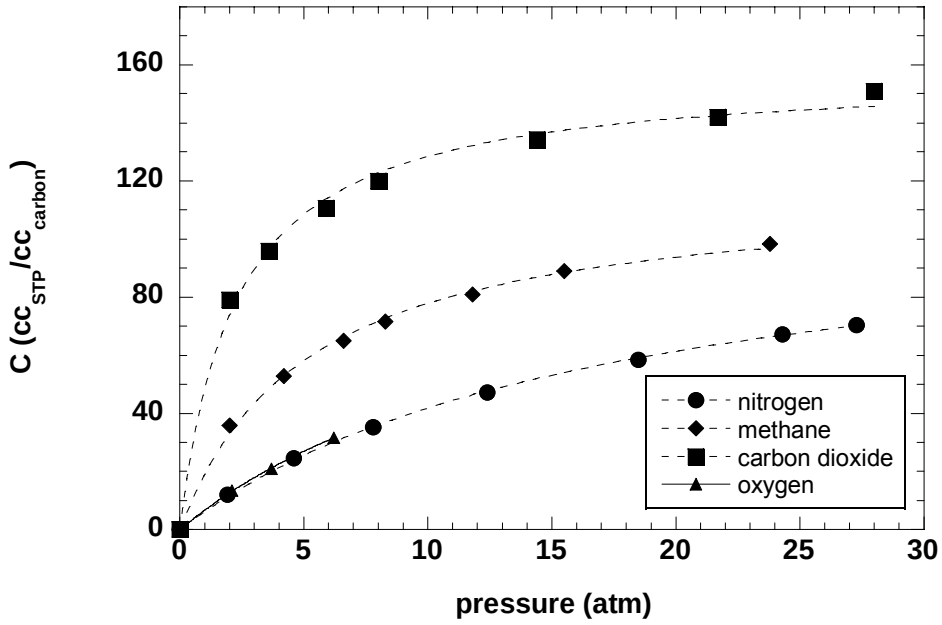

Figure 4.10 Sorption isotherms for CMS membranes from 6FDA:BPDA(1:2)-DAM at 550 ^{o}C

Table 4.5 Sorption coefficients of CMS membranes derived from 6FDA:BPDA(1:1)-DAM and 6FDA:BPDA(1:2)-DAM using 550 ^{o}C pyrolysis protocol

Precursor	S_{N2}	S_{o2}	S_{CH4}	S_{CO2}	S_{O2}/S_{N2}	S_{CO2}/S_{CH4}
	(cc_{STP}/cc_{carbon}-atm)					
1:1	5.6	6.2	16.0	35.7	1.1	2.2
1:2	5.8	6.2	15.7	34.0	1.1	2.2

4.3.4 Diffusion coefficients in CMS membranes

The diffusion coefficients of the 550 ^{o}C membranes synthesized under <0.005 torr of air were obtained from steady state permeation/equilibrium sorption using the method described in Appendix A. The sorption isotherms from Section 4.3.3 were used to obtain the sorption coefficients. Though the membranes in Section 4.3.3 were synthesized under slightly different atmospheric conditions, it was assumed that differences in the isotherms when synthesizing in 0.005 torr vacuum and 0.030 torr vacuum are not very significant based on the results in Appendix A. The diffusion coefficients for the membranes can be found in Table 4.5. The results show that the diffusion coefficients for 1:2 membranes are lower for all gases than for 1:1 membranes. These results suggest that the differences in the microstructure of the 1:1 precursors lead to membranes with a higher average ultramicropore size than the 1:2 membranes. The results also show that the selectivity in CMS membranes is controlled almost entirely by diffusion selectivity, which is expected from a molecular sieving material.

Table 4.6 Diffusion coefficients for 6FDA:BPDA(1:1)-DAM and 6FDA:BPDA(1:2)-DAM based CMS membranes pyrolyzed at 550 ^{o}C under <0.005 torr air

Precursor	D_{N2}	D_{o2}	D_{CH4}	D_{CO2}	D_{O2}/D_{N2}	D_{CO2}/D_{CH4}
		(10^{-8}) cm^2/s				
1:1	9.8	76.3	1.7	54.9	7.8	31.6
1:2	6.0	52.6	1.1	37.0	8.8	35.0

4.4 HYPOTHESIS DISCUSSING THE EFFECT OF POLYMER COMPOSITION ON THE SEPARATION PERFORMANCE OF CMS MEMBRANES

The microstructure of CMS membranes consists of irregularly packed sheets of sp^2 hybridized carbon. Amorphous carbon has a high degree of defects in the carbon sheets, which contribute to the very disordered, amorphous structure. The porosity of amorphous carbon membranes comes from the spaces between carbon planes, and convergence of the planes is believed to lead to the slitlike pore structure. When a polymer used for CMS membrane synthesis decomposes, a variety of by-products are evolved, most of which eventually evolve from the membrane. During the evolution of the gaseous by-products, new chemical bonds between carbon molecules are formed which eventually form the structure of the CMS membrane. The formation of the carbon structure can be inhibited if stable by-products inhibit the formation of the carbon-carbon bonds. Therefore, the size and quantity of light by-products evolved during pyrolysis may affect the formation of the CMS structure, and in turn the ultimate porosity of the CMS membranes. Also, when stable and light by-products are large, the diffusion coefficient of the by-products through the membrane will be lower than for small by-products so the larger by-product will remain in the membranes for a longer time during

CMS formation. This inhibits the formation of a regular carbon structure. This hypothesis can be used to describe the difference between CMS membranes formed from 6FDA:BPDA(1:1)-DAM and 6FDA:BPDA(1:2)-DAM. TGA has shown that when 6FDA:BPDA(1:1)-DAM decomposes, it loses more weight than 6FDA:BPDA(1:2)-DAM. FTIR results suggest that the majority of the difference in weight loss is due to the evolution of higher amounts of CF_3H, especially at 550 ^oC. It is speculated that CF_3H, a large molecule in comparison to the gases used for permeation testing, hinders the molecular rearrangement of the CMS structure during pyrolysis, and therefore, increases the average pore size. It is also likely that this effect is more apparent for the ultramicropores than the sorptive pores. Small changes in the pore size of the ultramicropores can have a considerable impact on both the permeability and diffusion coefficients because the ultramicropores are similar in size to the gas penetrant. On the other hand, small changes in the micropore (adsorptive pore) size may have only a minimal impact on the sorption coefficient and permeability.

It is also hypothesized that the free volume of glassy polymer precursors can also contribute to the CMS microstructure. During pyrolysis, the glassy polymer precursors are heated above their glass transition point. It is speculated that in rigid polymers, the diffusion of free volume out of the membrane above glass transition takes a finite time. If the polymer is rigid, then this time may be considerable. Therefore, when glassy polymers that have high free volume are decomposed, the large distance between polymer chains at the onset of decomposition inhibits the formation of chemical bonds between carbon atoms and formation of the carbon structure. Therefore it is speculated that the increased free volume of 6FDA:BPDA(1:1)-DAM might also contribute to the

high permeability and diffusion coefficients as compared to 6FDA:BPDA(1:2)-DAM. Unfortunately, it is difficult to deconvolute the effects of free volume and increased amounts of by-products with this series of copolymers. In Chapter 5, a series of polyimides will be used to help deconvolute these effects.

The overall results of this study show that the composition of the polymer precursor has a considerable effect on the microstructure and separation performance of CMS membranes. It has been determined that the polymer decomposition products and the polymer free volume are two factors which contribute to CMS performance and therefore should be carefully considered when choosing a polymer precursor. On the other hand, one can use co-polymer composition to "tune" final carbon properties by including inherently "packing disruptive" or "packing promoting" entities.

4.5 REFERENCES

1. Vu, D.Q., Koros, W.J., and Miller, S.J., *High Pressure CO2/CH4 Separation Using Carbon Molecular Sieve Hollow Fiber Membranes.* Industrial and Engineering Chemistry Research, 2002. **41**: p. 367-380.

2. Vu, D.Q., *Formation and characterization of asymmetric carbon molecular sieve and mixed matrix membranes for natural gas purification*, in *Department of Chemical Engineering*. 2001, University of Texas at Austin: Austin, TX.

3. Steel, K.M. and Koros, W.J., *Investigation of porosity of carbon materials and related effects on gas separation properties.* Carbon, 2003. **41**: p. 253-266.

4. Steel, K.M., *Carbon membranes for challenging separations*, in *Department of Chemical Engineering*. 2000, University of Texas - Austin: Austin, TX.

5. Singh-Ghosal, A. and Koros, W.J., *Air separation of flat sheet homogeneous pyrolytic carbon membranes.* Journal of Membrane Science, 2000. **174**: p. 177-188.

6. Singh, A. and Koros, W.J., *Significance of Entropic Selectivity for Advanced Gas Separation Membranes.* Industrial and Engineering Chemistry Research, 1996. **35**: p. 1231-1234.

7. Singh, A., *Membrane materials with enhanced selectivity; an entropic interpretation.* Ph. D. Dissertation, The University of Texas at Austin, 1997.

8. Jones, C.W. and Koros, W.J., *Characterization of Ultramicroporous Carbon Membranes with Humidified Feeds.* Industrial and Engineering Chemistry Research, 1995. **34**: p. 158-163.

9. Jones, C.W. and Koros, W.J., *Carbon Composite Membranes: A Solution to Adverse Humidity Effects.* Industrial and Engineering Chemistry Research, 1995. **34**: p. 164-167.

10. Jones, C.W. and Koros, W.J., *Carbon molecular sieve gas separation membranes-II. Regeneration following organic exposure.* Carbon, 1994. **32**(8): p. 1427-1432.

11. Jones, C.W. and Koros, W.J., *Carbon molecular sieve gas separation membranes-I. Preparation and characterizaton based on polyimide precursors.* Carbon, 1994. **32**(8): p. 1419-1425.

12. Geiszler, V.C. and Koros, W.J., *Effects of Polyimide Pyrolysis Conditions on Carbon Molecular Sieve Membrane Properties.* Industrial and Engineering Chemistry Research, 1996. **35**: p. 2999-3003.

13. Geiszler, V., *Polyimide Precursors for Carbon Molecular Sieve Membranes.* 1997, University of Texas, Austin: Austin.

14. Park, H.B., Kim, T.K., Lee, J.M., Lee, S.Y., and Lee, Y.M., *Relationship between chemical structure of aromatic polyimides and gas permeation properties of their carbon molecular sieve membranes.* Journal of Membrane Science, 2004. **229**: p. 117-127.

15. Bondi, A., *Physical Properties of Molecular Crystals, Liquids, and Glasses*`. 1968, New York: Wiley-Interscience.

16. Van Krevelen, D.W., *Properties of Polymers*. 1990, Amsterdam: Elsevier.

17. Park, J.Y. and Paul, D.R., *Correlation and prediction of gas permeability in glassy polymer membrane materials via modified free volume based group contribution method.* Journal of Membrane Science, 1997. **152**(1): p. 23-29.

18. Barsema, J.N., Klijnstra, S.D., van der Vegt, N.F.A., Koops, G.H., and Wessling, M., *Intermediate polymer to carbon gas separation membranes based on Matrimid PI.* Journal of Membrane Science, 2004. **328**: p. 93-102.

19. Barsema, J., *Carbon Membranes: Precursor, preparation, and functionalization*. 2004, University of Twente: Twente.

CHAPTER 5

FORMATION AND CHARACTERIZATION OF CMS MEMBRANES FROM 6FDA-6FMDA AND 6FDA-6FPDA

In Chapter 4, co-polyimides of similar structure were used as precursors to produce CMS membranes. In this chapter, a similar study was performed using two different polyimides, 6FDA-6FmDA and 6FDA-6FpDA to test the effect of polymer free volume on the separation performance of CMS membranes. Section 5.1 will discuss the reason these polymers were chosen as precursors as well as properties of these polymer precursors. Section 5.2 will discuss methods used to characterize the CMS microstructure and the pyrolysis process. Section 5.3 will discuss separation performance of these membranes in terms of gas transport properties of the membranes.

5.1 POLYMER PRECURSORS

5.1.1 Selection of precursors

In the previous chapter, it was hypothesized that the two important factors for determining the separation of CMS membranes are (1) the free volume in the polymer and (2) the composition and amount of by-products that evolve. It is difficult to elucidate the effect of each of these factors individually for most polyimide systems because free volume is often controlled by the composition of pendant groups along the polymer chain. During pyrolysis these pendant groups decompose and often evolve as light by-products. Chapter 4 briefly discussed how the choice of pendant groups could be utilized to control CMS separation performance. The goal of the present study was to examine the effect that intrinsic polymer free volume has on the separation performance of CMS

membranes. In pursuit of this goal, two well characterized polyimides, 6FDA-6FpDA and 6FDA-6FmDA were chosen as precursors. The structure of these two polymers can be found in Figure 5.1. These two polymers have the same general structure, the only difference between the structures of the two polymers comes from the location of the phenylene linkages in the polyimide backbone. 6FDA-6FmDA contains a meta- linkage while 6FDA-6FpDA contains a para- linkage. It was expected (and will later be proven) that as these materials decompose, similar light by-products evolve. In subsequent sections, it will be shown that the fractional free volume of these two materials varies considerably. Therefore, this series of precursors proved useful for determining the effect of polymer free volume on the separation performance of CMS membranes.

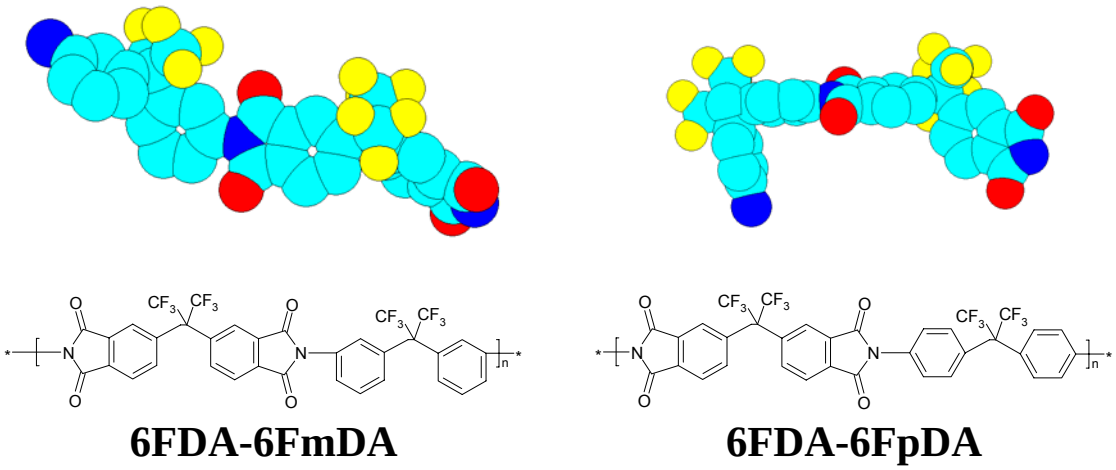

Figure 5.1 Model of the repeat units for 6FDA-6FmDA and 6FDA-6FpDA. The models were obtained using Hyperchem. The atoms correspond to the following colors: C-cyan, N-blue, O-red, F-yellow.

5.1.2 Fractional free volume (FFV) of 6FDA-6FmDA and 6FDA-6FpDA

The densities of 6FDA-6FmDA and 6FDA-6FpDA were obtained from Coleman [1]. Coleman [1] performed an extensive study on the separation performance of polyimide membranes produced from 6FmDA and 6FpDA diamines and different dianhydrides, including 6FDA. In that study, the fractional free volume was estimated using group contribution theory similar to that described for the 6FDA:BPDA(x:y)-DAM polyimides. The reported density and FFV are listed in Table 5.1. Park and Paul [2] also replicated the FFV calculated by Coleman [1] in their study. Using the data provided by Park and Paul [2] and the densities reported by Coleman [1], the FFV was again calculated in the present study. There is some discrepancy between the results, as shown in Table 5.1. The differences are likely associated with the assignment of the groups used to calculate the van der Waals volume. Though there is some disagreement in the exact value of the free volume of the two polyimides, the FFV of 6FDA-6FmDA is about 8% lower than that of 6FDA-6FpDA with either method.

Table 5.1 Density and fractional free volume of 6FDA-6FpDA and 6FDA-6FmDA polymer membranes used as precursors

Polymer	Density (g/cm^3)	FFV	Reference
6FDA-6FpDA	1.466	0.190	[1, 2]
		0.186	
6FDA-6FmDA	1.493	0.175	[1, 2]
		0.171	

5.1.3 WAXD of 6FDA-6FpDA and 6FDA-6FmDA

WAXD was also used to investigate the characteristics of the polymer precursors. The results are shown in Figure 5.2. Both of the polymers are characterized by a broad amorphous peak at approximately 15 degrees (2 theta) and a second small, broad amorphous peak around 27 degrees (2 theta). The crystalline peaks around 13 (2 theta) and between 25 and 45 degrees (2 theta) are due to the sample holder used in the experiment. The average d-spacing for 6FDA-6FmDA was approximately 5.9 Å while the average d-spacing for 6FDA-6FmDA was approximately 5.7 Å. The average d-spacing for 6FDA-6FmDA contains some degree of uncertainty because the distribution is very broad. The d-spacings obtained in this study agree with Coleman [1] and compare with the free volume trends. The 6FDA-6FpDA appears to be a more loosely packed polymer than 6FDA-6FmDA based on the larger d-spacing and larger inherent free volume.

The two different "amorphous" peaks may be due to two distinct areas along the polymer chain that have different packing characteristics. The large amorphous peak is characteristic of areas where packing in significantly hindered, likely due to the $-C(CF_3)_2-$ groups. Both polymers have a second small, broad peak centered around 3.3 Å which might be associated with the distance between polymer chains in areas where fewer "kinks" are located, such as the imide-phenyl connection as shown in Figure 5.3. The "kinks" in 6FDA-6FpDA are much larger than in 6FDA-6FmDA, which are believed to lead to a larger d-spacing and increased free volume.

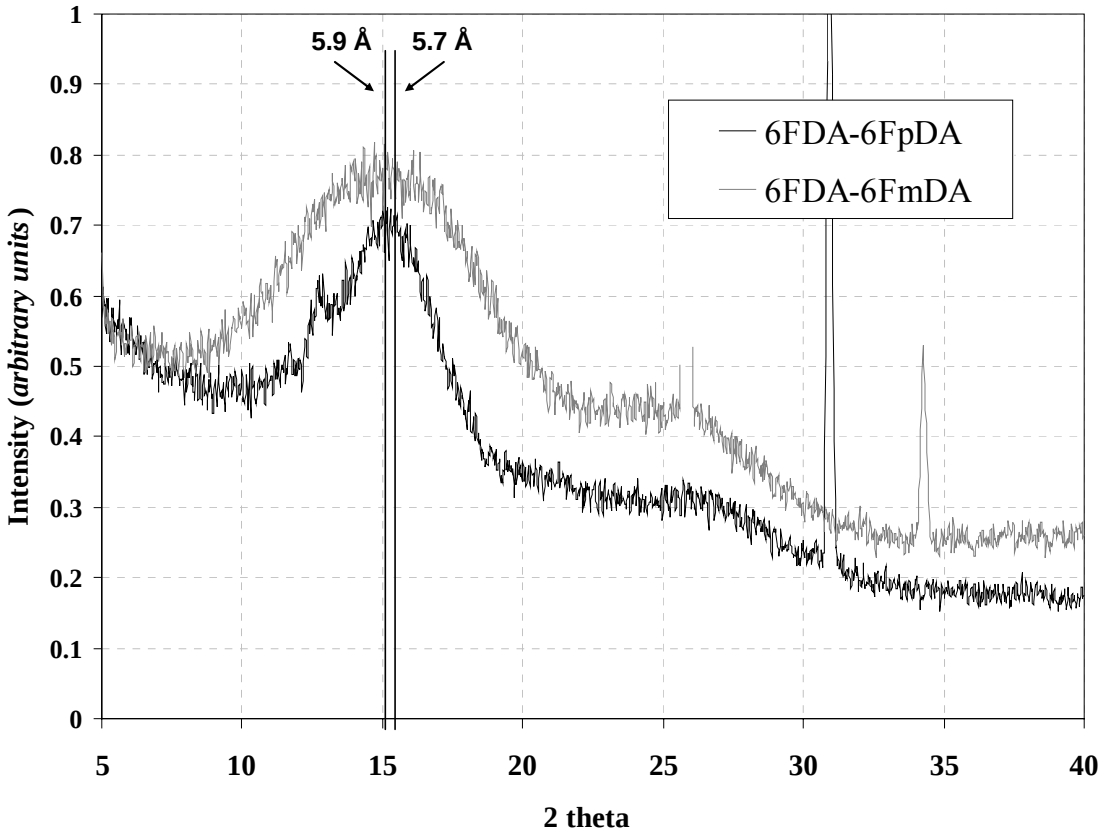

Figure 5.2 XRD pattern of 6FDA-6FpDA and 6FDA-6FmDA.

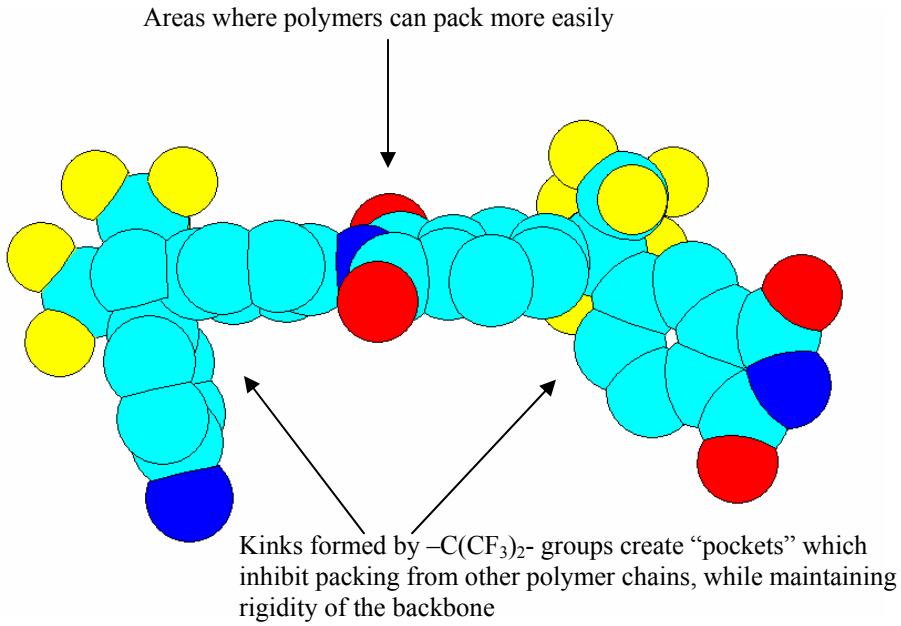

Figure 5.3 6FDA-6FpDA monomer showing areas where packing is inhibited leading to high free volume

5.2 CHARACTERIZATION OF DECOMPOSITION PROCESS AND CMS MEMBRANES

5.2.1 TGA-IR of 6FDA-6FmDA and 6FDA-6FpDA decomposition

In this study, it was useful to perform TGA-IR experiments similar to those performed for the 6FDA:BPDA(x:y)-DAM precursors in the previous section in order to verify that the two polyimides decompose to form the same decomposition products, in the same quantities. Therefore, TGA was used to monitor the weight loss during simulated pyrolysis protocols. The results of the TGA experiments can be found in Figures 5.4 and 5.5. The TGA decomposition curves for both the 550 ^{o}C decompomposition profile and the 800 ^{o}C decomposition profile are identical, within the error of the test. These results were replicated several times for each sample. These results suggest that the decomposition of 6FDA-6FmDA and 6FDA-6FpDA follow the same mechanisms with the same decomposition products.

The weight loss for both these polyimides utilizing either the 550 ^{o}C and 800 ^{o}C thermal profile is higher than the corresponding thermal profile for both 6FDA:BPDA(x:y) precursors. This result was expected because there is a much higher content of -CF_3 groups on 6FDA-6FmDA and 6FDA-6FpDA, which likely evolve during decomposition. The residual mass for both of these polymers is approximately 55% at 550 ^{o}C and 49% at 800 ^{o}C. The rate of weight loss for these precursors is much more rapid than the 6FDA:BPDA(x:y)-DAM series. This is also likely associated with the cleavage of CF_3 groups on both the 6FDA dianhydride of the 6FmDA and 6FpDA diamines. The cleavage of –CF_3 groups occurs at the first stage of decomposition and accounts for a large percentage of the mass loss. Since these polymers have at least twice

the amount of CF_3, the total mass loss and the rate of mass loss is higher for these polyimides than the 6FDA:BPDA(x:y)-DAM polyimides. There is very little weight loss during the 800 ^{o}C thermal soak for the 6FDA-6FmDA and 6FDA-6FpDA polymer, and thus it is presumed that the extent of carbonization is very high at 800 ^{o}C.

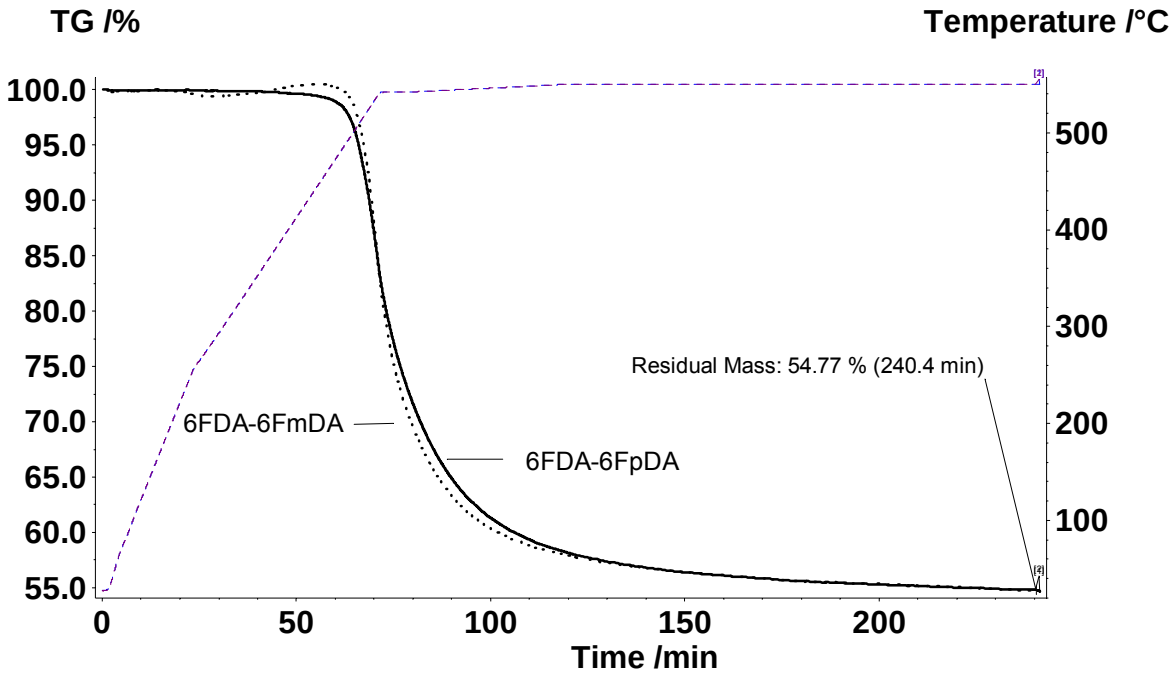

Figure 5.4 TGA of 550 ^{o}C pyrolysis protocol using 6FDA-6FpDA and 6FDA-6FmDA polymer precursors. Both materials have the same weight loss curves, within the error of the experiment.

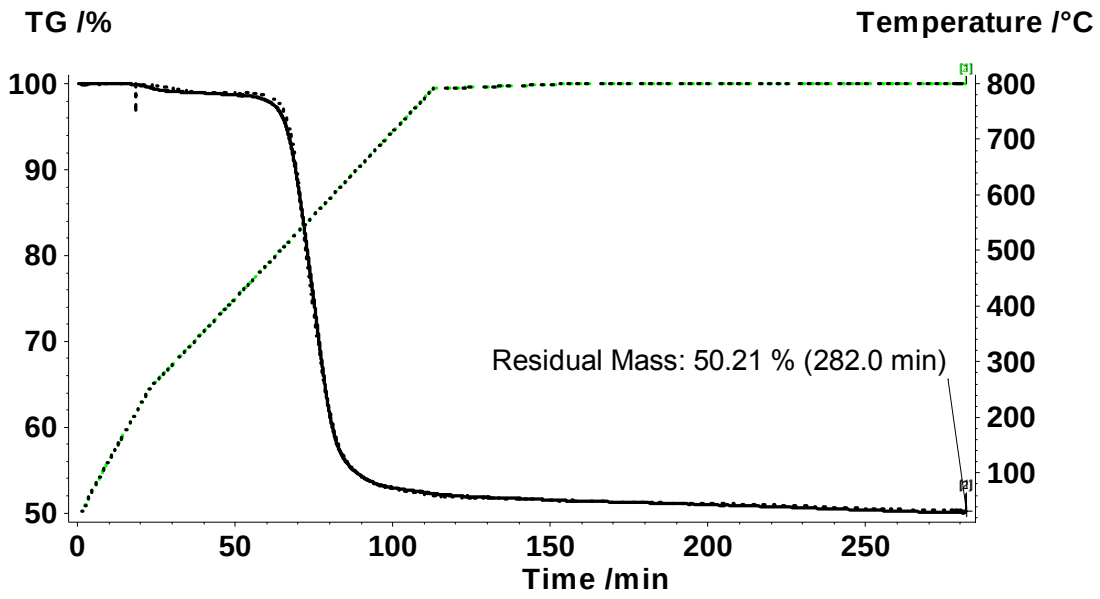

Figure 5.5 TGA of 800 °C pyrolysis protocol using 6FDA-6FpDA and 6FDA-6FmDA polymer precursors. Both materials have the same weight loss curves, within the error of the experiment.

FTIR was again used to analyze the gaseous by-products evolved during decomposition. The spectra for both precursors are similar but due to the IR software limitations, it is not possible to directly compare the two spectra on the same plot. Therefore, only the 550 °C 6FDA-6FmDA spectra is included, Figure 5.6. The major decomposition products are again CF_3H, HF, CO, and CO_2. The large peak between 3000 and 3500 cm^{-1} is due to ice formation around the IR detector during the experiment. Unlike the 6FDA:BPDA(x:y)-DAM polymers, methane was not evolved during 6FDA-6FmDA decomposition. This result was expected because there are no methyl groups in these polymers. Figure 5.7 contains plots of the intensity of certain IR peaks for the individual compounds evolved during pyrolysis. As with the 6FDA:BPDA(x:y)-DAM based polymers, there is a small amount of CO_2 evolved before the major decomposition peak. The onset of decomposition involves the evolution of CF_3H followed by HF, most

likely from cleavage of the C-C bonds in $-C(CF_3)_2-$. The hydrogen likely comes from the aromatics in the diamine. At a slightly higher temperature, CO and CO_2 evolve, which likely come from the cleavage of the imide bond. The CO peak is very strong initially and slowly dissipates. This is possibly due to (1) the initial cleavage of imide bonds and then (2) further decomposition of larger by-products which are a result of imide ring cleavage. There is a strong peak evolved after the evolution of the fluorinated materials which has a strong intensity at 1020 cm^{-1}. This is likely a large aromatic by-product which results from imide ring cleavage.

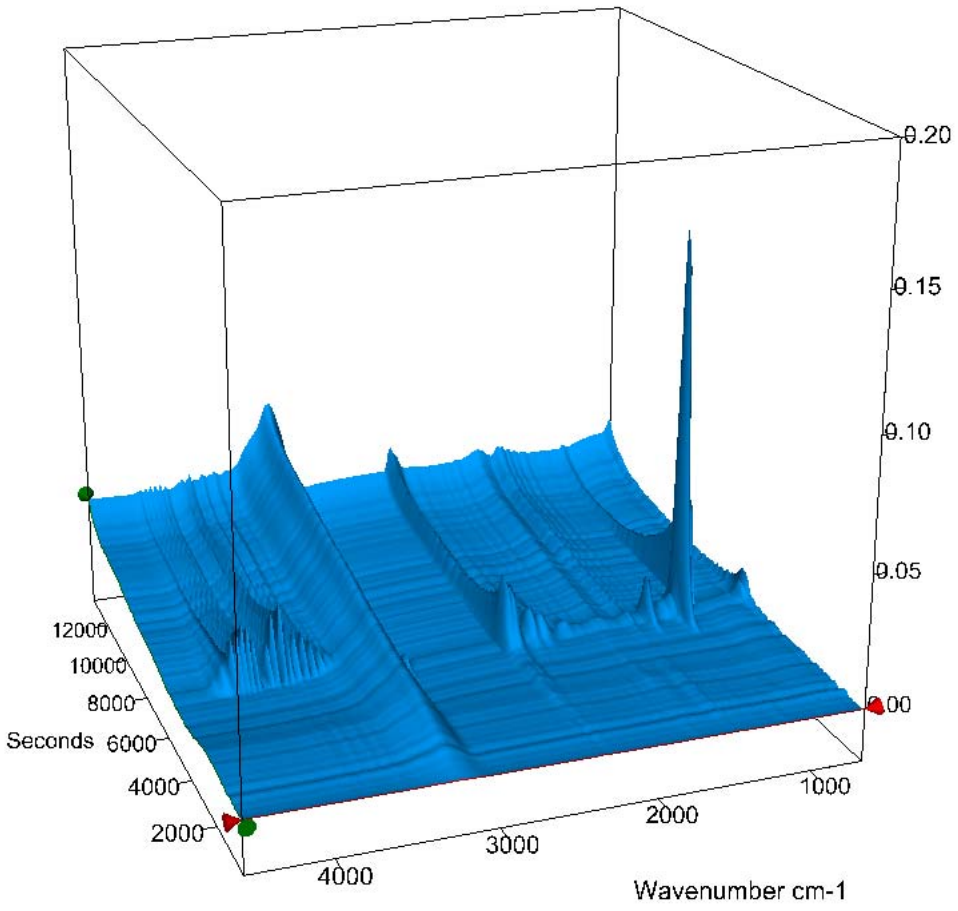

Figure 5.6 IR spectrum of the decomposition products evolved during 6FDA-6FmDA pyrolysis using 550 ^{o}C thermal profile

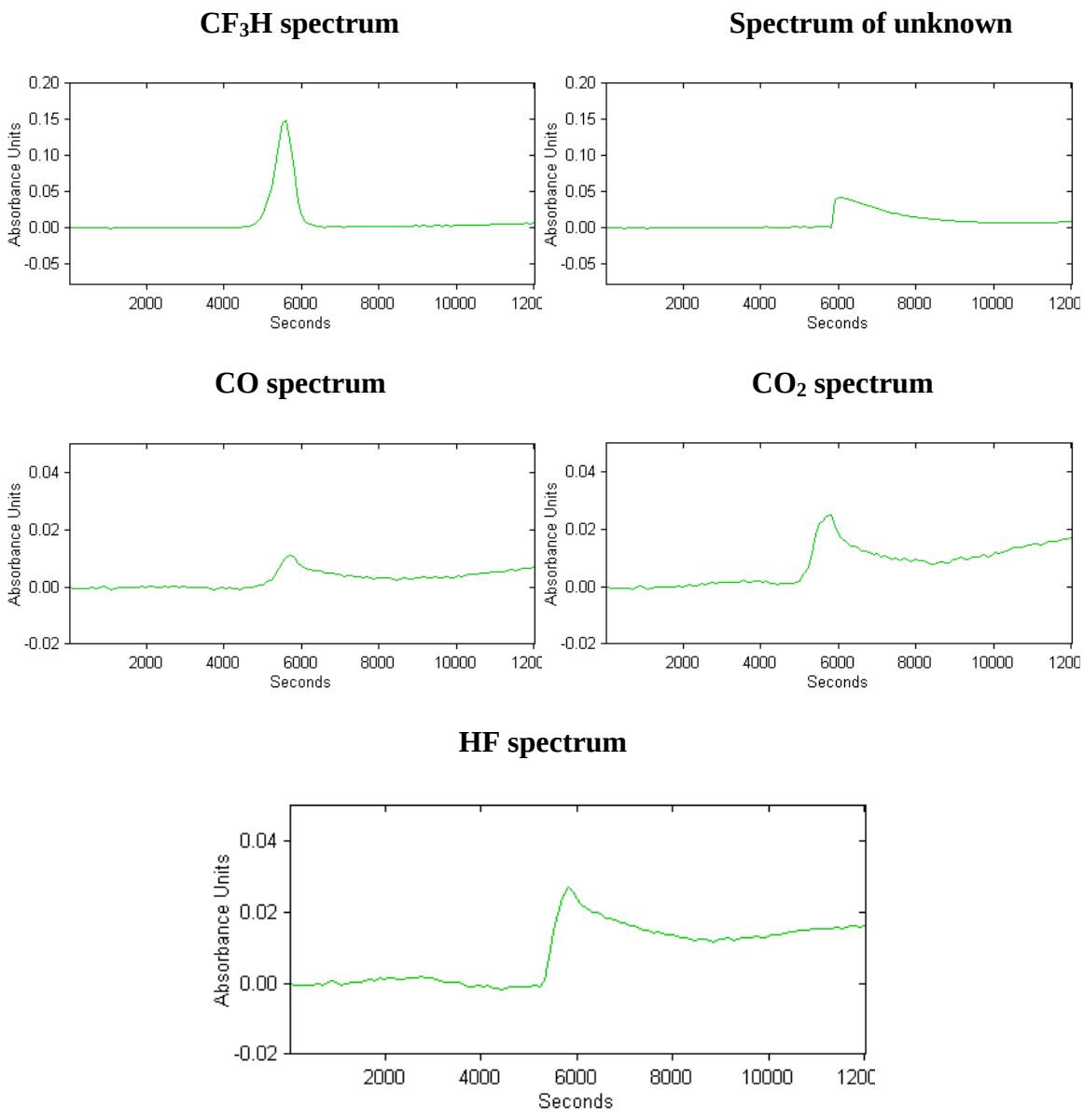

Figure 5.7 FTIR absorbance versus time plot for individual decomposition products using the 550 ^{o}C thermal decomposition profile

5.2.2 FTIR analysis of polymer and CMS membranes derived from 6FDA-6FmDA and 6FDA-6FpDA

ATR spectroscopy was used to investigate the structure of CMS membranes to determine whether or not any functional groups remained in the membranes after pyrolysis. Spectra for membranes produced at 550 ^{o}C and 800 ^{o}C, as well as the polymer membranes from which they were derived are shown in Figures 5.8 and 5.9. The only discernable peaks in the IR spectra for the CMS membranes are associated with CO_2. The ATR cell used for analysis is in open to the atmosphere and the scans were taken were for long periods of time to increase the signal to noise ratio. Therefore, the CO_2 could be from changes in the amount of CO_2 in the atmosphere or more likely, the peaks are associated with CO_2 adsorbed onto the surface of the carbon membranes. IR spectra suggest that after pyrolysis, the CMS membranes are composed of mostly amorphous carbon and have a structure that is dissimilar from the polymer from which they were produced.

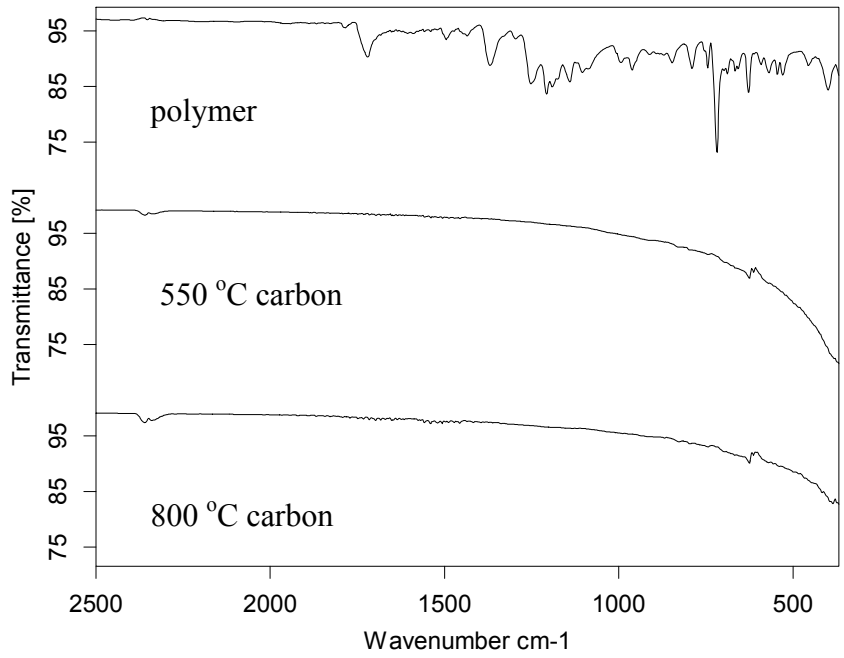

Figure 5.8 IR spectra of 6FDA-6FmDA and carbons derived from the polymer

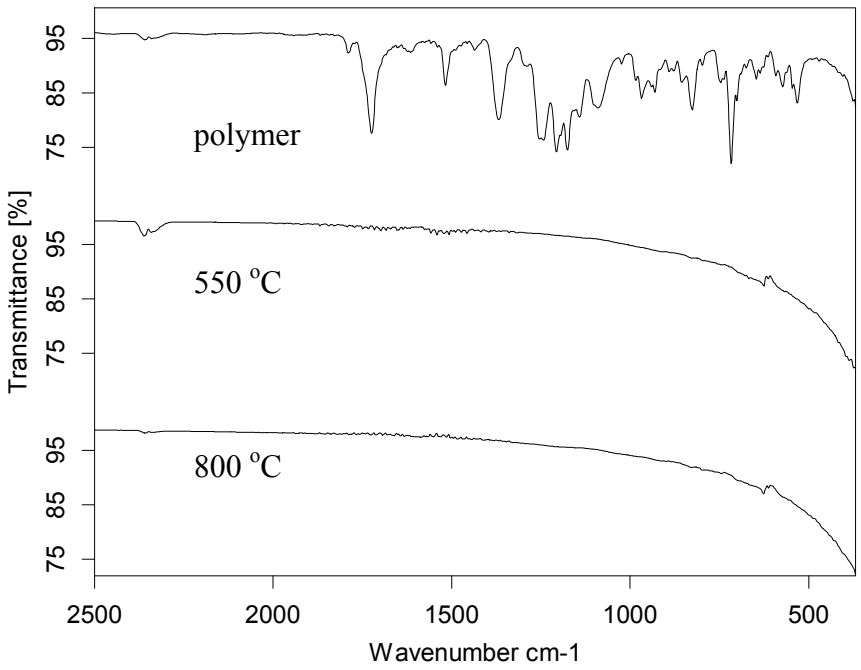

Figure 5.9 IR spectra of 6FDA-6FpDA and carbons derived from the polymer

5.2.3 WAXD of CMS membranes derived from 6FDA-6FmDA and 6FDA-6FpDA

The microstructure of the CMS membranes was also investigated using WAXD, Figures 5.10 and 5.11. The membranes produced at 550 ^{o}C have two characteristic peaks, a broad peak associated with the distance between carbon planes, similar to the amorphous peak in polymers, and a broad peak at ~42 degrees (2 theta), which characterizes the distance between carbon atoms in the same plane. For graphite, the second peak (100) occurs at 2.13 Å. The amorphous peak for both membranes at 550 ^{o}C is very broad, which is characteristic of a distribution of pore sizes. The peak for 6FDA-6FpDA is centered at ~3.95 Å while the peak for 6FDA-6FmDA is centered around ~3.8 Å. Estimation of the location of the peak is difficult because of the breadth of the peak. More importantly, it appears that the average d-spacing for 6FDA-6FpDA is larger than for 6FDA-6FmDA. This suggests that the higher free volume polymer produces CMS membranes that are, on average, less compact than the low free volume polymer.

The trends observed at 800 ^{o}C are similar to those at 550 ^{o}C. The intensity of the amorphous peak as well as the (100) peak has increased for both membranes. The amorphous peak is much broader for the 6FDA-6FpDA than for the 6FDA-6FmDA. For both membranes, though, the peak is centered at around 3.5 Å. The results suggest that the distance between carbon planes decreases when the pyrolysis temperature is increased, as expected from previous results with similar precursors. Also, the breadth of the amorphous peaks suggests that the "pore" size distribution in the 6FDA-6FmDA membrane is narrower than in the 6FDA-6FpDA membrane. The pore structure of the CMS membrane is defined by the decomposition by-products and the free volume of the precursor. At 800 ^{o}C, pore sintering causes a narrowing of the pore size distribution.

The 6FDA-6FpDA originally had a higher free volume than the 6FDA-6FmDA and some of that free volume is maintained throughout the pyrolysis process. This may explain why the carbon membrane based on 6FDA-6FpDA has a broader distribution of pore sizes that 6FDA-6FmDA.

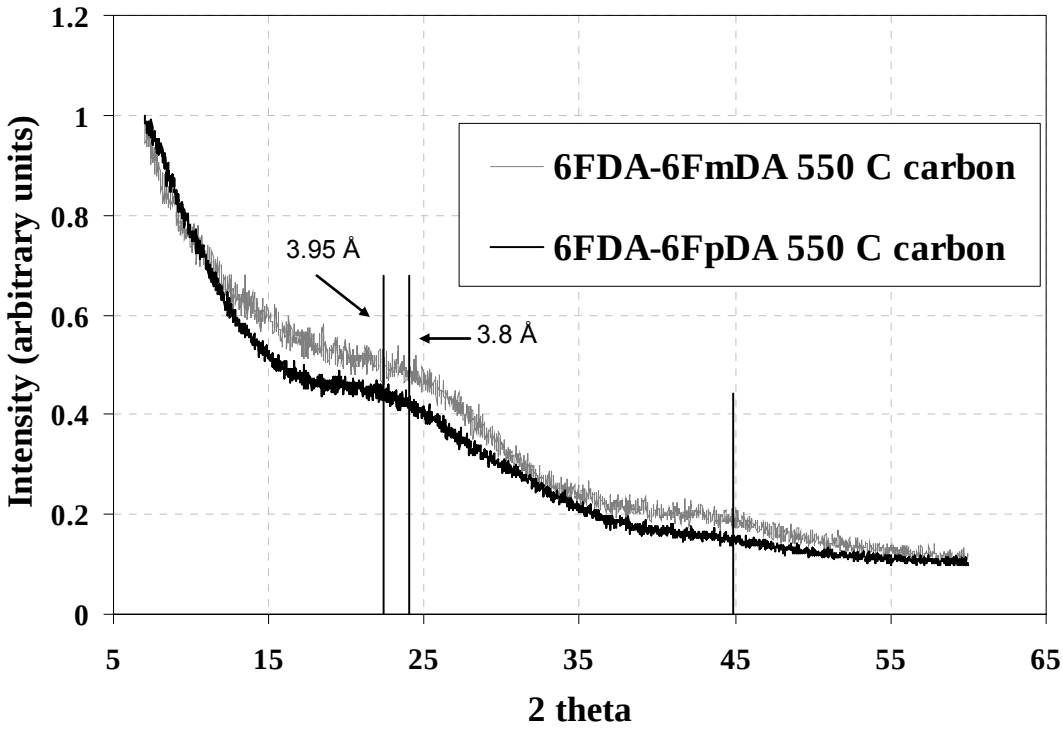

Figure 5.10 WAXD pattern of CMS membranes from 6FDA-6FpDA and 6FDA-6FmDA at 550 ^{o}C

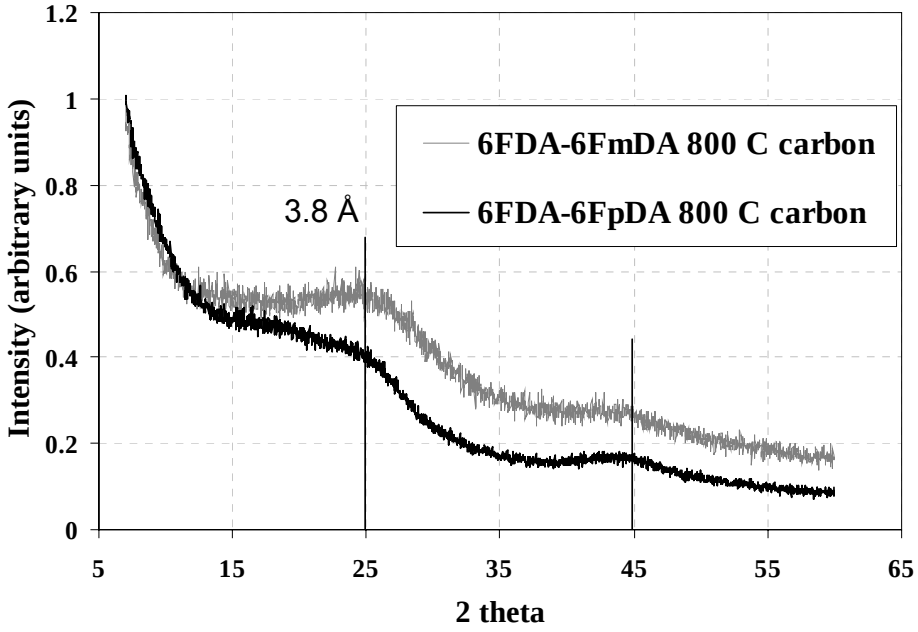

Figure 5.11 WAXD pattern of CMS membranes from 6FDA-6FpDA and 6FDA-6FmDA at 800 ^{o}C

5.3 GAS SEPARATION PERFORMANCE OF CMS MEMBRANES

The ultimate goal of this study was to determine the effect of intrinsic polymer precursor free volume on the microstructure and gas separation performance of CMS membranes. In this section, the gas separation performance will be investigated and the results discussed in comparison to material properties obtained in the previous section.

5.3.1 Permeation performance of CMS membranes derived from 6FDA-6FmDA and 6FDA-6FpDA

5.3.1.1 Permeation testing and permeation performance

In section 5.2.3 of this chapter, WAXD results suggested that 6FDA-6FmDA based CMS membranes are more compact than 6FDA-6FpDA based membranes, especially using the 550 ^{o}C pyrolysis protocol. In this section, gas permeation was used to support these results. Table 5.2 lists the permeation properties for membranes

produced using the 550 °C and 800 °C pyrolysis profile. These membranes were pyrolyzed using ~0.03 torr vacuum and had a thickness of ~2 mil. The ultimate goal of permeation testing was to determine whether changes in the polymer free volume have an effect on separation performance. Since these membranes were synthesized under the same conditions, the results can be used to compare the microstructure of CMS membranes formed from the two precursors, as discussed in the previous chapter and Appendix A.

One of the difficulties when testing CMS membranes is that they are rather brittle. During permeation testing, considerable pressure is placed on the upstream side of the membrane. It is not uncommon to have membranes break during testing. Due to limited availability of polymers in this study, lower pressures were used on the upstream side of the membrane during permeation testing to minimize the amount of film broken during testing. The average upstream pressure was 17 psia for all of the gases tested. The permeabilities listed are for an average of 2-3 films from multiple batches.

Table 5.2 Permeation properties of CMS membranes produced from 6FDA-6FpDA and 6FDA-6FmDA. The name of each film corresponds to the polymer diamine and the pyrolysis temperature. All permeabilities are in Barrers.

Film	P_{O2}	P_{CO2}	P_{O2}/P_{N2}	P_{CO2}/P_{CH4}	P_{CO2}/P_{N2}
6FmDA 550	255 ± 9	1283 ± 38	8.4 ± 0.3	74 ± 5	42 ± 1
6FpDA 550	417 ± 52	2146 ± 73	6.4 ± 0.3	69 ± 8	33 ± 1
6FmDA 800	18 ± 9	32 ± 19	5.0 ± 0.7	23± 2	14 ± 3
6FpDA 800	45 ± 12	166 ± 55	7.8 ± 1.2	37 ± 9	29 ± 3

5.3.1.2 Effect of precursor composition on CMS separation properties

The permeability of CMS membranes was tested using O_2, N_2, CO_2, and CH_4. Figure 5.12 shows that for all of the membranes, the permeability follows the order $CO_2>O_2>N_2>CH_4$, which is also the order of kinetic diameter. In addition, the extremely high sorption of CO_2 versus all of the other gases is a factor making CO_2 much more permeable than similarly sized O_2. Most important to this study was to compare CMS membranes produced under identical conditions with different precursors. 6FpDA 550 had an O_2 permeability of approximately 400 Barrers with a O_2/N_2 selectivity of approximately 6.4. 6FmDA had a permeability of 255 Barrers with an O_2/N_2 selectivity of 8.4. Due to the limited amount of samples, there is some uncertainty in the permeability values, but notwithstanding, the permeability for 6FpDA 550 is higher than 6FmDA 550, well beyond the uncertainty, with a lower selectivity. The CO_2 permeability for 6FpDA 550 is almost double that of 6FmDA 550. The average CO_2/CH_4 selectivity for 6FpDA 550 is lower than 6FmDA 550, but within experimental error, there is no difference between the two membranes. Therefore, no general conclusions can be drawn from the CO_2/CH_4 selectivity data. Later in this chapter, these results will be related to the diffusion coefficient of the membranes. The CO_2/N_2 selectivity of 6FmDA 550 is about 30% higher in than 6FmDA 550. Therefore, the results show that CMS membranes produced from 6FmDA at 550 ^oC have a lower permeability but generally a higher selectivity than those produced from 6FpDA.

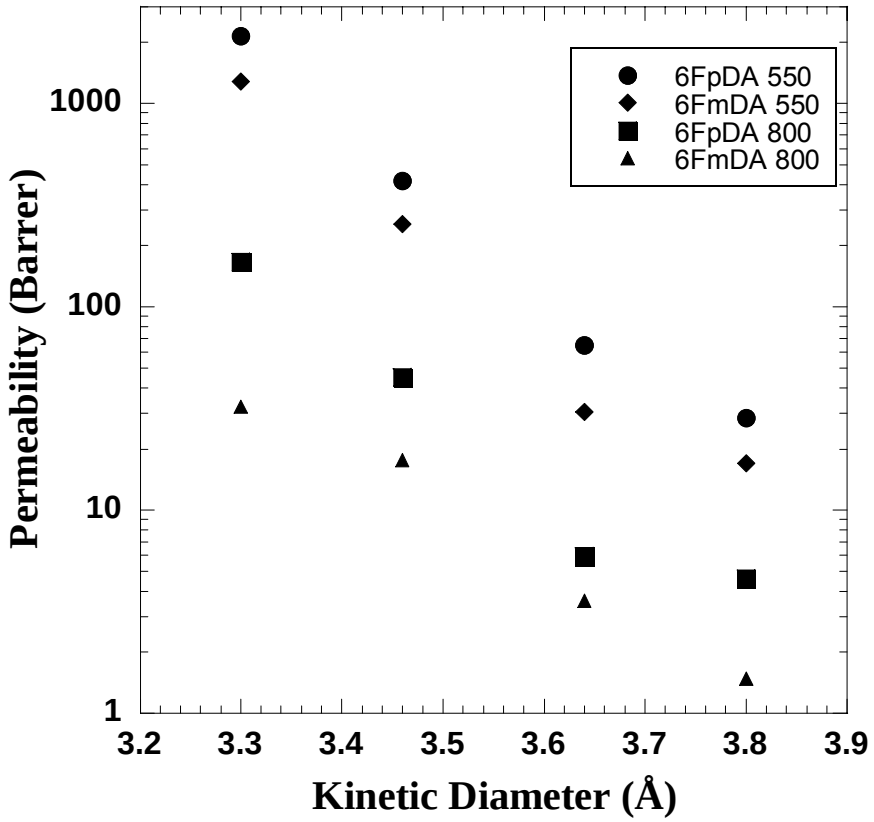

Figure 5.12 Permeability of CMS membranes derived from 6FDA-6FpDA and 6FDA-6FmDA as a function of kinetic diameter of gas penetrant

The permeability of 800 ^{o}C films is approximately 10% of the 550 ^{o}C films from the same precursor. The permeability for 800 ^{o}C membranes also follows the order of kinetic diameter of the gas penetrant. The selectivities of the membranes do not follow the same trends as the 550 ^{o}C membranes, though. The O_2/N_2 selectivity of 6FmDA 800 is only 5.0 while 6FpDA 800 has a selectivity of 7.8. The selectivity for 6FpDA 800 is higher than 6FpDA 550, while the selectivity for 6FmDA 800 is lower than 6FmDA 550. This unexpected result was repeated for several batches of membranes. The CO_2/CH_4

selectivity drops by ~1/2 when changing from 550 ^{o}C to 800 ^{o}C, independent of precursor.

It is useful to discuss these permeability and selectivity results when combined with XRD data. The average d-spacing obtained for 6FpDA 800 and 6FmDA 550 using XRD is approximately 3.5 Å, while the average d-spacing for the 550 ^{o}C membranes was 3.8-4.0 Å. Though XRD is not a direct measure of pore size, it can be used to speculate changes in the pore structure. A hypothetical *ultramicropore* size distribution for CMS membranes is shown in Figure 5.13. The distribution, adapted from Steel [3], assumes that the majority of ultramicropores are in a fairly small range. It has been speculated that the sizes of pores in CMS membranes are related to the size of decomposition by-products as well as the polymer precursor free volume. Pore sintering likely occurs during periods of thermal soak, therefore thermal soak time also affects the ultramicropore size distribution. Figure 5.13 speculates that the ultramicropore size is characterized by a broad distribution. The majority of pores are believed to be in a small range but there may be few large pores which likely have low selectivity. It is speculated that as the pyrolysis temperature of 6FDA-6FmDA based membranes is increased from 550 ^{o}C to 800 ^{o}C, the distribution shifts to a much smaller pore size. These results are in agreement with the WAXD spectra which showed that the average pore size shifts from ~3.8 Å to 3.5 Å. The d-spacing distribution, characterized by WAXD, represents the interplanar spacing of carbon sheets which is speculated to include both aspects of ultramicropores and pores for adsorption. Therefore, the average ultramicropore size is likely smaller than the d-spacing and therefore, smaller than the size of any of the gas molecules tested in this study. In that case, diffusion only occurs through a small amount

of larger pores in the membrane, which are fairly nonselective. Even though diffusion occurs through fairly large pores, there are very few of them, and therefore, the tortuosity of the membrane may be increased. The overall result is a decrease in both permeability and selectivity in the 800 ^{o}C samples as opposed to the 550 ^{o}C samples. Similar results were observed by Steel [3] when investigating the permeability of propane and propylene in membranes pyrolyzed at high temperatures and to some extent when investigating O_2/N_2 separation performance for CMS membranes produced at high temperatures with long thermal soaks. When compared to 6FmDA 800, the ultramicropores of 6FpDA 800 likely have a larger average pore size and therefore there is not the dramatic decrease in selectivity from 6FpDA 550 to 6FpDA 800. Diffusion in these films is speculated to occur mainly through larger, fairly unselective pores but there are also a significant amount of selective pores. Therefore, both the permeability and selectivity of 6FpDA 800 membranes are higher than 6FmDA 800.

Overall, permeability results show that when using the same pyrolysis conditions, the permeabilities of 6FDA-6FpDA based CMS membranes are higher than that of 6FDA-6FmDA. Thus, it appears that free volume of the polymer precursor has an effect on the separation performance of CMS membranes. In the next sections, equilibrium sorption and gas diffusion calculations will be used to further investigate the CMS structure.

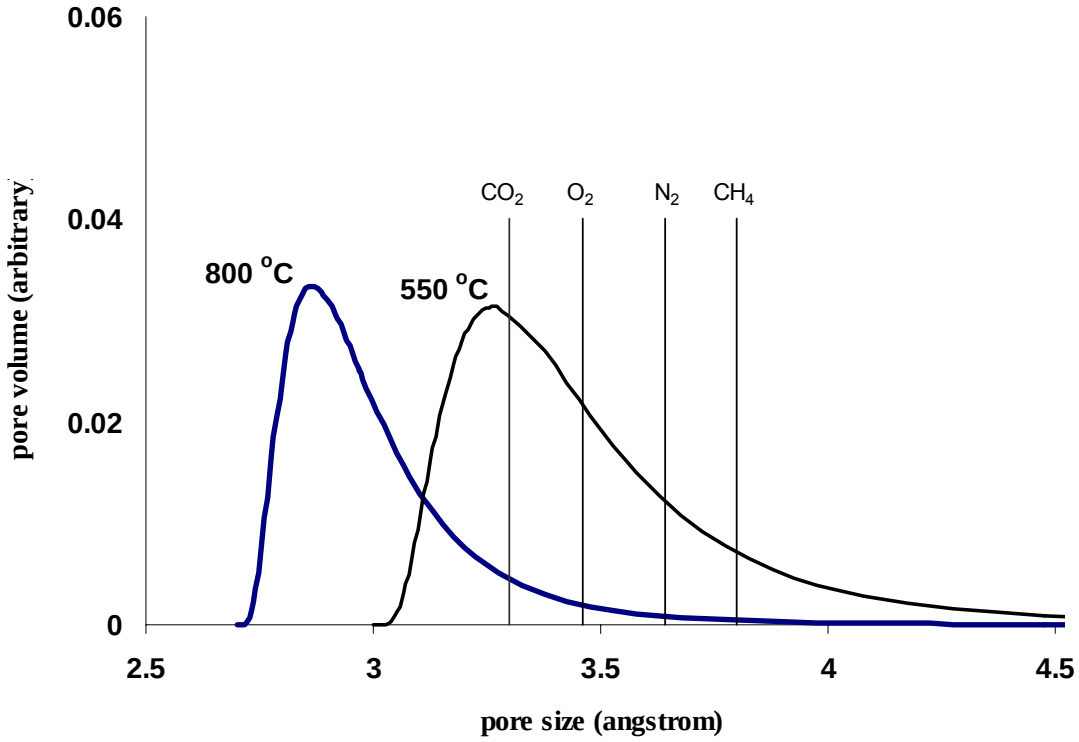

Figure 5.13 Hypothetical ultramicropore size distributions for CMS membranes. The majority of pores in the distribution at 550 °C are accessible to all gases while there are very few accessible pores at 800 °C.

5.3.2 Equilibrium sorption of CMS membranes derived from 6FDA-6FmDA and 6FDA-6FpDA

Equilibrium sorption isotherms were obtained for each of the CMS membranes using the pressure decay method. In CMS membranes, the majority of the pore volume available for sorption is contained in the large micropores. The ultramicropores, though important for diffusion, are speculated to account for a very small percentage of the sorption capacity. Therefore, analysis of sorption isotherms gives information about the changes in large pores. Each isotherm was obtained at 35 °C, which allows correlation with permeation data. The isotherms for each material are shown in Figures 5.14-5.17.

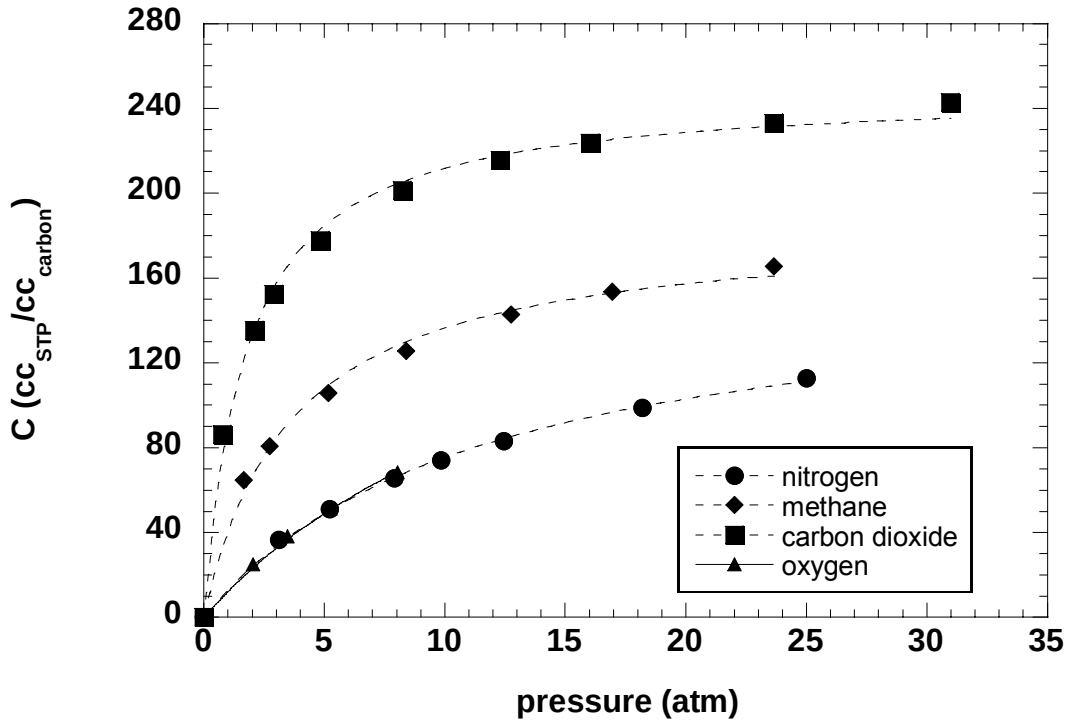

Figure 5.14 Sorption isotherms for 6FmDA 800 modeled using the Langmuir isotherm

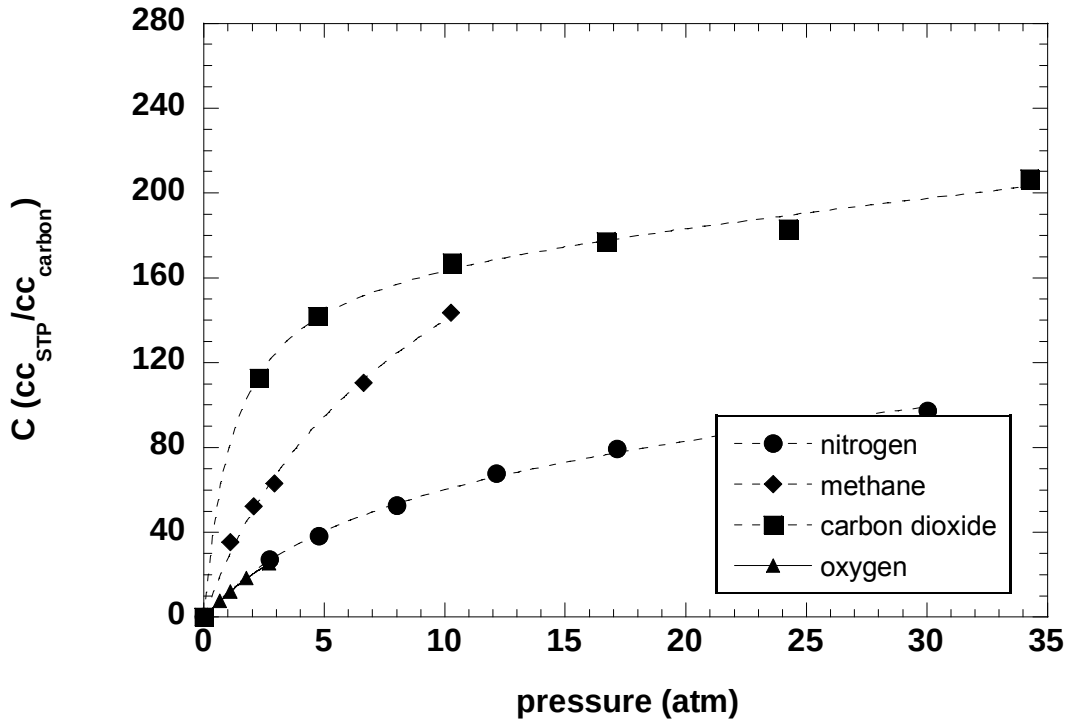

Figure 5.15 Sorption isotherms for 6FmDA 550 modeled using the Langmuir isotherm

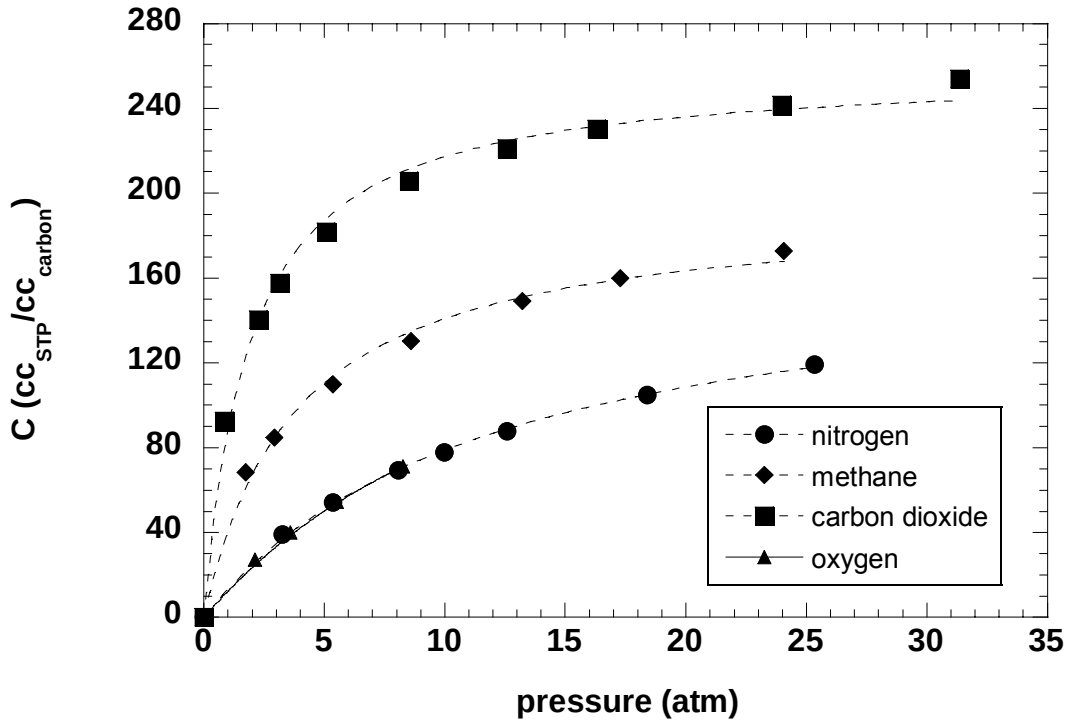

Figure 5.16 Sorption isotherms for 6FpDA 800 modeled using the Langmuir isotherm

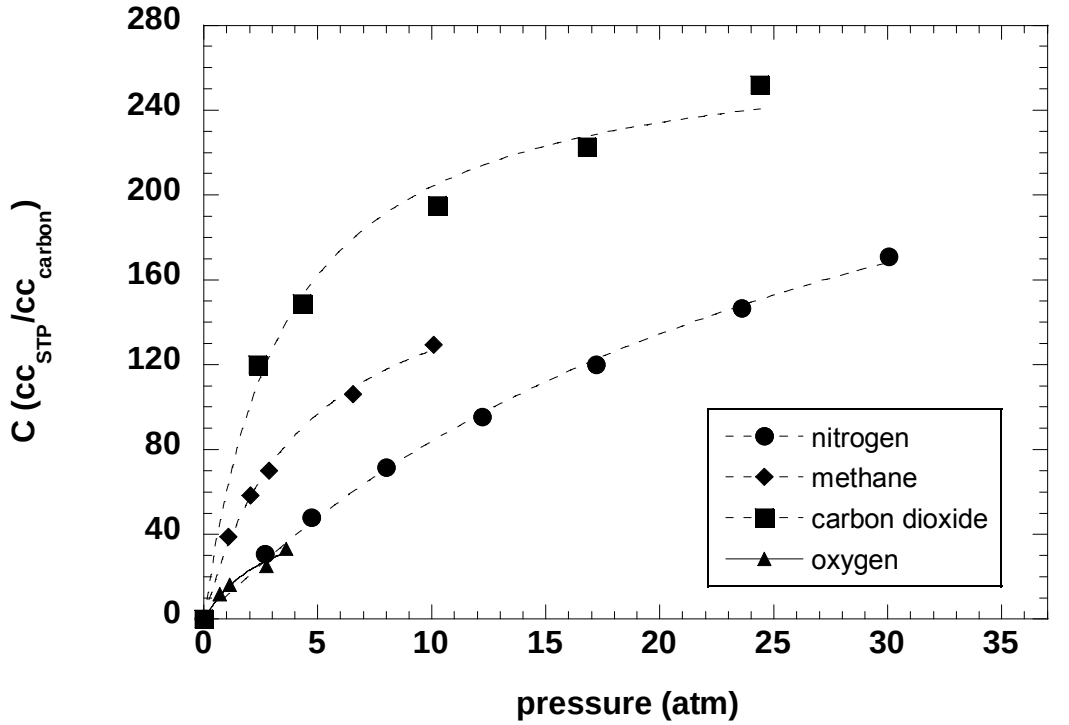

Figure 5.17 Sorption isotherms for 6FpDA 550 modeled using the Langmuir isotherm

Each sorption isotherm was modeled using the Langmuir isotherm, Equation 2.11. The Langmuir model accurately described most of the isotherms, except carbon dioxide in 6FpDA 550. The Langmuir coefficients were obtained using a least means squared algorithm in Kaleidagraph. These were in turn used to calculate the sorption coefficient of each of the gases at 17 psia, the average upstream pressure used for permeation, Table 5.3.

The sorption coefficients follow the order $N_2 \sim O_2 < CH_4 < CO_2$, which is approximately the order of critical temperature. The sorption coefficients are higher for the 800 ^{o}C films than for the 550 ^{o}C films. In CMS membranes, as with other porous materials, the majority of sorption occurs in the large pores in the membrane, whereas selective diffusion is controlled by the size of the ultramicropores connecting the large pores. The weight loss associated with 550 ^{o}C pyrolysis is ~5% less than for 800 ^{o}C pyrolysis. Therefore, the overall pore volume in the 800 ^{o}C is higher than at 550 ^{o}C as determined by the sorption capacity. This suggests that the pore volume is likely associated with the volume of decomposition products. Although additional pore sintering also occurs when heating from 550 ^{o}C to 800 ^{o}C, the effect is much more important for the small ultramicropores than for adsorptive pores, therefore sintering does not a have a large impact on the size of the adsorptive pores. Steel also observed an increase in the sorption capacity when heating from 550 ^{o}C to 800 ^{o}C when using both 6FDA:BPDA-DAM and Matrimid® precursors.

The sorption coefficient for 6FpDA 550 is approximately 5-10% higher than for 6FmDA 550. When the pyrolysis temperature is increased to 800 ^{o}C, the sorption

coefficient of the two precursors is very similar. Therefore, at 550 ^{o}C, the difference in sorption coefficients between 6FDA-6FpDA and 6FDA-6FmDA is greater than at 800 ^{o}C.

At 550 ^{o}C, the pore size distribution (both micropores and ultramicropores) in the membranes is likely broad, especially in 6FpDA 550 because the polymer has a high free volume. At 550 ^{o}C, the material is in an earlier state of decomposition and therefore the structure is speculated to be highly disordered. The adsorptive pore size at 550 ^{o}C is likely affected by both by-product evolution and by the initial free volume in the polymer precursor. As the temperature is increased to 800 ^{o}C, the material has almost completely decomposed and the pore volume has increased. The material is in a much more ordered state, as shown by the height of the WAXD peak representing the C-C spacing in graphite planes. The combination of the addition of more pores during pyrolysis followed by extensive molecular rearrangement apparently leads to the similarity in pore structure at 800 ^{o}C, as shown by the sorption coefficients for each membrane. This result is likely due to the similarities in the structure of the initial precursors. Steel has found that membranes pyrolyzed from different precursors at 800 ^{o}C for 8 hours have dissimilar sorption isotherms [3].

The sorption selectivity for the gas pairs of interest, O_2/N_2, CO_2/CH_4, and CO_2/N_2 is nearly constant for all of the membranes. The sorption selectivity is approximately 1 for O_2/N_2, 2.3 for CO_2/CH_4, and 6.5 for CO_2/CH_4. These results agree well with a similar study by Steel using Matrimid® and 6FDA:BPDA-DAM precursors. The O_2/N_2 sorption selectivity varied from 1.0 to 1.6 for O_2/N_2 while the CO_2/CH_4 selectivity varied from 4.0 to 5.8 (at different pressures from this study), though the precursor compositions were

very dissimilar. Since the structure of carbon membranes produced from all precursors consists mainly of amorphous carbon, the sorption affinity is rather similar for all membranes. This leads to similar sorption selectivities.

Table 5.3 Sorption coefficients for CMS membranes derived from 6FDA-6FmDA and 6FDA-6FpDA

Film	S_{N2}	S_{o2}	S_{CH4}	S_{CO2}	S_{O2}/S_{N2}	S_{CO2}/S_{CH4}	S_{CO2}/S_{N2}
		(cc_{STP}/cc_{carbon}-atm)					
6FmDA 550	10.2	10.6	26.9	64.3	1.0	2.4	6.3
6FpDA 550	10.8	14.5	32.0	70.5	1.3	2.2	6.6
6FmDA 800	12.8	12.0	38.2	86.1	0.9	2.3	6.7
6FpDA 800	13.2	12.4	38.3	84.6	0.9	2.2	6.4

5.3.3 Diffusion coefficients of CMS membranes derived from 6FDA-6FmDA and 6FDA-6FpDA

The diffusion coefficient of each of the membranes was calculated using steady state permeation/equilibrium sorption. Table 5.4 contains the diffusion coefficients for each of the membranes. The diffusion coefficients follow a similar trend as the permeability. The diffusion coefficients for each individual gas follows the order 6FpDA 550>6FmDA 550>>6FpDA 800>6FmDA800. The diffusion coefficients for the 800 ^{o}C films are approximately one order of magnitude lower than those at 550 ^{o}C. The results show that selectivity in these CMS membranes is primarily controlled by the diffusion coefficient, with sorption playing only a minor role. Though there was little difference in the sorption capacity of membranes produced from the two different precursors, there are considerable differences in the diffusivity. It was originally speculated that changing the free volume of the precursor would only have a very subtle effect on the pore structure of

the resulting CMS membrane. However, for ultramicropores, which are very close to the size of the gas pentrants, a decrease in the pore size by 0.1 Å can have a considerable effect on the diffusion coefficient. Since adsorptive pores are speculated to be on the order of ~1 nm, a 0.1 Å decrease in the pore size may have a negligible effect on the adsorption capacity. Therefore, changes in free volume appear to affect the diffusivity of the membranes while having a negligible effect on the sorptivity.

One unexpected result obtained in this section was that the CO_2 diffusion coefficient in 6FpDA 550 is larger than the O_2 diffusion coefficient. Similar results were also obtained by Steel for CMS produced from 6FDA:BPDA-DAM at 550 ^oC for 8 hours. Also, even more unexpectedly, the CO_2/CH_4 diffusion selectivity for 6FpDA 550 was larger than 6FmDA 550, even though the diffusion coefficients for 6FpDA are larger. These results are likely attributed to "entropic" selectivity as described by Singh for O_2 and N_2. This will be described in more detail below.

CO_2, N_2, and O_2 are spherocylindrical molecules while methane is fairly spherical. The diffusion selectivity is a product of an energetic factor and an entropic factor, Equation 2.14. The energetic selectivity is related to the activation energy required to overcome repulsions from the wall of the ultramicropore and is therefore related to the size of the minimum dimension of a gas molecule and the interaction energy with the pore wall. When separating CO_2 and CH_4, increasing the pore size would lower the activation energy that must be acquired to make a diffusive jump. Since the minimum dimension for CO_2 is smaller than CH_4, there will be a loss in selectivity because the change in activation energy will be more for CH_4 than CO_2 when the pore size in increased. The entropic contribution to diffusivity is related to the loss of degrees

of freedom as the molecule diffuses through an ultramicropore. Since methane is fairly spherical, it does not give up degrees of freedom as it diffuses through an ultramicropore. On the other hand, CO_2 is cylindrical and therefore, gives up rotational degrees of freedom if the pore size is smaller than the length of the molecule. Thus, entropic factors in diffusion generally favor methane. If the pore size is increased to a size where CO_2 gains a rotational degree of freedom, then the entropic selectivity will not favor CH_4 as much. Since the observed diffusivity is a product of both of these factors, it is possible that a small increase in pore size could increase both the permeability and the selectivity of CO_2/CH_4 because CO_2 gains a degree of freedom and the entropic factor overcomes the difference in the energetic factor.

Table 5.4 Diffusion coefficients obtained from steady state permeability/equilibrium sorption for 6FDA-6FpDA and 6FDA-6FmDA polyimides.

Film	D_{N2}	D_{o2}	D_{CH4}	D_{CO2}	D_{O2}/D_{N2}	D_{CO2}/D_{CH4}	D_{CO2}/D_{N2}
		(10^{-8} cm^2/s)					
6FmDA 550	2.3	18.2	0.50	15.1	8.1	30.6	6.7
6FpDA 550	4.5	20.0	0.68	25.0	4.4	37.4	5.6
6FmDA 800	0.21	1.11	0.03	0.29	5.4	9.2	2.0
6FpDA 800	0.34	2.8	0.09	1.5	8.3	16.7	4.4

5.4 OVERVIEW OF CORRELATION BETWEEN PRECURSOR STRUCTURE AND CMS PERFORMANCE

The primary goal of this portion of the study was to determine correlations between the free volume of a polymer precursor and the transport properties of the resulting CMS membranes. The free volume of 6FDA-6FpDA is 0.190 while the free volume for 6FDA-6FmDA is 0.175. TGA-FTIR has proven that the decomposition mechanism of both precursors is identical. The porosity in CMS membranes is controlled by the evolution of by-products along with any initial free volume in the precursor at the onset of polymer pyrolysis. The transport performance of CMS membranes derived from 6FDA-6FpDA have higher permeability and diffusion coefficients than 6FDA-6FmDA based CMS membranes, while the sorption capacities are fairly similar. The transport properties are controlled primarily by the diffusion coefficient, which is expected since diffusion in CMS membranes follows a molecular sieving mechanism. Therefore, these results suggest that precursors which have higher free volumes will produce CMS membranes with higher diffusion coefficients, all else being equal. This is a very important result when considering new materials to be used as precursors for CMS membranes. As an example, the oxygen permeability of 6FpDA 550 is approximately double that of 6FmDA 550, while the O_2/N_2 selectivity is only 6.4 as compared to 8.4 for 6FmDA 550. When the pyrolysis temperature is increased to 800 ^oC, O_2 permeability decreases by approximately one order of magnitude using either precursor. Therefore, the pyrolysis temperature is still one of the most important factors to consider when tailoring the separation performance of CMS membranes, but when optimizing for a specific separation, the polymer precursor free volume should be considered, particularly for the separation of large molecules such as hydrocarbons.

Though it is difficult to directly compare the membranes tested here with those tested in Chapter 4 and Appendix A due to dissimilar amounts of oxygen in the pyrolysis atmosphere during pyrolysis, some discussion is possible. The sorption capacities of the membranes formed in this chapter are higher at the respective temperatures than those produced in Chapter 4. This is likely due to the differences in the amount of by-products evolved during pyrolysis. Both of the precursors in this chapter have at least twice the amount of CF_3- groups as compared to the 6FDA:BPDA(x:y)-DAM polymers. Therefore, they have higher weight loss during decomposition and form a much higher pore volume.

Comparison of the permeability of 6FDA:BPDA-DAM 550 ^{o}C membranes formed in ~0.03 torr of oxygen (presented in Appendix A) shows that the permeabilities of the membranes produced in this chapter are higher. This is likely due to the two important structural factors mentioned in Chapter 4. First, both of the precursors in this chapter evolve more CF_3H during decomposition, which likely increases the pore size in both the micropore and ultramicropore range. Second, the two membranes in this study have higher free volumes than those in Chapter 4. These results suggest that both of these properties play a significant role in the formation of CMS membranes.

5.5 REFERENCES

1. Coleman, M.R., *Isomers of fluorine-containing polyimides for gas separation membranes*. 2002, University of Texas, Austin: Austin, TX.

2. Park, J.Y. and Paul, D.R., *Correlation and prediction of gas permeability in glassy polymer membrane materials via modified free volume based group contribution method.* Journal of Membrane Science, 1997. **152**(1): p. 23-29.

3. Steel, K.M., *Carbon membranes for challenging separations*, in *Department of Chemical Engineering*. 2000, University of Texas - Austin: Austin, TX.

CHAPTER 6

FORMATION AND CHARACTERIZATION OF CMS MEMBRANES UNDER DIFFERENT PYROLYSIS ENVIRONMENTS

This chapter will discuss the formation and characterization of CMS membranes under nominally inert pyrolysis atmospheres. Section 6.1 will present the background behind the study and the reason it was performed. Section 6.2 will discuss CMS membranes formed under inert environments at atmospheric pressure and compare the trends obtained in this study to similar studies. Section 6.3 will discuss CMS membranes formed in inert gases at sub-atmospheric pressures.

6.1 BACKGROUND

Appendix A presents a comparison between CMS membranes formed under different vacuum environments. It was determined that the amount of oxygen in the pyrolysis atmosphere had a significant effect on the separation performance. In this section, pyrolysis atmospheres containing an inert gas at both atmospheric pressure and sub-atmospheric pressure will be investigated. Limited studies have been performed to compare the separation performance of CMS membranes produced under different pyrolysis atmospheres. The most detailed study came from Geiszler and Koros [1, 2], who compared the performance of CMS asymmetric hollow fiber membranes produced in (1) vacuum and (2) inert gas purge systems. A similar study was performed by Vu [3], but only one inert purge gas was investigated.

6.1.1 Comparison of vacuum and inert purge pyrolysis

Geiszler [1, 2] produced asymmetric CMS hollow fibers from 6FDA:BPDA(1:1)-DAM asymmetric hollow fibers supplied by Dupont® (ID 157 μm, OD 231 μm) using

pyrolysis protocols similar to the two protocols used in this study (550 ^{o}C and 800 ^{o}C). The fibers were first placed on either a stainless steel mesh or a ribbed quartz plate and held in place using aluminum wire. The same pyrolysis equipment used in the current study was used by Geiszler [1, 2]. The fibers were placed in a quartz tube and the tube was either evacuated (<0.1 mm Hg) or the system was purged with an inert gas. The maximum pressure used for vacuum pyrolysis was higher than any of the previous studies detailed in this thesis, typically 0.03 or 0.05 torr. Three different inert gases were used, argon, helium, and carbon dioxide, at two different flow rateS (20 and 200 ccSTP/min). The earlier CO_2 results will not be discussed here because CO_2 was not investigated in the present study. The separation performance was investigated by testing the permeance and selectivity for both O_2/N_2 and H_2/N_2. Table 6.1 shows the separation performance of fibers produced in vacuum and in a flowing stream at 200 ccSTP/min at 550 ^{o}C. The results show that fibers pyrolyzed in inert gases have a much higher permeance but lower selectivity than fibers produced in vacuum. It should be noted that these values are permeances and not permeabilities because the thicknesses of the selective layer for asymmetric hollow fibers are not known precisely. Geiszler [1, 2] suggested that within the error of the permeance data, that there is no difference in permeance between fibers produced in helium and argon, even though the average O_2 and N_2 permeances for the fibers produced in argon was approximately twice that for fibers produced in helium.

Table 6.1 O_2/N_2 and H_2/N_2 separation performance for asymmetric CMS hollow fiber membranes produced at 550 ^oC [1, 2]. The argon and helium were flowing at 200 cc(STP)/min.

Pyrolysis Atmosphere	O_2 flux (GPU)	O_2/N_2	H_2 flux (GPU)	H_2/N_2	N_2 flux (GPU)
Vacuum	19.4 ± 3.0	10.2 ± 0.6	306 ± 28	179 ± 28	1.9±0.4
Argon	174 ± 75	4.3 ± 1.4	594 ± 97	15.5 ± 9.6	40.5±22
Helium	97 ± 37	5.4 ± 0.7	511 ± 96	23.8 ± 8.8	18.0±12

Vu performed a similar study to investigate the effect of purge gas pyrolysis on CMS asymmetric hollow fiber membranes produced from Matrimid® precursors [3]. In that study, the same general procedure was used to produce the CMS hollow fiber membranes and the separation performance of the membranes was investigated using a 90% CH_4/10% CO_2 mixture. The results for membranes produced at 550 ^oC are shown in Figure 6.1. The results show the same trends as seen by Geiszler [1, 2]. Membranes produced in a 200 ccSTP/min helium purge stream had twice the permeance of those produced in vacuum with a 65% decrease in the selectivity. Therefore, these results suggest that for asymmetric hollow fibers, no matter the nature of the precursor, inert purge pyrolysis produces higher permeance than vacuum pyrolysis, with an accompanying decrease in selectivity.

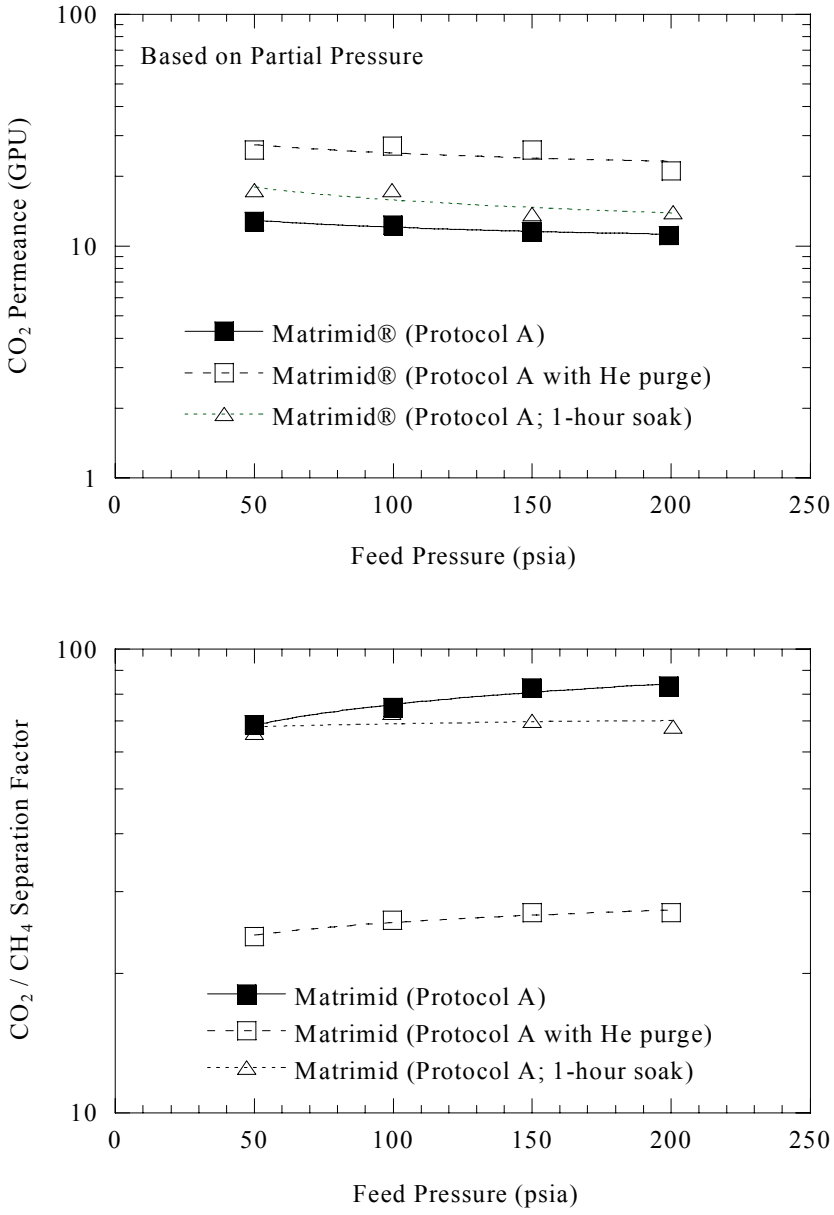

Figure 6.1 Separation performance of asymmetric hollow fiber CMS membranes under vacuum and under a 200 ccSTP/min helium purge at 550 ^{o}C (Protocol A). The feed gas was 10% CO_2/90% methane [3].

There have been no studies, up to now, that probe the subtle effect of pyrolysis environment on the separation performance of dense flat CMS membranes produced using the same thermal profile. Suda and Haraya [4] have compared the results for dense CMS membranes produced from Kapton polyimide in 500 ccSTP/min argon and in vacuum. Unfortulately, the pyrolysis conditions for the samples are not identical. The membranes produced in vacuum had a heating rate of 10 ^{o}C/min and were produced at 873, 1073 and 1273 K. Membranes produced in argon utilized a final pyrolysis temperature of 1223 K with heating rates of 1.33, 4.5, and 13.3 K/min. Though these differences seem very subtle, the authors have shown that subtle changes in pyrolysis temperature and heating rate have a significant impact on separation performance. Table 6.2 compares the results for the 1273 K vacuum film and the 1223 K film produced at 13.3 K/min in argon. The separation performances of the two films are very similar. Therefore, these results appear to contradict those for the CMS hollow fibers in the previous studies in that there is no difference in properties between inert purge and vacuum pyrolysis. Another major difference between the studies of Geiszler [1, 2] and Suda and Haraya [4] is the pyrolsis temperature used. Membranes produced by Suda and Haraya [4] are produced at very high temperatures, and therefore have permeabilities that are very low. High temperature pyrolysis might influence the separation performance to a much greater extent than the purge gas, and therefore differences between the two different pyrolysis environments in that study may be negligible. Suda and Haraya [4], though, have also shown that subtle changes in the pyrolysis rate can have a significant impact on the separation performance, even at 1223 K.

Table 6.2 Comparison of CMS dense membranes produced under different atmospheres using Kapton precursors. Permeabilities are in Barrer [4]

	KP1273 (10 K/min, 1273 K, vacuum)	KP1223 (13.3 K/min, 1223 K, 500 ccSTP/min Ar)
P_{HE}	27.9	26.4
He/N_2	680	618
P_{H2}	59.4	53.1
H_2/N_2	1450	1240
P_{CO2}	4.15	3.54
CO_2/N_2	101	82.7
P_{O2}	0.96	0.92
O_2/N_2	23.4	21.6
P_{N2}	0.04	0.04

6.1.2 Influence of inert purge flow rate

As mentioned previously, Geiszler and Koros [1, 2] have also investigated the effect of inert purge flow rate on the separation performance of CMS hollow fiber membranes. Two different flow rates were investigated, 20 ccSTP/min and 200 ccSTP/min at atmospheric pressure. These flow rates correspond to superficial velocities of 3.1 and 31 cm/min at 550 ^{o}C and 1 atm. The results for membranes produced at 550 ^{o}C in argon and in helium can be found in Table 6.3. The permeance for the membranes produced in 20 ccSTP/min are at least two orders of magnitude lower than those produced in 200 ccSTP/min flow rates. There is very little difference in the selectivity at different flow rates.

The data in Table 6.3 also show that the average weight loss is ~2% higher for films pyrolyzed under 200 ccSTP/min of helium than for 20 ccSTP/min. Therefore, the purge flow rate appears to influence the decomposition of the polyimide and therefore influences the microstructure of the resulting CMS membrane.

Table 6.3 Permeation performance and weight loss of asymmetric hollow fiber CMS membranes produced under different atmosphere and different flow rates [2]

Pyrolysis Atmosphere	Flow rate (ccSTP/min)	O_2 Flux (GPU)	O_2/N_2 selectivity	Average % weight loss
Argon	200	174 ± 75	4.3 ± 1.4	-----
Argon	20	0.24 ± 0.21	4.5 ± 2.5	-----
Helium	200	97 ± 37	5.4 ± 0.7	36.1 ± 2.0
Helium	20	0.08 ± 0.05	4.6 ±0.9	33.9 ± 3.8

6.1.3 Hypotheses concerning the effect of pyrolysis atmosphere and gas flow rate

To explain the differences in membrane performance between inert purge pyrolysis and vacuum pyrolysis, Gieszler and Koros [1, 2] have suggested that the "mechanism" of the carbonization reaction may change when a conductive mode of heat transfer is added to the primarily radiative mode in vacuum pyrolysis. Mass transfer is also influenced by adding a convective mode to the existing conductive mode. This hypothesis was based on work by Dickens [5, 6] which showed that the activation energies of decomposition for polyethylene and isotactic polypropylene are strongly dependent on the pressure under which they are decomposed.

Figure 6.2 is a cartoon that was used to demonstrate the hypothesis. As the polyimide begins to degrade, by-products evolve from the backbone of the molecule. The by-products are mainly light molecules such as CF_3H, CO_2, CO, and CH_4. Some larger aromatics also evolve, presumably due to the decomposition of the imide along the polymer backbone, as discussed in Chapter 4. The aromatic by-products have the potential to further decompose (and attach to the carbon structure) or to evolve from the

membrane without further decomposition. It was speculated that as the by-products evolve from the existing membrane (which is in a transient state in terms of morphology), diffusion is limited by the selective pores already formed. Therefore, larger molecules may further decompose at selective ultramicropores and therefore reduce the pore size even further. The authors suggested that by increasing convection, by increasing the mass flow rate, by-products are more easily swept away from the surface.

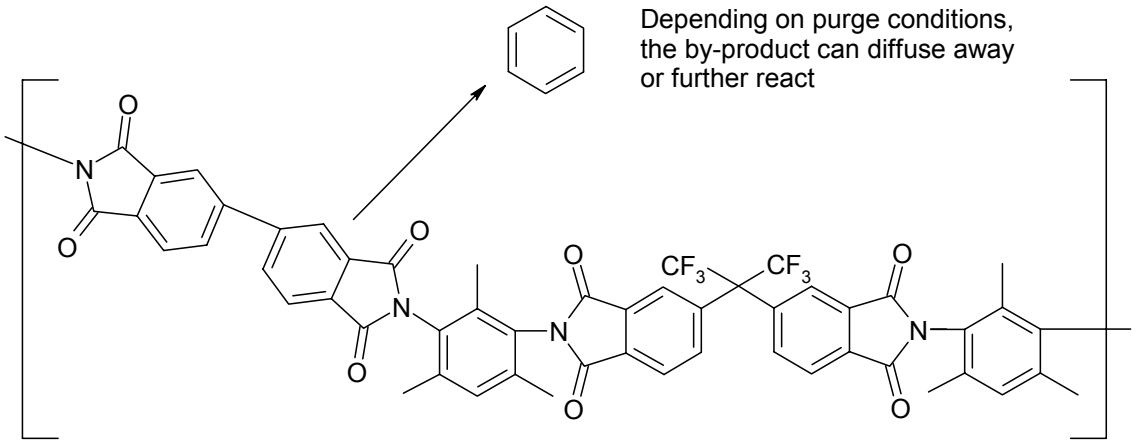

Figure 6.2 Cartoon depicting by-products evolving from the carbon membranes during pyrolysis. The by-products can diffuse out of the membrane or further react and form part of the carbon structure [2].

The hypothesis would explain two phenomena: (1) membranes produced at 200 ccSTP/min have a higher overall mass loss than those produced at 20 ccSTP/min and (2) membranes produced at 200 ccSTP/min have higher permeability that those at 20 ccSTP/min. This hypothesis seems valid when comparing films produced under different flow rates. The theory does not explain why membranes produced in vacuum have a higher permeability and higher selectivity than those produced at a flow rate of 20 ccSTP/min. It may be that the complex morphology of asymmetric hollow fibers creates a variety of factors which affect the permeation properties of membranes produced under different environments. Therefore, analysis using a more simplified geometry is warranted.

6.1.4 Description of current study and motivation

The studies of Geiszler and Koros [1, 2], Vu and Koros [3, 7, 8], and Suda and Haraya [4] do not lead to any general trends which can be used to explain the effect of atmospheric conditions on the separation performance of CMS membranes. Several factors may contribute to these results: (1) Geiszler and Koros [1, 2] along with Vu and Koros [3] performed studies using asymmetric hollow fibers as the precursor, which has a complex morphology and makes CMS formation somewhat more complicated and (2) the flat sheet membranes produced by Suda and Haraya [4] under different atmospheres were not produced under identical pyrolysis conditions, and therefore comparison between the two will inherently contain uncertainty.

In this study, dense flat CMS membranes were produced under vacuum and in helium and argon purges. The effects of purge flow rate as well as atmospheric pressure were also investigated. The purpose of this study was to verify the trends of Geiszler and

Koros [1, 2] using a more simplified (non-asymmetric) morphology and expand on the hypotheses explaining the observed phenomena to include the influence that oxidation has on the separation performance of CMS membranes .

6.2 SYNTHESIS AND SEPARATION PERFORMANCE OF CMS MEMBRANES PRODUCED IN INERT PURGE ENVIRONMENTS AT ATMOSPHERIC PRESSURE

CMS membranes were produced using the same equipment as in the previous studies for vacuum pyrolysis. The flow rate of purge gas was controlled by a MKS mass flow controller. Helium (O_2<0.1 ppm) and argon (O_2<4 ppm) were used as the purge gases. The volumetric flow rate through the pyrolysis furnace was verified using a bubble flow meter. Purge flow rate was varied from 50 cm^3/min to 200 cm^3/min, at room temperature. Before pyrolysis, the inert gases were used to purge the pyrolysis apparatus for approximately 4 hours. All films had a thickness of approximately 2 mils.

Table 6.4 shows the separation performance of CMS membranes produced from 6FDA:BPDA(1:1)-DAM using the 550 ^oC thermal profile. The results for two of the vacuum pyrolysis conditions discussed in Appendix A have also been included for comparison. The results show that there is very little difference between the permeability of membranes produced at different inert purge flow rates. Within the error associated with these experiments, no trends can be developed which relate separation performance to flow rate. The data for the argon purge gases may suggest that increasing the flow rate increases the permeability, but this trend is only true for some of the gases tested, and therefore no *overall* trend can be speculated. There is also very little difference between membranes produced under argon and helium purges. It could be speculated that the

selectivity for films produced in helium is higher than those produced in argon, but this is only observed for the O_2/N_2 separation, and it is not a strong trend.

The permeability of membranes produced using inert purge pyrolysis is similar to that obtained using 0.005 torr vacuum pyrolysis. The selectivity of the films produced in vacuum is higher than those produced using an inert purge. When compared to membranes produced in higher pressures of air (0.042 torr), the inert purge membranes have a much higher permeability and a lower selectivity than with vacuum pyrolysis.

The results obtained in this study are in agreement with many of the results obtained by Geiszler and Koros [2] as well and Vu and Koros [3]. Both studies show that membranes produced at 200 ccSTP/min have a much higher permeability and lower selectivity than those produced in vacuum. It should be noted that in this study, the flow rate is somewhat lower because the flow rate was measured at room temperature. Therefore, flow rates for 50, 100, and 200 cm^3/min correspond to 46, 93, and 185 ccSTP/min, respectively. In the previous studies, the maximum pressure of vacuum pyrolysis were 0.050 torr and 0.1 torr. Therefore, vacuum pyrolysis was likely performed under conditions similar to the 0.042 torr films in the current study. If that was the case, the results are in agreement with the current study.

The results from the current study suggest that the flow rate of purge gas does not have a significant effect on the separation performance. These results are in disagreement with Geiszler and Koros [1, 2], who showed that flow rate had a major effect on gas permeance. Several factors may be the cause of this discrepancy, the most likely is associated with the complex morphology of asymmetric hollow fiber membranes

when compared to flat sheet membranes. This surprising discovery is beyond the scope of this study to pursue; however, it certainly should be clarified.

Table 6.4 Separation performance of dense flat CMS membranes produced at 550 ^{o}C, atmospheric pressure. The flow rate was measured at the temperature of the laboratory, 295 K. The argon contains ≤4 ppm O_2 and the He contains ≤ 0.1 ppm O_2.

Purge Gas	Flow rate (cm^3/min)	P_{O2} (Barrer)	O_2/N_2	P_{CO2} (Barrer)	CO_2/CH_4
He	50	620	7.5	2850	58.4
He	200	581	7.3	2845	68.6
Ar	50	537	7.1	2997	75.3
Ar	100	599	6.3	3064	43.8
Ar	200	647	6.4	3110	54.9
0.005 torr Air		630	8.8	2580	71
0.042 torr air		52	10	240	110

The hypothesis developed in Appendix A can be used to describe the similarities and differences between membranes produced in the presence of an inert purge gas and in vacuum environments. Normalization of all pyrolysis atmospheres can be performed by considering the "total oxygen exposure coefficient", q_{o2}, which describes the total number of moles of oxygen available for reaction during the pyrolysis run. Appendix B discusses the calculations used to determine this value and all assumptions used in the calculation, but a few key points are noted here. First, the ultramicropores are considered "active" from the onset of thermal decomposition until the temperature in the quartz tube is below 500 ^{o}C. This choice was arbitrary but has very little impact on the trends observed in the data. Second, the source of oxygen is considered the volume above the

quartz plate during pyrolysis. Finally, all calculations are based on an oxygen concentration of 4 ppm in the argon cylinder. The actual concentration in the cylinder is unknown and therefore the values calculated represent the maximum amount of oxygen possibly available during pyrolysis. Table 6.5 lists the total oxygen exposure coefficient for all pyrolysis conditions. Follow-up studies should probe the detailed effects of trace amounts of O_2 in the inert sweep gas.

Table 6.5 Comparison of the total oxygen exposure coefficient for different pyrolysis atmospheres. The flow rate was measured at 295 K using a bubble flow meter. A discussion of the method used to estimate the flow rate of gases in the vacuum systems as well as the calculation q_{o2} can be found in Appendix B.

Purge Gas	Flow rate (cm^3/min)	Pressure (torr)	q_{O2} (10^{-8} mol)
He	50	760	2.8
He	200	760	11.2
Ar	50	760	110
Ar	100	760	220
Ar	200	760	440
Air	vacuum	0.005	93
Air	vacuum	0.042	3100

The largest oxygen exposure coefficient was obtained for vacuum pyrolysis at 0.042 torr. Though this system is under vacuum, air leaks result in oxygen exposure. The oxygen exposure coefficient for the 0.042 torr vacuum condition is approximately an order of magnitude larger than any other condition, including 0.005 torr vacuum. The minimum pressure obtained while pulling active vacuum is associated with the steady state between the pumping speed and the leak rate. At low pressures, the pumping speed is highly dependent on pressure and therefore the leak rate of atmospheric air into the 0.042 torr system is much faster than at the 0.005 torr condition. The leak rates, represented by the molar flow rate of gas into the system, are discussed in Appendix B.

The oxygen exposure coefficients for all of the inert purge systems are much lower than the 0.042 torr vacuum system and comparable to the 0.005 torr system. This result is not intuitive. Even though a constant purge is allowed to flow during the inert purge systems, the oxygen concentration in the purge streams is very low, and therefore the total oxygen exposure coefficient is low. Even though the 0.042 torr system is at a low pressure, leaks are attributed to air, which has 21% (210,000 ppm) oxygen. Therefore, leaks contribute significantly to the exposure of oxygen. Of course, the oxygen exposure in the purge systems is proportional to the flow rate of purge gas.

The trends obtained in the total oxygen exposure coefficient compare well with the trends in the permeation data in Table 6.4. Assuming the illustration in Figure A.2 is valid, higher oxygen exposure coefficients could have two effects on the ultramicropores near the surface of the CMS membrane. First, if there is not a significant amount of oxygen to react with all of the ultramicropores on the surface of the membrane, then a higher exposure coefficient would suggest a higher “surface coverage” of oxidized pores.

Second, if there was significant oxygen to react with all ultramicropores on the surface, then any additional oxygen would diffuse into the membrane and react to increase the thickness of the surface oxidized layer. Both of these situations lead to a decrease in the permeability (and increase in the selectivity), but the second condition is more likely. Therefore, since the system under 0.042 torr of vacuum has a much higher oxygen exposure coefficient than the other systems, CMS membrane produced in it have a lower permeability and higher selectivity.

Even though the oxygen exposure coefficient is dependent on the flow rate of purge gases through the quartz tube, the difference in oxygen exposure coefficients for systems with different purge flow rates is very small in comparison to the difference between inert purges and the 0.042 torr vacuum system. This is likely why there is no true trend in the permeation data at different flow rates. It is likely that within experimental error, the effect of oxygen exposure coefficient is not noticeable at different flow rates. Also, the hypothesis concerning the data would suggest that the argon systems should have a lower permeability than the helium systems due to a considerably higher oxygen exposure coefficient. It is speculated that two factors could attribute to the discrepancy in permeation data. First, the oxygen concentration in the argon purge streams is overestimated, or second, the difference between the two is still negligible in comparison to the 0.042 torr system.

Overall, trends in the permeation data correlate well with the oxygen exposure coefficient derived in this section, though admittedly, the oxygen exposure coefficient is only a crude measure of O_2 availability. There is still a small discrepancy in the selectivity data. All membranes produced under inert purges have a lower selectivity

than the 0.005 vacuum pyrolysis, even though the permeabilities are similar. Therefore, there are likely other factors which contribute to changes in the membrane morphology when converting from inert purge pyrolysis to vacuum pyrolysis, but the most significant factor appears to be the level of exposure to oxygen during pyrolysis.

6.3 SYNTHESIS AND SEPARATION PERFORMANCE OF CMS MEMBRANES PRODUCED IN INERT PURGE GAS ENVIRONMENTS BELOW ATMOSPHERIC PRESSURE

CMS membranes were also produced in an inert purge pyrolysis system at reduced pressure. In these experiments, a gas cylinder with a regulator was attached to the left side of the quartz tube used for pyrolysis. A needle valve was used to control the flow rate of gas through the quartz tube. The pressure was measured on the left side of the furnace as in vacuum experiments. A vacuum pump was attached to the right side of the pyrolysis furnace. The vacuum pump pulled active vacuum throughout the experiment. During each experiment, the needle valve between the pressure regulator on the gas cylinder and the quartz tube was adjusted until a desired pressure was achieved. The MKS metering valve was not designed to operate at low pressures, and therefore was disconnected during these experiments. Two pressures were used in this study, 3 torr and 8 torr. These pressures were chosen for two reasons: (1) the pressure transducer had a pressure limit of 10 torr and (2) these pressures correspond to flow rates similar to the previous experiments performed at atmospheric pressure. The molar flow rate of gas through the pyrolysis system was estimated by attaching a bubble flow meter to the outlet of the vacuum pump.

The separation performances for membranes produced using the 550 ^{o}C profile are listed in Table 6.6. The permeability for these membranes are approximately double those of the membranes produced in atmospheric pressure inert purge environments. As with the membranes produced at atmospheric pressure, no conclusions can be drawn about the effect of flow rate or purge gas composition. Membranes produced in helium have a lower permeability and generally have a higher selectivity than those produced in argon, but the differences are very small. Table 6.7 compares to total oxygen exposure coefficient for the membranes.

Table 6.6 Separation performance of dense flat CMS membranes produced at 550 ^{o}C, reduced pressure. Flow rates were measure at 295 K.

Gas	Flow rate (cm^3/min)	Pressure (torr)	P_{O2} (Barrer)	O_2/N_2	P_{CO2} (Barrer)	CO_2/CH_4
He	46	3	1186	7.6	5407	61.8
He	270	8	1341	6.6	6551	46.3
Ar	46	3	1527	6.7	7281	46.0
Ar	270	8	1311	6.2	6874	41.9

Table 6.7 Comparison of oxygen concentrations in quartz tube for CMS membranes produced under reduced pressure inert purge pyrolyses

Purge Gas	Flow rate (cm^3/min)	Pressure (torr)	q_{O2} (10^{-8} mol)
He	46	3	2.5
He	270	8	14
Ar	46	3	100
Ar	270	8	565

The oxygen exposure coefficient for these membranes is similar to those produced at atmospheric pressure. Therefore, it appears that a factor other than oxygen exposure coefficient has an effect on the permeability and selectivity of these membranes. It is hypothesized that the difference could be related to the velocity of the purge gas as it flows through the quartz tube. The molar flow rates of purge gas are similar to those produced under the previous conditions at atmospheric pressure, but the pressure is reduced. Therefore, the volumetric flow rate of gas inside the pyrolysis tube is considerably different. Table 6.8 lists the residence time of a gas molecule in the "reaction zone" during pyrolysis for each of the pyrolysis conditions. The results show that the residence time is significantly dependent on the pyrolysis conditions. The residence time for the reduced pressure inert purge systems are at least an order of magnitude lower than the systems at atmospheric pressure and the systems under vacuum. Though not entirely quantitative, these result suggest that the likelihood of an oxygen molecule to come in contact with a reactive site on the surface of the CMS membrane is lower in the low pressure inert systems than under any of the other conditions because each oxygen molecule spends much less time in the "reaction zone".

Table 6.8 Residence times of oxygen molecules in the "reaction zone" of the pyrolysis furnace. Flow rates are at 295 K and 1 atm.

Purge Gas	Flow rate (cm^3/min)	Pressure (torr)	residence time (s)
He	50	760	43
He	200	760	11
Ar	50	760	43
Ar	100	760	21
Ar	200	760	11
He	46	3	0.18
He	270	8	0.086
Ar	46	3	0.18
Ar	46	8	0.086
Air	vacuum	0.005	16
Air	vacuum	0.042	2.3

6.4 DISCUSSION AND REVIEW OF RESULTS

In this section, the effect of pyrolysis atmosphere on the separation performance of CMS membranes has been investigated. The results show that membranes produced in inert purge gases at atmospheric pressure have similar results to those produced in vacuum at 0.005 torr. To compare these systems, the total oxygen exposure coefficient was calculated and the results show that the coefficient is similar for all atmospheric pressure inert purge conditions and in 0.005 torr of vacuum. The oxygen exposure coefficient at 0.042 vacuum, though, is one to two orders of magnitude higher. The membranes at 0.042 torr, therefore, have a much lower permeability and higher selectivity because the extent of oxidation of the ultramicropores is higher.

The permeability of membranes produced at low pressures in inert purges have a higher permeability than those produced at atmospheric pressure, though the oxygen exposure coefficients are similar for both sets of membranes. These results are attributed

to a decreased residence time of oxygen molecules during pyrolysis for the reduced pressure systems. That is, even though the total oxygen exposure in the reaction zone is similar in both atmospheric pressure and low pressure systems, in the low pressure systems the oxygen molecules flow through the reaction zone at a much higher rate and therefore the likelihood of contact with an "active" ultramicropore is much lower.

Up to this point, the hypothesis describing the difference in separation performance for all membranes produced under different environments has been associated with oxygen exposure. Though it is hypothesized that this is the most important factor related to changes in the pyrolysis environment, there are likely other differences, between environments. Geislzer and Koros suggested that the inclusion of an inert purge at atmospheric pressure could affect both the heat transfer and mass transfer characteristics of the pyrolysis environment. Though it is speculated that these effects are likely small, Appendix C contains an analysis of the mass transfer and heat transfer coefficients of each of the conditions used in this study, as well as a discussion of the effects that each might have on separation performance.

From the results in this study, it appears that optimizing the separation performance of CMS membranes should include an analysis of the total oxygen exposure during pyrolysis. All of the membranes produced in this study were exposed to small amounts of oxygen, and therefore the level of oxidation is limited. It is speculated that the oxygen in the membranes produced here reacted with the ultramicropores and decreased the effective critical ultramicropore size. It is well known that exposure to high levels of oxygen has a different effect on CMS membranes. In Chapter 2 it was mentioned that exposure to air at high temperatures is a well known method for

increasing the pore sizes. Therefore, if the extent of oxidation is high enough, oxygen will attack the membrane and there will be an accompanying evolution of CO_2. In that case the membranes are effectively being burned at the ultramicropores, which increases the average pore size. Fuertes has used oxidative post treatment to form selective surface diffusion membranes from molecular sieving membranes, as an example of the effect of oxidation on increasing the pore size [9, 10]. Therefore, the use of oxygen as an engineering tool to form CMS membranes will require optimization. It may be possible to narrow the pore size distribution of membranes with oxidative post treatment if the total oxygen exposure coefficient in the membrane is kept low. This could be particularly important in the production of asymmetric hollow CMS fiber membranes, where the selective layer is thin. Doping the selective layer with oxygen molecules could be a tool to tailor the separation performance for a desired separation.

6.5 REFERENCES

1. Geiszler, V.C. and Koros, W.J., *Effects of Polyimide Pyrolysis Conditions on Carbon Molecular Sieve Membrane Properties.* Industrial and Engineering Chemistry Research, 1996. **35**: p. 2999-3003.

2. Geiszler, V., *Polyimide Precursors for Carbon Molecular Sieve Membranes.* 1997, University of Texas, Austin: Austin.

3. Vu, D.Q., *Formation and characterization of asymmetric carbon molecular sieve and mixed matrix membranes for natural gas purification*, in *Department of Chemical Engineering*. 2001, University of Texas at Austin: Austin, TX.

4. Suda, H. and Haraya, K., *Gas Permeation through Micropores of Carbon Molecular Sieve Membranes Derived from Kapton Polyimide.* Journal of Physical Chemistry B, 1997. **101**: p. 3988-3994.

5. Dickens, B., *Thermally Degrading Polyethylene Studies by Means of Factor-Jump Thermogravimetry.* Journal of Polymer Science, Polymer Chemistry, 1982. **20**: p. 1065-1087.

6. Dickens, B., *Thermal Degradation Study of Isotactic Polypropylene Using Factor-Jump Thermogravimetry.* Journal of Polymer Science, Polymer Chemistry, 1982. **20**: p. 1169-1183.

7. Vu, D.Q., Koros, W.J., and Miller, S.J., *Effect of Condensable Impurities in CO2/CH4 Gas Feeds on Carbon Molecular Sieve Hollow-Fiber Membranes.* Industrial and Engineering Chemistry Research, 2003. **42**: p. 1064-1075.

8. Vu, D.Q., Koros, W.J., and Miller, S.J., *High Pressure CO2/CH4 Separation Using Carbon Molecular Sieve Hollow Fiber Membranes.* Industrial and Engineering Chemistry Research, 2002. **41**: p. 367-380.

9. Fuertes, A.B., *Effect of air oxidation on gas separation performance of adsorption-selective carbon membranes.* Carbon, 2001. **39**: p. 697-706.

10. Fuertes, A.B., *Adsorption-selective carbon membranes for gas separation.* Journal of Membrane Science, 2000. **177**: p. 9-16.

CHAPTER 7

SUMMARY, CONCLUSIONS, AND RECOMMENDATIONS

7.1 SUMMARY AND CONCLUSIONS

Currently, CMS membranes provide the most attractive pure material alternative to polymer membranes for high performance gas separation. Over the last 20 years, CMS membranes have been formed from the thermal decomposition of polymer precursors, though the relationship between CMS synthesis methods and separation performance is only partially understood. The goals of this study were to determine the impact of two key CMS formation parameters on the separation performance of CMS membranes: 1) polymer precursor composition and 2) pyrolysis atmosphere. Though parameters such as pyrolysis temperature and thermal soak time have been investigated extensively in relation to CMS separation performance, the two parameters investigated in this study have only recently been explored.

In Chapter 4, the synthesis of CMS membranes from 6FDA:BPDA(1:1)-DAM and 6FDA:BPDA(1:2)-DAM was investigated. The decomposition mechanism of the polymer was analyzed using TGA-IR and revealed to involve evolution of CO, CO_2, CH_4, CF_3H, HF, and some aromatics during pyrolysis. The average d-spacing of the CMS membranes as determined by WAXD is smaller for the 6FDA:BPDA(1:2)-DAM films. The separation performance was investigated using permeation and to some extent equilibrium sorption. The results show that films produced using 6FDA:BPDA(1:1)-DAM are more permeable and generally less selective than those produced from 6FDA:BPDA(1:2)-DAM. These results are attributed to an increase in the average ultramicropore size of 6FDA:BPDA(1:1)-DAM due to the evolution of larger amounts of

CF_3H during pyrolysis and an increase in polymer free volume as compared to 6FDA:BPDA(1:2)-DAM.

In Chapter 5, the synthesis of CMS from 6FDA-6FpDA and 6FDA-6FmDA was investigated. The structures of these two polymers are similar and TGA revealed that the weight loss in the two materials during pyrolysis is essentially the same. The polymer free volume of these two materials is quite different. 6FDA-6FpDA has a free volume of ~0.190 while 6FDA-6FmDA has a free volume of ~0.175. The separation performance of CMS membranes produced from these materials showed that membranes produced from 6FDA-6FpDA had higher permeabilities and diffusivities than those produced from 6FDA-6FmDA. These results were attributed to increased free volume in the polymer precursor which is maintained to some extent after thermal decomposition as differences in membrane structure.

In Chapter 6, the separation performance of CMS membranes produced under nominally inert flowing gases were compared to membranes produced in vacuum in Appendix A. The results were also compared to a study performed by Geiszler, who performed a similar study but used asymmetric hollow fibers as the precursor. A "total oxygen exposure coefficient" was used to describe the amount of oxygen available under each pyrolysis condition. The results from this study showed that the total amount of oxygen available during pyrolysis had a significant impact on CMS separation performance. The results also suggest that increased convection could affect mass transfer, heat transfer, and the residence time of oxygen in the quartz tube during pyrolysis. Appendix A also contains work related to Chapter 6 and discusses the repeatable formation of CMS membranes under "vacuum pyrolysis" conditions as well as

the effect of polymer precursor thickness on the separation performance and repeatable membrane formation.

The following specific conclusions can be drawn from this study.

- The separation performance of CMS membranes produced from 6FDA:BPDA(x:y)-DAM copolyimides depends on the 6FDA:BPDA ratio. Increasing the ratio of 6FDA:BPDA results in an increase in CMS permeability for membranes produced at 550 ^{o}C and 800 ^{o}C.
- 6FDA-6FmDA and 6FDA-6FpDA are a useful series of polymers for determining the effect of polymer free volume on the separation performance of CMS membranes. Analysis of the decomposition of two precursors using TGA shows that the weight loss curves are virtually identical. Differences in the pore structure (and separation performance) between membranes produced from the two precursors are therefore related to only the free volume and not the evolution of different amounts of by-products. The permeabilities of CMS membranes produced from 6FDA-6FpDA are higher than for 6FDA-6FmDA and therefore it appears that increasing the polymer free volume increases the ultramicropore size in CMS membranes.
- The gas separation performance of all of the CMS membranes produced in this study was controlled by the diffusion rate.

The sorption selectivities of all membranes are similar. Increasing the pyrolysis temperature lowered the permeability of all membranes in this study.

- The separation performance of carbon materials formed at different pyrolysis pressures between 0.005 and 0.42 torr is strongly dependent on the pressure of pyrolysis, or more specifically the atmosphere during the latter stages of pyrolysis and "cool-down." This is attributed to changes in the amount of oxygen in the pyrolysis environment atmosphere during CMS membrane formation. Increasing the pressure (assuming the pressure is comprised of an air atmosphere) decreases the CMS permeability and generally increases the selectivity.
- In general, the separation performance of CMS membranes produced from the same precursor, using the same thermal profile, is related to the total amount of oxygen available to the CMS membrane during pyrolysis.

7.2 Recommendations

In this section, several recommendations are listed to develop more detailed relationships between the pyrolysis atmosphere and the resulting microstructure of CMS membranes. Of particular interest are experiments which elucidate the relationship between oxygen exposure during pyrolysis and CMS separation performance. The recommended experiments are designed to expand on the current study.

Accurately control the total oxygen exposure coefficient during pyrolysis and post pyrolysis cool down

One of the difficulties encountered in this study was accurate determination of the oxygen exposure coefficient. Vacuum pyrolyses involve very low molar flow rates, and therefore, direct measurement of the flow rate is difficult. Therefore, indirect methods based on pump performance must be used. To more accurately determine the oxygen exposure during pyrolysis, it is recommended that purge gases which have specified concentrations of oxygen be used as the primary method of pyrolysis.

For consistency, a study investigating the affect of helium purge with 0.1, 1, 25, and 100 ppm of oxygen would provide a significant range of investigation, similar to that investigated in the current study. It is also suggested that a portable ppm level oxygen analyzer (such as a Teledyne 311XL) be attached to the outlet of the quartz tube to measure oxygen concentrations. This would be particularly useful during "thermal soak" to determine the amount of oxygen consumed. Using this type of system, more accurate relationships could be developed between oxygen exposure and CMS properties.

Deconvolute the effects of purge flow rate and oxygen exposure coefficient

The results in the current study suggest that the residence time of oxygen in the quartz tube during pyrolysis may impact the separation performance. To investigate this effect to a greater extent, it is important to keep the total oxygen exposure constant, while changing the residence time of oxygen molecules. This study could also be performed using the gases suggested in the previous section. For example, the oxygen exposure coefficient of a 25 ppm stream at 200 ccSTP/min is the same as a 100 ppm stream at 50 ccSTP/min, while the residence time is 4 times higher for the first stream. Analysis of

membranes produced under both conditions could allow the effects of oxygen exposure and residence time to be deconvoluted.

Determine the relationship between oxidation and pore formation

The microstructure of CMS membranes is related to the precursor composition, the thermal degradation profile, and the pyrolysis atmosphere. In the current study, it has been assumed that the pore size is mainly dependent on the thermal profile and the precursor composition, and that oxidation is supplemental. This suggests that there is an intrinsic pore structure related to the polymer precursor composition and the thermal profile. Controlled oxidation (or other reactions) can then be used to alter the intrinsic properties. It is likely that the intrinsic properties are related to the amount of oxygen available during microstructure formation and are not entirely independent. Therefore, methods to determine the relationship between the "intrinsic" properties and oxidation should be investigated.

To test the hypothesis, it is suggested that CMS membranes be pyrolyzed in an atmosphere that has a constant molar flow rate of oxygen throughout the profile. This method should be compared to a method involving a low amounts of oxygen during decomposition followed by exposure to a higher amount of oxygen after initial decomposition. During the first system, oxygen is available to react during decomposition and "intrinsic" pore formation while in the second system, oxygen is available after the "intrinsic" pores have been formed. Using this method, the total oxygen exposure and the thermal soak time could be kept constant while only varying the method of exposure.

Compare the microstructures of CMS membranes produced under different oxygen exposures.

One of the assumptions in this study was that oxygen exposure has a significant impact on the diffusion rate while there is negligible impact on the sorption capacity of the membrane. This assumption should be investigated by testing the sorption capacity of membranes produced with different oxygen exposure levels. It may also be beneficial to obtained CO_2 adsorption isotherms the more accurately determine the pore size distribution in the materials.

A second method of analysis may involve milling the surface of CMS membranes to determine the depth of the "oxidized layer". A particularly interesting, but difficult experiment would be to obtain the permeation properties for a film and then mill the surface using an argon beam. Argon beams can be used to precisely mill a thin layer from the surface. The permeation performance could again be determined. Using this method repeatedly could accurately determine whether oxidation is limited to a surface layer. An alternate method is to mill the surface of a CMS membrane with fine sandpaper. This method was investigated in the current study but consistently led to defects in the membrane.

Study "aging" effects in CMS membranes

Membranes used industrially for air separation are exposed to atmospheric oxygen for months at a time. Since oxidation is an important issue when forming CMS membranes at high temperature, the effect of high levels of oxygen under industrial operating conditions should also be investigated. Membranes in the current study were exposed to pure oxygen over a period of several days with little change in the separation performance but more extended studies are warranted for industrial applications.

Oxidation may lead to changes in the separation performance, particularly a loss of permeability over time.

APPENDIX A

COMPARISON OF CMS MEMBRANES PRODUCED UNDER EVACUATED ENVIRONMENTS

A.1 INTRODUCTION

The work presented in this chapter involves exciting and unexpected results. Initial groundwork determining the relationship between pyrolysis environment, CMS membrane microstructure, and CMS membrane separation performance will be described. This will provide the basis for a previously unexplored but important parameter in the synthesis of CMS membranes.

A.1.1 Difficulties with reproducibility in CMS membranes

6FDA:BPDA(1:1)-DAM polyimide has been used previously by Koros and coworkers to produce CMS membranes. Singh [1, 2] and Steel [3, 4] have studied the effect of pyrolysis conditions on the separation performance of CMS flat sheet membranes while Jones [5-9], Vu [10-12], and Geiszler [13, 14] have studied CMS asymmetric hollow fibers. In the earliest studies, Geiszler [13-15] and Jones [6-9, 16] showed that CMS asymmetric hollow fiber membranes produced in vacuum have a lower permeance and higher selectivity than those produced under inert environments. Vacuum pyrolyzed membranes have properties that are orders of magnitude "better" than upper bound polymer membranes, therefore the majority of CMS membranes produced in the Koros research group have been formed in vacuum environments.

One of the challenges in CMS membrane synthesis is understanding and controlling factors responsible for sample to sample variability. Figure A.1 compares the performance of CMS membranes produced by Singh [2] at 535, 550, and 800 ^{o}C to the

polymeric upper-bound. The permeability and selectivity of films produced under nominally the same conditions have a considerable amount of scatter in comparison to corresponding polymers. Foley and coworkers [17, 18] have suggested that scatter in CMS data is caused by defects in the membrane. In their hypothesis, a defect is a continuous, nonselective channel that is percolated through the membrane. This theory was discussed in detail in Chapter 2. Defects could be formed from dust particles in the polymer membrane, which decompose during pyrolysis and leave voids, or a variety of other factors.

Due to the rigorous synthesis procedure utilized by Singh [2], it is difficult to attribute reproducibility issues entirely to defects. It could be argued that scatter in separation performance is inherent due to the amorphous nature of carbon membranes. On the other hand, from experiments presented in this chapter, it is hypothesized that a major factor contributing to irreproducibility is associated with variability in the amount of oxygen in the pyrolysis atmosphere during pyrolysis. This is likely not the only cause of scatter in separation performance data, but as is shown in this chapter, it is clearly a factor that must be carefully considered.

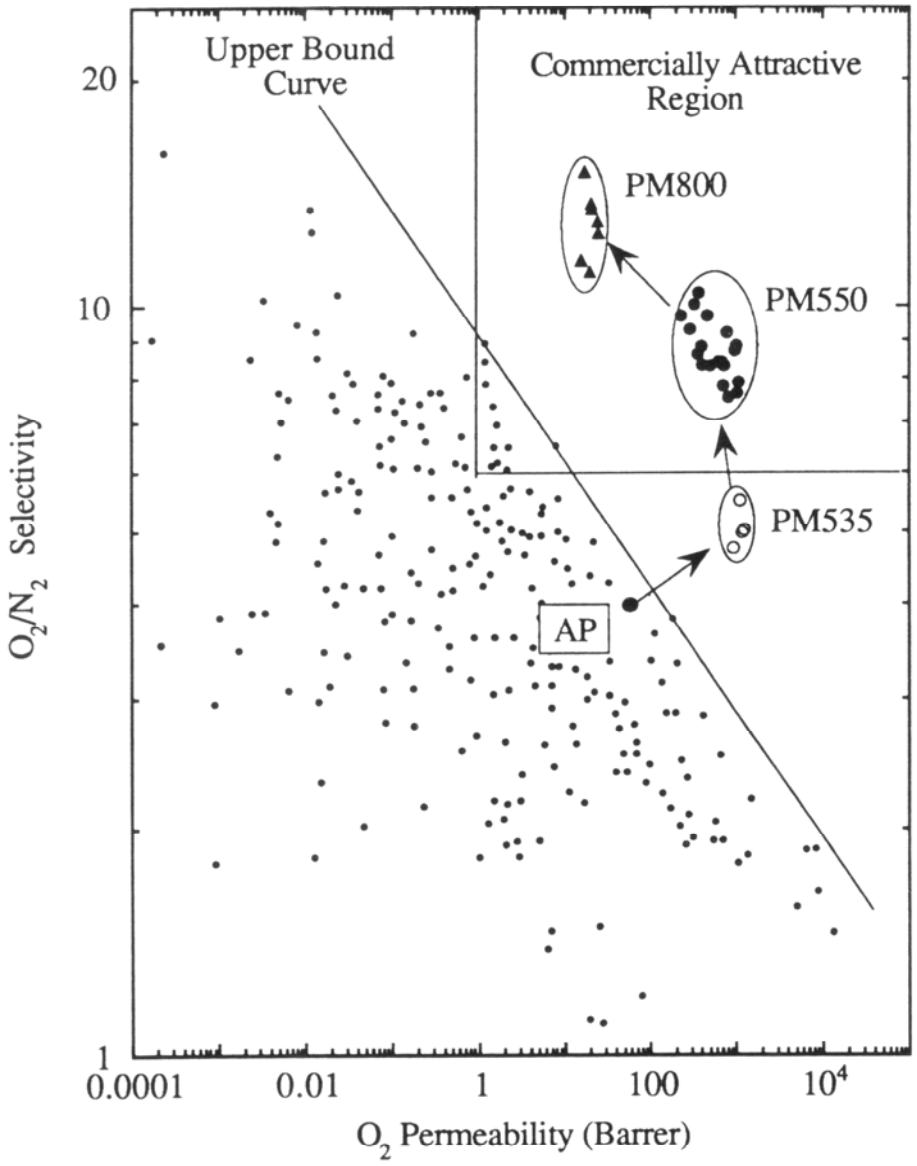

Figure A.1 Gas separation performance of CMS flat sheet membranes produced by Singh. AP is the abbreviation for "aromatic polyimide 6FDA:BPDA-DAM." PM535 were produced at 535 ^{o}C, PM550 were produced at 550 ^{o}C, and PM800 were produced at 800 ^{o}C. All other points are various polymer membranes [2].

A.2 ANALYSIS OF CMS MEMBRANES PRODUCED IN OTHER STUDIES

Singh [2] and Steel [4], in independent studies, produced dense flat CMS membranes using similar experimental set-ups to those described in Chapter 3. There are two main differences between their apparatuses and the one in the present study. In both of the previous studies, only vacuum pyrolysis was performed. Therefore, there was no purge line to allow inert gas into the quartz tube during pyrolysis. Also, instead of a pressure tranducer, the pressure was measured using a McLeod's gauge attached to the left hand side of the quartz tube, see Figure A.2. Before each pyrolysis, the pressure was evacuated to <0.03 torr in the study by Singh [2] and <0.05 torr in the study by Steel [4]. Once the pressure in the quartz tube was maintained below the maximum allowed pressure for an extended period of time, the valve to the McLeod's gauge was closed and pyrolysis was initiated. After pyrolysis, the valve was reopened to verify that the pressure had maintained the desired level throughout pyrolysis. Therefore, the exact pressure in the system is unknown throughout the pyrolysis run. Also, it should be noted that the readings on a McLeod's gauge are on a logarithmic scale and that the smallest unit is ~0.01 torr, so the accuracy of the pressure reading is somewhat limited. This is likely the reason that a maximum pressure was stated and not an exact pressure.

There are subtle differences between the pyrolysis protocols of Singh [2] and Steel [4]. Singh [2] produced membranes by heating at a rate of 13.3 ^{o}C to 250 ^{o}C, the rate was slowed to 3.85 ^{o}C/min to 535 ^{o}C, slowed again to 0.25 ^{o}C/min to 550 ^{o}C and then held at 550 ^{o}C for 2 hours. For membranes heated to 800 ^{o}C, an additional heating step was performed. Steel [4] heated quickly (unspecified rate) to 250 ^{o}C and held at that temperature for 2 minutes, followed by heating at 4 ^{o}C/min to 550 ^{o}C or 800 ^{o}C and a 2

hour thermal soak. There are only minor differences between the 550 ^{o}C protocols. Therefore, the separation performance of 550 ^{o}C membranes is comparable for the two studies. Table A.1 lists the separation performance of membranes produced in both studies at 550 ^{o}C.

Table A.1 Separation performance of CMS membranes produced at 550 ^{o}C by Steel [4] and Singh [2].

Film reference	P_{O2}	P_{N2}	P_{CO2}	P_{CH4}	P_{O2}/P_{N2}	P_{CO2}/P_{CH4}
	(Barrers)					
Steel {Steel, 2000 #98}	1108	175	5274	113	6.3	46.7
	995	128	4454	74	7.8	60.2
Singh {Singh, 1997 #108}	238	24.2			9.8	
	826	115			7.2	
(mixed gas)	1010	114			8.9	
(mixed gas)	1069	136			7.9	
(mixed gas)	791	86			9.2	
(mixed gas)	724	87			8.3	
(mixed gas)	363	42.5			8.5	

Singh [2] investigated the separation performance of CMS membranes for air separation, and therefore only O_2/N_2 data will be discussed for both studies. The films produced by Steel [4] were tested with pure gases at 75 psia for N_2 and 22 psia for O_2. The first two membranes from Singh [2] were tested using 48 psia nitrogen and 10 psia oxygen. All mixed gas films were tested at a total pressure of 57 psia. Singh [2] has shown that for O_2/N_2, the permeabilities are similar in both mixed gas and pure gas streams, therefore comparison is appropriate. Also, the permeability is only slightly affected by pressure so comparison of the two data sets is accepted.

The results show that the O_2 permeability ranges from 1108 Barrers (O_2/N_2=6.3) to 238 Barrers (O_2/N_2=9.8), for nominally similar membranes. Therefore, there is considerable scatter in the data. Of particular interest are films which have an O_2 permeability of ~1000 Barrers. The selectivity of those films ranges from 6.3 to 8.9. These results show that an increase in the membrane permeability is not always accompanied by a decrease in the selectivity.

As previously mentioned, Foley and coworkers speculated [17, 18] that defects in the CMS membranes cause scatter in the separation performance by creating a parallel transport pathway through which Knudsen diffusion occurs. Though this argument may be valid for some CMS membranes, it is difficult to argue here. The selectivity for O_2/N_2 for Knudsen diffusion is approximately 1, while the diffusion coefficients are approximately four orders of magnitude higher than those obtained from the CMS membranes. Therefore, increases in permeability will be accompanied by decreases in selectivity. The current data shows scatter in selectivity, even over a very narrow permeability range. Thus, the underlying cause of scatter in separation performance is not likely to be associated with defects.

A.3 EFFECT OF OXYGEN CONTENT ON SEPARATION PERFORMANCE OF CMS MEMBRANES

A.3.1 Changes in permeability with oxygen concentration

Recently, it was discovered that an unexpected, but strong correlation exists between the permeability and selectivity of CMS membranes and the pressure under which vacuum pyrolysis occurs. As the average pressure used for pyrolysis increases, the permeability of CMS films decreases, with a corresponding increase in selectivity. It was

speculated that changes in separation performance could be related to the amount of oxygen in the quartz tube during pyrolysis. Several experiments were used to test this hypothesis. First, the pyrolysis system was overhauled and the number of fittings was minimized. Fittings sometimes act as leak points, and therefore limit the minimum pressure which can be achieved. Also, to verify that the capacitance manometer was properly zeroed, the manometer reading was compared to an absolute pressure transducer from Kurt J. Lesker. After reconstruction, the minimum pressure maintained in the system was 0.005 ± 0.002 torr. For most other studies presented in this thesis, the operating pressure is 0.03 ± 0.01 torr. To minimize the amount of oxygen in the system, the quartz tube was purged four times with research grade helium (0.1 ppm O_2) before pyrolysis. Between each purge, the pressure was lowered to ~0.005 torr. Pyrolysis was then performed using the 550 ^{o}C profile described in Chapter 3.

To induce an intentional leak in the pyrolysis system, two Swagelok metering valves were also attached at the point where the inlet for the inert purge is normally attached. The valves were cracked to maintain a pressure of ~0.04 torr in the pyrolysis system, when under active vacuum. Table 4.2 compares the separation performance of several films produced under these two conditions along with a variety of films produced at ~0.03 torr throughout the rest of the study. The film thickness was maintained at ~2 mils for consistency. The significance of this consistency will be discussed in the next section.

The data in Table A.2 show that the permeability of CMS membranes is related to the pressure in the quartz tube during pyrolysis. The permeability of oxygen decreases from 652 to 32 Barrers as the pressure is increased from 0.005 torr to 0.042 torr while the

selectivity increases. While there is not a perfect correlation between selectivity and pyrolysis vacuum pressure, films produced at 0.005 torr have *lower selectivity* than the other two conditions, for all separations. It is likely that the variations in the pyrolysis oxygen content and the film thickness (discussed later) in the 0.025-0.035 torr Air films contribute to scatter in the data. Other than the O_2/N_2 separation, there is considerable scatter in the selectivity data. These films were produced well before the discovery of the importance of oxygen and therefore the pressure in the pyrolysis system was not rigorously maintained.

Table A.2 Separation performance of CMS membranes produced under different levels of oxygen. The actual amount of oxygen in the system was not determined directly and therefore the maximum pressures used for pyrolysis are used for comparison. The <0.005 torr system was evacuated and purged with helium before pyrolysis so the oxygen concentration is likely lower than pure air at 0.005 torr. Italicized values in parentheses represent the scatter (1 standard deviation) in the data. All films are approximately 2 mils and permeabilities are reported in Barrers.

Environment	P_{N2}	P_{O2}	P_{CH4}	P_{CO2}	O_2/N_2	CO_2/CH_4	CO_2/N_2
4 films from 3 batches (<0.005 torr Air)	71.8 *(7.5)*	632.8 *(57.4)*	36.5 *(5.0)*	2578.8 *(237.0)*	8.8 *(0.2)*	71.1 *(5.2)*	36.0 *(2.3)*
2 films from 1 batch (~0.042 torr air)	5 *(0.2)*	52 *(1.5)*	2 *(0.2)*	240 *(8.7)*	10 *(0.2)*	110 *(11.8)*	47 *(0.4)*
5 films from 4 batches (0.025-0.035 torr Air)	17 *(3)*	185 *(26)*	6 *(2)*	742 *(204)*	10.7 *(0.2)*	129.3 *(21.7)*	43.1 *(5.0)*

Figure A.2 contains a diagram to illustrate the basis for the hypothesis explaining these results. During pyrolysis, the polymer precursor is known to decomposed into amorphous carbon that consists of irregularly packed sheets of sp^2 hybridized carbon. As discussed previously, the slit-like pore structure consists of large pores which act as adsorption sites and ultramicropores which act as molecular sieves, see Figures 2.1 and 2.2. The ultramicropores are believed to be created at a "kink" in the carbon sheet or from the edge of a carbon sheet. These "kinks" are hypothesized here to be more reactive and prone to oxidation than other sites in the membrane. Studies of the reactivity of single walled carbon nanotubes have shown that defects are prone to high temperature oxidation and that oxidation can be used to cut nanotubes at defect locations [19]. Others have used thermal oxidation to purify carbon nanotubes and remove carbon from the tube ends [20, 21]. These aggressive treatments have shown that the reactivity of the tube ends and defects are much higher than the tube walls. Therefore, when pyrolyzed in the presence of oxygen, it is hypothesized that oxygen reacts and binds to the reactive sites on CMS membranes at locations which create the ultramicropores, thereby narrowing the average ultramicropore size. This process, in turn, is hypothesized to lower the permeability of the membrane, and to increase the selectivity.

The main source of oxygen in the pyrolysis system comes from the pyrolysis atmosphere. Decomposition occurs at over 450 ^{o}C and pressures below 0.05 torr. Under these conditions, it is speculated that there is negligible sorbed oxygen in the membrane at the onset of pyrolysis. Since the major source of oxygen is the pyrolysis atmosphere, it is hypothesized that oxygen will react with pores on the surface of the membrane first. It is hypothesized that oxygen reacts with the ultramicropores due to dissociative

chemisorption to form carbonyls, though the exact mechanism of the reaction is not known. Increasing the amount of oxygen available for reaction would first increase the amount of oxidized pores on the surface. Once all of the highly reactive pores on the surface are oxidized, oxygen likely diffuses into the membrane and reacts with the next available site. Therefore, the thickness of the surface oxidized layer is hypothesized to depend on the total amount of oxygen available during pyrolysis. The thickness of the layer would also affect the overall permeability of the membrane.

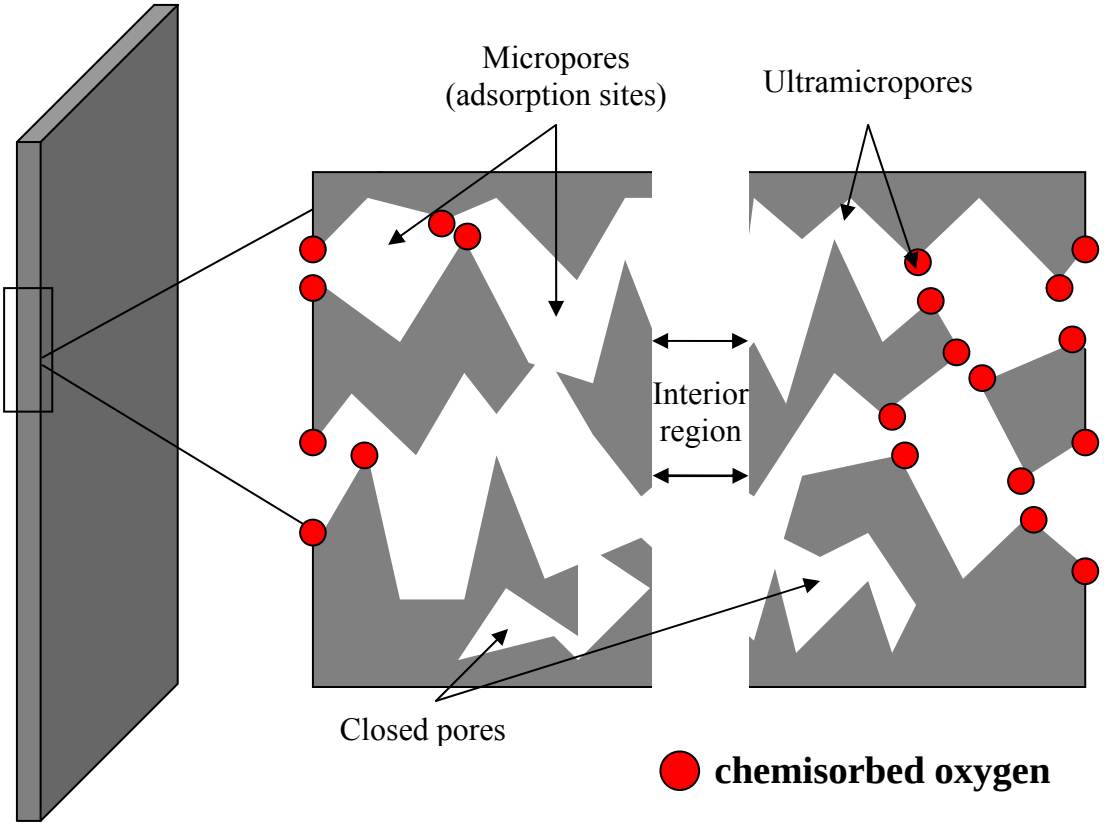

Figure A.2 Hypothetical structure of CMS membrane with oxygen bound at the ultramicropores. Chemisorbed oxygen would reduce the permeability to gases by reducing the ultramicropore size. The majority of the interior is unaffected by oxygen. Increasing the oxygen content would increase the depth of the oxidized layer.

A.3.2 Effect of oxygen content on gas diffusion

The pore volume of micropores in CMS membranes accounts for the majority of the overall pore volume. Ultramicropores are much smaller in comparison and therefore, the sorption capacity of ultramicropores pores is limited. On the contrary, gas diffusion is primarly controlled by the ultramicropores, and small changes to the ultramicropore size distribution can have a substantial effect on the gas diffusivity, and permeability. To further investigate the relationship between pore structure and pyrolysis oxygen content, the methane diffusion coefficient for two sets of membranes produced at different pressure was calculated using transient permeation. The gas diffusion coefficient is related to the permeation time lag as described in Equation 3.1.

$$\theta_A = \frac{\ell^2}{6D_A} \qquad (3.1)$$

Methane was chosen as the penetrant for this analysis. Methane has the lowest diffusion coefficient of the four gases tested. It is the only gas that has a reasonable time lag (>30 seconds) for both sets of membranes, which decreases the error associated with the measurement. Table A.3 compares the diffusion coefficients obtained from transient permeation for two pyrolysis conditions. The results show that that diffusion coefficient is *strongly* dependent on the pyrolysis conditions, as speculated. The diffusion coefficient for the membranes produced at 0.042 torr is more than an order of magnitude lower for the membranes produced at <0.005 torr. These results support the hypothesis that the ultramicropore size is smaller when pyrolyzed under higher amounts of oxygen, most likely associated with oxidation of the pore mouths.

Table A.3 Diffusion coefficients obtained from transient permeation. Values in parentheses represent one standard deviation in the data.

Environment	Average D_{CH4} (time lag) *(10^{-8} cm^2/s)*
5 films from 3 batches (<0.005 torr Air)	1.03 *(0.51)*
3 films from 1 batch (~0.042 torr air)	0.038 *(0.015)*

If the hypothetical structure discussed in Figure A.2 is accurate, the sorption capacity (and in turn the sorption coefficient) for membranes produced under different oxygen concentrations should be essentially unaffected. At this time, sorption isotherms for membranes produced under different conditions are unavailable. As an alternative test, the diffusion coefficient based on equilibrium sorption and steady state permeation can be calculated using a single isotherm which represents all of the data sets. The average diffusion coefficient is related to the equilibrium sorption coefficient and steady state permeation by Equation 2.6:

$$P_A = D_A S_A \qquad (2.6)$$

The diffusion coefficient from steady state permeation/equilibrium sorption (P/S) was then compared to the diffusion coefficient obtained from transient permeation. If the diffusion coefficients obtained using the two methods are similar, then the sorption coefficient is likely unaffected by oxidation and a single isotherm can be used to represent all vacuum conditions. Figure A.3 shows the methane sorption isotherm for a set of CMS membranes pyrolyzed at 550 ^{o}C under ~0.03 torr of air. The data were fit with the Langmuir sorption isotherm (Equation 2.10) to allow for easy calculation of the

sorption coefficient. Using the single isotherm, the average diffusion coefficient was calculated for two conditions. Table A.4 contains diffusion coefficients from both transient permeation and P/S.

The diffusion coefficients obtained by P/S for membranes produced under 0.042 torr of air are again approximately one order of magnitude lower than those produced in <0.005 torr of air. For both sets of membranes, the diffusion coefficient obtained by transient permeation is of the same order of magnitude as those obtained by steady state permeation. The difference (based on the percentage of transient permeation diffusion coefficient) between the two diffusion coefficients is 35% (for 0.042 torr air) and 70% (<0.005 torr air). For both sets of membranes, lower diffusion coefficients were obtained for transient permeation than from steady state permeation/equilibrium sorption. Zimmerman et al [22] obtained similar results when comparing diffusion coefficients from transient sorption, transient permeation, and steady state permeation. The authors attribute differences using the three methods to blind non-selective pores in the membrane, such as those shown in Figure A.2. The "blind" pores increase the tortuosity of the membrane during transient permeation. Once steady state is achieved, diffusion of gas molecules into and out of closed pores occurs at equal rates. The resulting diffusion coefficients from transient permeation are lower than for P/S.

When comparing the diffusion coefficients obtained in the current study from P/S and transient permeation, the major assumption in this analysis was that the sorption capacity of films produced under different atmospheres are similar. If this assumption was not valid, one would expect that there would be a large difference between the diffusion coefficients obtained from the two methods, which is not the case.

The results suggest that the diffusion coefficient is strongly influenced by the pyrolysis conditions while the sorption capacity is not strongly affected. Further studies analyzing the sorption isotherms of the two types of membranes are warranted to verify these results.

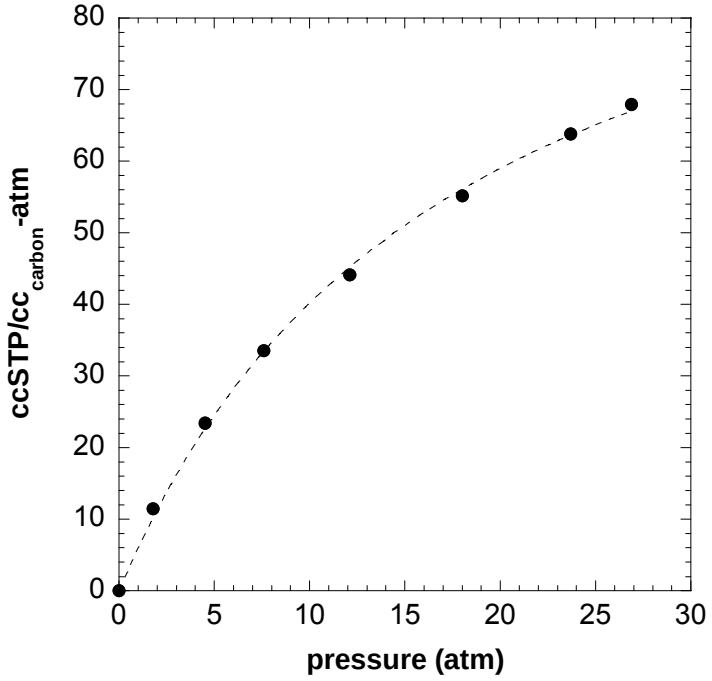

Figure A.3 Methane sorption isotherm for CMS membrane produced from 6FDA:BPDA-DAM in 0.03 torr of air. The data is fit with the Langmuir sorption isotherm.

Table A.4 Comparison of methane diffusion coefficients determined using transient permeation and steady state permeation/sorption data. The percent differences are based on the difference in the "time lag" D's relative to the diffusion coefficient evaluated from P/S. For membranes this estimate of mobility is the most meaningful measure of practical mobility under steady state conditions. The values in parentheses represent one standard deviation in the data.

Environment	D_{CH4} (time lag) *(10^{-8} cm^2/s)*	D_{CH4} (P/S) *(10^{-8} cm^2/s)*	Average % difference
5 films from 3 batches (<0.005 torr Air)	1.03 *(0.51)*	1.64 *(0.75)*	35%
3 films from 1 batch (~0.042 torr air)	0.038 *(0.015)*	0.129 *(0.044)*	70%

A.4 RELATIONSHIP BETWEEN CMS MEMBRANE PERFORMANCE AND POLYMER PRECURSOR THICKNESS

During experiments in a supplementary project, it was discovered that the thickness of the polymer precursor membrane has a substantial effect on the permeability and selectivity of the resulting CMS membrane. This result was somewhat unexpected because this factor had not been previously investigated and it had been assumed that CMS membranes were isotropic and unaffected by thickness. Figure A.4 compares the separation performance for 10 membranes with thicknesses ranging from 2-4.5 mils. All of the membranes were produced using pressures between 0.030-0.045 torr using the 550 ^oC pyrolysis protocol. The results show that the permeability increases from P_{O2}=200 Barrer to P_{O2}=900 Barrer as the thickness is increased from 2-4.5 mils. This is accompanied by a decrease in O_2/N_2 selectivity from around 10.5 to 8.5.

The CMS structure described in Figure 4.3 can be used to describe these data. Assuming that the "intrinsic" structure of the CMS membrane is independent of the level of

oxidation and more dependent on variables such as pyrolysis protocol and precursor composition, the bulk structure of the membrane will be similar irrespective of thickness. As the CMS structure is formed, the ultramicropores are "doped" with O_2 present in the pyrolysis atmosphere. If a uniform and reproducible amount of oxygen is available to react with the CMS membrane during pyrolysis, then the thickness of the highly-selective oxidized layer should be fairly similar for all membranes. The permeability in the bulk of the membrane will be higher than the surface of the membrane if the situation in Figure 4.2 applies. The difference between films of varying thickness in such a case, which alters the separation performance, is the percentage of the film thicknesses containing such a selective layer. Therefore, in such a case the apparent permeability will increase for thick films, with a corresponding decrease in selectivity. These results are consistent with the hypothesis that a thin, selective, oxidized layer of ultramicropores exists on the surface of CMS membranes, however, they do not comprise a proof that such a structure exists.

Though oxidiation of the ultramicropore mouths is likely the leading factor which contributes to the CMS properties shown in Figure A.3, it may not be the only reason why films of different thickness have different separation properties. It is also possible that there are differences in the bulk properties as the thickness of the membrane changes, independent of O_2 attack at the kink points. During pyrolysis, gaseous by-products are evolved from the membrane which contribute to the pore structure as discussed in Chapter 4. Polymer precursor decomposition involves active microstructural rearrangements. During decomposition, light, stable by-products must migrate out of the membrane. It is a likely possibility that the diffusion of large, stable by-product

molecules out of the membrane hinders the ability of carbon sheets to arrange and therefore, creates a more open porosity. The idea is similar to a pillar holding two floors apart in a building. The evolution of by-products is limited by their interpore diffusion coefficient, which may be low since by-product molecules can be large. Thick films will contain large, stable by-products for a longer period of time than thin films and therefore, may be more affected by the by-product molecules. This would result in a larger average pore size. Therefore, the relationship observed between CMS thickness and CMS separation performance supports the hypothesis of an oxidized selective layer on the surface of the membrane, but there may be other factors which also contribute to differences in separation performance.

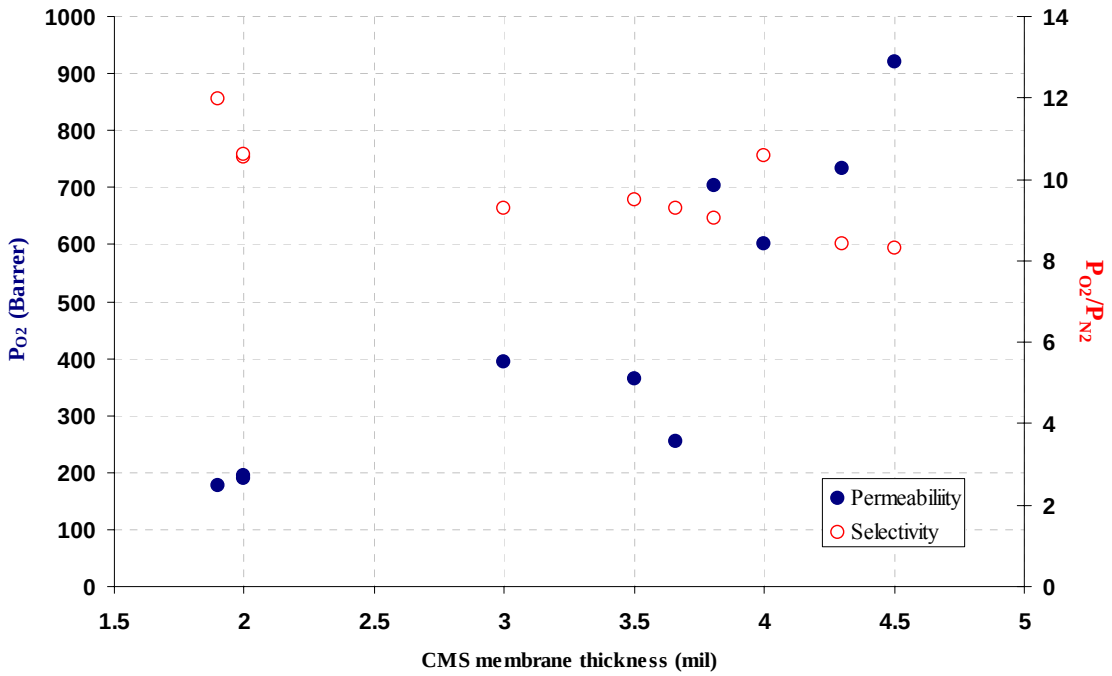

Figure A.4 Relationship between CMS membrane thickness and separation performance for O_2/N_2.

A.5 SUMMARY OF OXIDATION STUDY IN RELATION TO REPEATABILITY

There are several factors which can affect the conditions under which vacuum pyrolysis is performed. When preparing for evacuation, the quartz tube is sealed with an o-ring and fittings are attached to each end of the pyrolysis tube. Between successive pyrolysis runs, several changes are often made to the pyrolysis system, such as removal of the liquid nitrogen trap for cleaning, changing pump oil or cleaning of the quartz tube. Therefore, the starting pressure used during pyrolysis tends to vary. As mentioned previously, the starting pressure varied by more than 0.01 torr in earlier studies pertaining to this work. Singh [2] and Steel [4] also followed similar procedures during their studies on CMS formation. In both of the studies, a maximum pressure was used to describe the pyrolysis protocol and therefore, there were possibly subtle batch to batch protocol variations related to both precursor thickness and pyrolysis atmosphere. The combination of these two factors could lead a range of separation performances.

In the present study, it has been proven that there is a strong correlation between the pressure within the pyrolysis tube and the separation performance of the resulting CMS membranes, even when the pressure is maintained below 0.05 torr. Therefore, it is speculated that a major factor which has contributed to the batch to batch variation in CMS membrane synthesis is the pressure of pyrolysis, and more importantly, the amount of oxygen available during pyrolysis. A second, smaller, but less understood factor may be related to the thickness of the polymer precursor. Both of these factors need to be further investigated if a thorough CMS membrane synthesis protocol is to be developed. In all of the other studies presented in this work, the film thickness was maintained at

approximately 2 mils and the pyrolysis pressure was controlled. Therefore, these two factors do not contribute to any results presented elsewhere in this study.

A.6 REFERENCES

1. Singh-Ghosal, A. and Koros, W.J., *Air separation of flat sheet homogeneous pyrolytic carbon membranes.* Journal of Membrane Science, 2000. **174**: p. 177-188.

2. Singh, A., *Membrane materials with enhanced selectivity; an entropic interpretation.* Ph. D. Dissertation, The University of Texas at Austin, 1997.

3. Steel, K.M. and Koros, W.J., *Investigation of porosity of carbon materials and related effects on gas separation properties.* Carbon, 2003. **41**: p. 253-266.

4. Steel, K.M., *Carbon membranes for challenging separations*, in *Department of Chemical Engineering*. 2000, University of Texas - Austin: Austin, TX.

5. Sircar, S., Rao, M.B., and Thaeron, C.M.A., *Selective Surface Flow Membranes for Gas Separation.* Separation Science and Technology, 1999. **34**(10): p. 2081-2093.

6. Jones, C.W. and Koros, W.J., *Characterization of Ultramicroporous Carbon Membranes with Humidified Feeds.* Industrial and Engineering Chemistry Research, 1995. **34**: p. 158-163.

7. Jones, C.W. and Koros, W.J., *Carbon Composite Membranes: A Solution to Adverse Humidity Effects.* Industrial and Engineering Chemistry Research, 1995. **34**: p. 164-167.

8. Jones, C.W. and Koros, W.J., *Carbon molecular sieve gas separation membranes-II. Regeneration following organic exposure.* Carbon, 1994. **32**(8): p. 1427-1432.

9. Jones, C.W. and Koros, W.J., *Carbon molecular sieve gas separation membranes-I. Preparation and characterizaton based on polyimide precursors.* Carbon, 1994. **32**(8): p. 1419-1425.

10. Vu, D.Q., Koros, W.J., and Miller, S.J., *Effect of Condensable Impurities in CO2/CH4 Gas Feeds on Carbon Molecular Sieve Hollow-Fiber Membranes.* Industrial and Engineering Chemistry Research, 2003. **42**: p. 1064-1075.

11. Vu, D.Q., Koros, W.J., and Miller, S.J., *High Pressure CO2/CH4 Separation Using Carbon Molecular Sieve Hollow Fiber Membranes.* Industrial and Engineering Chemistry Research, 2002. **41**: p. 367-380.

12. Vu, D.Q., *Formation and characterization of asymmetric carbon molecular sieve and mixed matrix membranes for natural gas purification*, in *Department of Chemical Engineering*. 2001, University of Texas at Austin: Austin, TX.

13. Geiszler, V.C. and Koros, W.J., *Effects of Polyimide Pyrolysis Conditions on Carbon Molecular Sieve Membrane Properties.* Industrial and Engineering Chemistry Research, 1996. **35**: p. 2999-3003.

14. Geiszler, V., *Polyimide Precursors for Carbon Molecular Sieve Membranes.* 1997, University of Texas, Austin: Austin.

15. Wang, L.-J. and Hong, F.C.-N., *Surface structure modification on the gas separation performance of carbon molecular sieve membranes.* Vacuum, 2005. **78**: p. 1-12.

16. Hatori, H., Takagi, H., and Yamada, Y., *Gas separation properties of molecular sieving carbon membranes with nanopore channels.* Carbon, 2004. **42**: p. 1169-1173.

17. Strano, M.S. and Foley, H.C., *Modeling ideal selectivity variation in nanoporous membranes.* Chemical Engineering Science, 2003. **58**: p. 2745-2758.

18. Shiflett, M.B. and Foley, H.C., *Reproducible production of nanoporous carbon membranes.* Carbon, 2001. **39**: p. 1421-1446.

19. Qingwen, L., Hao, Y., Yinchum, Y., Jim, Z., and Zhongfan, L., *Defect Location of Individual Single-Walled Carbon Nanotubes with a Thermal Oxidation Strategy.* Journal of Physical Chemistry B, 2002. **106**: p. 11085-11088.

20. Ebbesen, T.W., Ajayan, P.M., Hiura, H., and Tanigaki, K., *Purification of nanotubes.* Nature, 1994. **6463**: p. 519.

21. Ajayan, P.M., Ebbesen, T.W., Ichihashi, T., Ilijama, S., Tanigaki, K., and Hiura, H., *Opening carbon nanotubes with oxygen and implications for filling.* Nature, 1993. **362**: p. 522.

22. Zimmerman, C.M., Singh, A., and Koros, W.J., *Diffusion in gas separation membrane materials: a comparison and analysis of experimental characterization techniques.* Journal of Polymer Science, Part B: Polymer Physics, 1998. **36**: p. 1747-1755.

APPENDIX B

CALCULATION OF THE TOTAL OXYGEN EXPOSURE COEFFICIENT

B.1 INTRODUCTION

Chapters 6 and Appendix A discussed the separation performance of CMS membranes formed under different pyrolysis atmospheres. This section will discuss the details used to calculate the total oxygen exposure coefficient introduced in Chapter 6.

B.2 DEFINITION OF "q_{O2}"

In Chapters 6 and Appendix A, the oxidation of CMS ultramicropores was hypothesized to occur due to the presence of oxygen in the pyrolysis environment during pyrolysis. The ultramicropores are speculated to be formed from "kinks" in sp^2 hybridized carbon sheets or from the ends of carbon sheets. Both of these areas are speculated to have a much higher reactivity than non-defective sp^2 carbon sheets, which have structures similar to graphite. It is our hypothesis that the reactivity of the kinked areas is very high and therefore oxidation is only limited by the availability of oxygen. Therefore, the most important factor to consider when determining the potential level of oxidation is the total amount of oxygen in the "source zone" during pyrolysis. In this analysis, the "source zone" is considered the entire area above the quartz plate in the pyrolysis tube, see Figure B.1. The factor q_{O2} will be defined as the total mols of oxygen available for reaction during pyrolysis. Equation B.1 defines the factor q_{O2} as the sum of the initial moles of oxygen in the reaction zone plus all oxygen that enters during the period of time that the ultramicropores are considered "active" (or prone to oxidation).

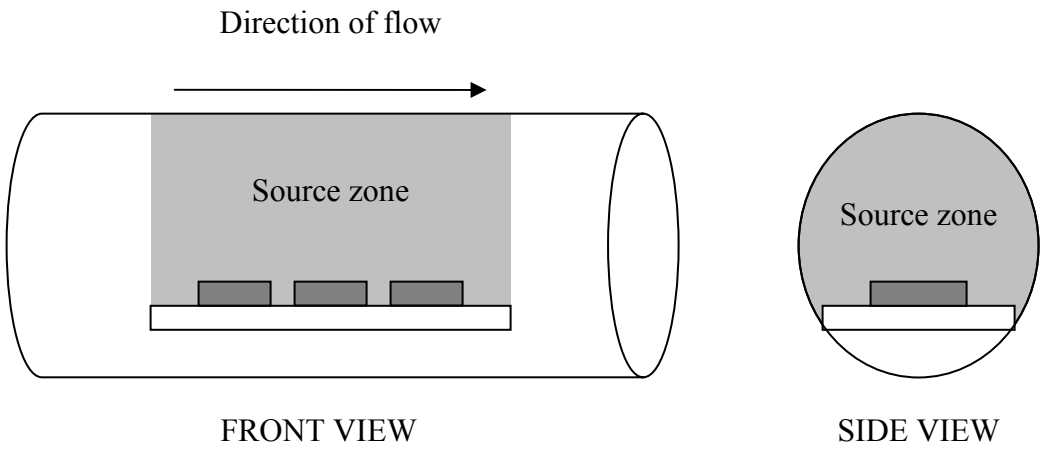

Figure B.1 Schematic of hypothetical "source zone" for oxidation in the quartz tube during pyrolysis

$$q_{O_2} = n_{O_2,initial} + n_{O_2,flow}\, t \qquad \text{(B.1)}$$

q_{O2} = total amount of oxygen available for reaction (mol)

$n_{O2,\ initial}$ = initial moles of oxygen in reaction zone (mol)

$n_{O2,\ flow}$ = molar flow rate of oxygen into reaction zone when sites are active (mol/s)

t = time when sites are active (s)

B.3 CALCULATION OF "q_{o2}"

The initial amount of oxygen available in the reaction zone when ultramicropores become active is governed by the pyrolysis atmosphere. In systems with inert purges operating at atmospheric pressure, the flow rate was controlled using a MKS flow controller and the volumetric flow rate verified using a bubble flow meter. For systems which had an inert purge bleeding into the system on the left side of the pyrolysis tube and active vacuum on the right side of the pyrolysis tube, the volumetric flow rate through the pyrolysis tube was measured using a bubble flow meter attached to the outlet of the pump.

When the pyrolysis system was operated under "vacuum", all flow through the quartz tube came from air leaks into the system. All vacuum systems have some level of leakage. At steady state, the rate that gas enters from leaks is equal to the amount of gas removed by the rotary pump. Therefore, the minimum pressure that be achieved during active vacuum is governed by the interplay between the pumping speed and the leak rate. The flow rate in vacuum systems in this study could not be directly measured without great difficulty and large modifications to the system. Measuring the volumetric flow rate from the discharge of the pump was attempted but the flow rates were too low for accurate (or reasonable) determination. Therefore, a second method was utilized. The pumps in this study were BOC Edwards Model RV3 rotary vane pumps. The performance characteristics of this pump can be found in Figure B.2. The maximum pumping speed was specified as 3.9 m^3/hr, using a 60 Hz electrical supply. Therefore, to determine the pumping speed, the inlet pressure to the pump was required. During pyrolysis, the inlet pressure was not measured directly. The pressure in the system was measured on the left side of the pyrolysis tube.

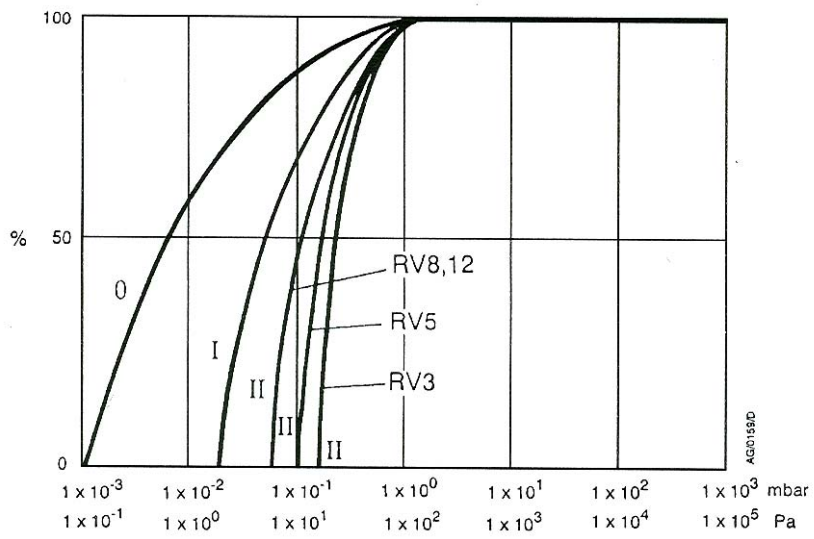

Figure B.2 Performance characteristics of pump in high vacuum mode [1]

The pyrolysis system was later modified to include a Kurt K. Lester absolute pressure transducer directly above the alumina trap on the pyrolysis pump, see Figure 3.2. The pressure in the system was set as before using the pressure transducer on the left side of the quartz tube and then, after several hours, the pressure was measured at the pump inlet. Table B.1 compares the pressure readings on the left side of the pyrolysis tube, to those at the pump inlet. The results show that there is a substantial pressure drop across the pyrolysis tube. Unfortunately, accurate measurement of the pump inlet pressure was limited by the absolute pressure transducer. The minimum pressure that could be accurately measured using the transducer was 0.001 torr and the readout is on a log scale. Therefore, though fairly accurate readings were obtained, there is still considerable error in the measurement, especially for the 0.005 torr run because the pump inlet pressure was below the scale of the transducer.

Table B.1 Comparison of pressure readings on left side of the pyrolysis tube compared with the pressure reading at the pump inlet. Readings on the pump inlet are also given in Pascals which correspond to Figure B.2

Pressure reading from left side (torr)	**Pressure reading at pump (torr, {Pa})**
0.005	<0.001, {<0.13}
0.042	0.002, {0.27}
3.03	0.25, {33}

Figure B.2 shows that as the pressure in the system approaches 0.1 Pa, the effective evacuation capacity at which the pump operates drops considerably. One major difficulty encountered was that the pump inlet pressure in the system which operated at 0.005 torr was below the detectable range (0.001 torr) and therefore the actual speed at which the pump was operating was unknown. As the pressure in the pump approaches 0.1 Pa (0.00075 torr) the flow rate approaches zero. Therefore, as an approximation, the flow rate was estimated to be 1% of the maximum pump speed. This was only an estimate but appears to be a reasonable value based on the shape of the pump curves. The flow rate for the 0.042 torr system was estimated from the pump curves using an inlet pressure of 0.002 torr. This is again an estimate and the actual value is extremely dependent on the exact pressure at the pump inlet, which was unknown. Therefore, these values were chosen to evaluate trends in the data and are not exact values.

The final variable in Equation B.1 is the exposure time. This value was estimated based on the TGA curve shown in Figure B.3. This curve is the same curve as shown in Figure 6.3 with some extended analysis. The onset of the major decomposition peak in the TGA occurs 65 minutes into the pyrolysis run and the total run time is 245 minutes.

It takes the pyrolysis furnace about one hour to cool down to 500 ^{o}C, but this value depends on the pyrolysis condition and room temperature. Therefore, the time the sample is above ~500 ^{o}C is likely on the order of 240 minutes (180 minutes during pyrolysis + 60 minute cool down). This value was chosen as the exposure time. Using the assumptions discussed here, the total oxygen exposure was calculated for each of the pyrolysis conditions. All volumetric flow rates were converted into molar flow rates using the ideal gas law. The oxygen flow rates were related to the total flow rates using the specified concentration of oxygen in the purge gas. For vacuum tests, air was considered 21% oxygen.

The results in Table B.2 show that the initial concentration of oxygen in the "reaction zone" has little effect on the total oxygen that is available in the reaction zone over the entire pyrolysis run, mainly because the molar flow rates of oxygen are so high. In fact, a simpler calculation may be based on just the total flow rate or the molar flux past the membranes. The results would give the same trends as those obtained for $q_{o2.}$ The highest oxygen exposure is obtained from membranes pyrolyzed in vacuum at 0.042 torr. The O_2 exposure for that experiment was approximately one order of magnitude higher than any other conditions. Even though the system is at low pressure, there is a considerable flow of oxygen from the leak. Most importantly, the oxygen content in air is approximately five orders of magnitude higher than the purge gases so a small air leak results in a substantial increase in oxygen exposure. Another important point that must be made is that the oxygen content of the argon purge streams is likely lower than the values reported here. The argon used in this study had a specified O_2 level of $\leq$4 ppm. The actual level is not known so the maximum possible amount was determined.

Discussion of these results in relation to permeation properties of the CMS membranes can be found in Chapter 5.

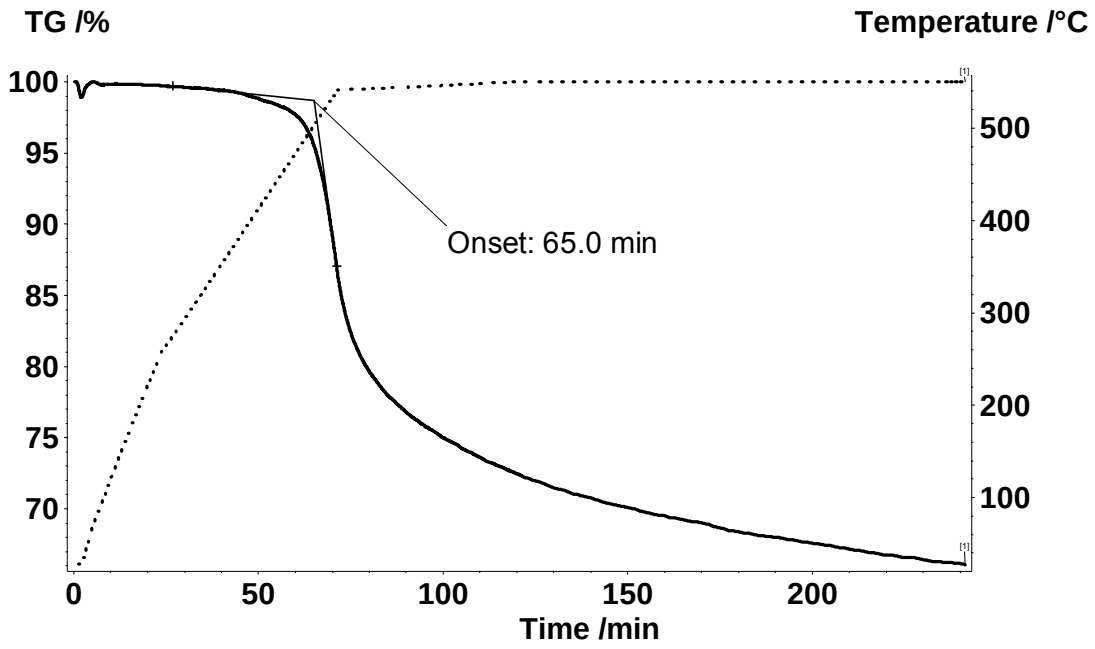

Figure B.3 TGA curve of decomposition of 6FDA:BPDA(1:1)-DAM precursor using 550 ^{o}C pyrolysis protocol.

Table B.2 Factors necessary for the calculation of q_{O2}. The flow rate at operating pressure is the flow rate through the reaction zone at operating pressure. Therefore, this value is a fraction of the total measured flow rate.

Purge gas	Measured flow rate (cm^3/min)	P (torr)	Flow rate at operating pressure (cc/min)	$n_{O2, initial}$ (mol)	$n_{O2, flow}$ (mol/min)	q_{o2} (mol)
He	50	760	28	4.8E-10	1.1E-10	2.76E-08
He	200	760	110	4.8E-10	4.5E-10	1.09E-07
Ar	50	760	28	1.9E-08	4.5E-09	1.10E-06
Ar	100	760	55	1.9E-08	9.0E-09	2.19E-06
Ar	200	760	110	1.9E-08	1.8E-08	4.35E-06
He	46	3	6400	1.9E-12	1.0E-10	2.50E-08
He	261	8	13673	5.1E-12	5.9E-10	1.41E-07
Ar	46	3	6451	7.6E-11	4.2E-09	1.00E-06
Ar	261	8	13673	2.0E-10	2.4E-08	5.65E-06
Air	vacuum	0.005	72	6.3E-09	3.8E-09	9.30E-07
Air	vacuum	0.042	282	5.3E-08	1.3E-07	3.08E-05

B.4 REFERENCES

1. *Instruction Manual for RV3, RV5, RV8, and RV12 Rotary Vane Pumps*, Manor Royal, Crawley, West Sussex, UK: BOC Edwards.

APPENDIX C

OTHER HYPOTHESES DESCRIBING THE EFFECTS OF PYROLYSIS ATMOSPHERE ON THE SEPARATION PERFORMANCE OF CMS MEMBRANES

C.1 INTRODUCTION

Chapter 6 and Appendix A have shown that the pyrolysis atmosphere has a considerable effect on the separation performance of CMS membranes. Up to this point, the hypothesis behind these results concerns the total oxygen exposure under different pyrolysis conditions. Lowering the oxygen exposure lowers the level of oxidation of ultramicropores at the surface of the CMS membranes. This, in turn, increases the average pore size at the surface and increases the permeability. Though it is speculated that the oxidation hypothesis is the major factor contributing to changes in separation performance under different pyrolysis atmosphere, there are likely other factors which contribute. One key point that supports this hypothesis is that the selectivity of films produced in vacuum are higher than those produced in inert purge, even when similar permeabilities are obtained.

C.2 ENHANCED MASS TRANSFER

Geiszler and Koros [1, 2] have suggested that the addition of an inert purge gas to the pyrolysis atmosphere could add a convective mode of mass transfer to the primarily diffusive mode found in vacuum environments. The addition of a convective mode of mass transfer could enhance the diffusion of large by-products away from the surface of the membrane. This would decrease the amount of by-products available to re-react with the carbon membrane, see Figure 7.3.

To determine the effect that convection has on the mass transfer from the surface of the pyrolysis plate, the average mass transfer coefficient was calculated. To determine the appropriate correlation to use to estimate the mass transfer coefficients, the flow regime was calculated. The Reynolds number for flow across a flat plate was calculated using Equation C.1 [3].

$$\mathrm{Re} = \frac{x\nu\rho}{\mu} \qquad \text{(C.1)}$$

x: distance from edge of pyrolysis plate (cm), full length was used to calculate maximum

υ: fluid velocity (cm/s)

ρ: density of gas (g/cm^3)

μ: viscosity of gas (g/cm-s)

The purge gas viscosity was estimated from simple kinetic theory of gases using Equation C.2 [4]:

$$\eta = 2.6693 \cdot 10^{-5} \frac{\sqrt{MT}}{\sigma^2} \qquad \text{(C.2)}$$

M: molecular weight of gas (g/mol)

T: temperature (K)

σ: collision diameter (cm)

The fluid density was estimated using the ideal gas law. The Reynolds number, along with the parameters used to calculate it are listed in Table C.1 for the conditions encountered in this study. To simplify the calculations, plug flow was assumed in the pyrolysis chamber. The velocity used was based on the tube area and the volumetric flow rate. The flow rate for the vacuum system could not be accurately measured because it is

very low. Therefore, it was estimated using pump curves supplied by BOC/Edwards as described in Appendix B.

The results in Table C.1 show that for all conditions, the flow across the surface of the plate is laminar. At 550 ^{o}C, the highest Reynolds number is approximately 25. The Reynolds numbers were also calculated at room temperature, and are approximately 50. Therefore, throughout the pyrolysis process, the flow across the pyrolysis plate is laminar.

Since the pressure in the vacuum systems are very low, it was speculated that Knudsen diffusion might play a role in mass transfer and therefore the Knudsen number was calculated for the 0.005 torr system. The Knudsen number is the ratio of the mean free path of a gas to the diameter of the tube flow through which the gas is flowing. The Knudsen number [5] can be calculated using Equation C.3:

$$\mathrm{Kn} = \frac{k_B T}{\sqrt{2}\pi\sigma^2 P D} \qquad \text{(C.3)}$$

D: diameter of the pyrolysis tube (m)

P: total pressure (atm)

k_D: Boltzman's constant

For the 0.005 torr system at 550 ^{o}C, the Knudsen number was 0.7. Therefore, for the 0.005 system, the system is more likely in the "slip flow" region than in laminar flow. As an approximation, though, laminar flow will be assumed in the remaining analysis. In a later analysis, the Knudsen diffusion coefficient and the bulk diffusion coefficients will be compared and the effect on the mass transfer coefficient will be discussed.

Table C.1 Parameters used for calculation of the Reynolds number at 550 ^{o}C. The flow rates were measured at 1 atm and 295 K.

Purge gas	T (K)	p (torr)	flow rate (cm^3/min)	μ (g/cm-s)	ρ (g/cm^3)	Re
Argon	873	760	50	3.76E-04	5.57E-04	5.6
Argon	873	3	46	3.76E-04	2.20E-06	5.1
Argon	873	760	200	3.76E-04	5.57E-04	22.3
Argon	873	8	270	3.76E-04	5.86E-06	30.1
Helium	873	760	50	3.32E-04	5.57E-04	6.8
Helium	873	3	46	3.32E-04	2.20E-06	6.3
Helium	873	760	200	3.32E-04	5.57E-04	27.3
Helium	873	8	270	3.32E-04	5.86E-06	36.9
Air	873	0.005	0.00086	2.97E-04	2.57E-09	0.0001
Air	873	0.042	0.028	2.97E-04	2.16E-08	0.0028

For flow across the surface of a flat plate in laminar flow, the average mass transfer coefficient can be estimated by [6]:

$$k^{*}_{c,avg} = \frac{0.664}{L} D_{AB} \left(\frac{L\upsilon\rho}{\mu} \right)^{1/2} \left(\frac{\rho}{\mu D_{AB}} \right)^{1/3} \qquad (C.4)$$

$k^{*}_{c.avg}$: average mass transfer coefficient across pyrolysis plate (cm/s)

D_{AB}: diffusion coefficient of component A in B (cm^2/s)

L: length of pyrolysis plate (cm)

υ: fluid velocity (cm/s)

ρ: density of gas (g/cm^3)

μ: viscosity of gas (g/cm-s)

The first and second dimensionless groups in Equation C.4 are the Reynolds number (Re) and the Schmidt number (Sc), respectively. The diffusion coefficient was estimated using Equation C.5 [4]:

$$D_{AB} = \frac{1.858 \cdot 10^{-27} T^{3/2}}{P\sigma_{AB}^2 \Omega_D} \left(\frac{1}{M_A} + \frac{1}{M_B} \right)^{1/2} \qquad (C.5)$$

σ_{AB}: average Lennard-Jones collision diameter (m)

Ω_D: collision integral based on Lennard-Jones potential

Of course, there are a variety of by-products that are evolved during 6FDA:BPDA(1:1)-DAM composition. It was speculated that the large by-products may be most affected by the introduction of a convective mode of mass transfer. Therefore, for simplification, benzene was chosen as the diffusing species. Table C.2 is a list of the bulk diffusion coefficients and mass transfer coefficients for both helium and argon purge streams at 550 ^{o}C as well as vacuum systems.

Table C.2 Diffusion coefficients and mass transfer coefficients of benzene for the various pyrolysis environments

Purge gas	**Pressure (torr)**	**Flow rate (cm^3/min)**	**D_{AB} (cm^2/s)**	**$k^*_{c,avg}$ (cm/s)**
Argon	760	50	5.47E-01	3.07E-02
Argon	3	46	1.39E+02	7.45E+00
Argon	760	200	5.47E-01	6.13E-02
Argon	8	270	5.19E+01	6.77E+00
Helium	760	50	1.97E+00	7.35E-02
Helium	3	46	5.58E+02	1.93E+01
Helium	760	200	2.20E+00	1.59E-01
Helium	8	270	2.09E+02	1.75E+01
Air	0.005	0.00086	9.14E+04	2.02E+01
Air	0.042	0.028	1.09E+04	1.37E+01

The results in Table C.2 show that the average mass transfer coefficient of benzene evolving from the quartz plate is strongly dependent on the pyrolysis conditions. The mass transfer coefficient is highly dependent on the pressure in the system, mainly due to heavy influence that pressure has on the diffusion coefficient. The highest mass transfer coefficient was found in the 0.005 torr vacuum system, followed by the low pressure inert purge systems and the 0.042 torr vacuum system. The mass transfer coefficients in the atmospheric pressure inert purge systems are approximately two orders of magnitude lower than the corresponding low pressure systems. The mass transfer coefficients for the vacuum systems are high due to the very high diffusion coefficients at low pressure.

The mass transfer coefficients listed in Table C.2 correlate with the permeation data obtained in this study for inert purge systems. The systems with the highest mass transfer coefficient (inert purge, low pressure) have the highest permeability. Therefore, it possible that the enhanced diffusion of by-products away from the membrane in these systems ultimately results in larger pore sizes, as compared to other inert purges. The atmospheric pressure systems have much lower mass transfer coefficients. Therefore, by-products remain in or near the CMS membrane and re-react, reducing the pore size and possibly the pore volume, which reduces the permeability. Therefore, a second (possibly complementary) explanation for the difference in permeability from systems utilizing low pressure inert purge gases is that enhanced mass transfer inhibits the re-reaction of large diffusion by-products with the membrane and therefore, increases the average pore size.

The mass transfer coefficient for the vacuum pyrolysis system was calculated based on nitrogen as the purge gas. Table C.3 shows that the mass transfer coefficient for vacuum systems is similar to that of the low pressure inert purge systems. If the primary difference between different pyrolysis atmospheres is due to variances in the mass transfer coefficients, membranes created under vacuum pyrolysis should have similar properties to those produced in low pressure inert purge systems. Therefore, the mass transfer coefficient cannot be used to accurately describe the difference in separation performance when comparing membranes produced in vacuum and in low pressure inert streams. Even if the flow rates in the pyrolysis chamber during vacuum pyrolysis are overestimated by an order of magnitude, the mass transfer coefficient is still similar to those of the low pressure inert systems. The mass transfer coefficient in vacuum systems is more heavily influenced by the very large diffusion coefficient than the flow rate.

In the above analysis, the diffusion coefficient in the 0.005 torr vacuum system determined using the correlations for the bulk diffusion coefficient. As mentioned above, in this system, Knudsen diffusion may play a role. Therefore the effective diffusion coefficient was estimated using Equation C.6.

$$\frac{1}{D_{A,e}} = \frac{1}{D_{AB}} + \frac{1}{D_{A,K}} \qquad \text{(C.6)}$$

$D_{A,e}$: effective diffusion coefficient

D_{AB}: bulk diffusion coefficient

$D_{A,K}$: Knudsen diffusion coefficient

The Knudsen diffusion coefficient was estimated using Equation 2.11. Using this analysis, the effective diffusion coefficient was estimated as 5.5×10^{-04} cm^2/s, which is 40% lower than if only bulk diffusion is considered. Using equation C.3 (which assumes

laminar flow), the mass transfer coefficient was 14.3 (cm/s), which is about 30% lower than the coefficient based on the bulk diffusion coefficient. These results have no effect on the trends discussed above because the above analysis was based on orders of magnitude.

C.3 ENHANCED HEAT TRANSFER

Another factor which may contribute to the properties of CMS membranes produced in inert environments is related to heat transfer to and from the membrane. Therefore, the following analysis will investigate the importance of heat transfer to and from CMS membranes during pyrolysis. Chapter 4 discussed some of the chemical reactions that occur during polyimide decomposition but a brief overview will be given here. These reactions were investigated to some extent by a variety of researchers including Geiszler [2], Steel [7], and Singh [8] and previously in this study. The onset of pyrolysis involves (1) the cleavage of the carbon-carbon bonds in the CF_3-C-CF_3 group on the 6FDA polyimide to form CF_3H, (2) cleavage of the CH_3 groups from the DAM monomer to form CH_4, and (3) cleavage of the imide to produce CO_2 and CO. It is undetermined where the hydrogens evolve from in the first two reactions, but they likely come from the hydrogens attached to aromatic rings. Geiszler [2] estimated the heat of these cleavage reactions to be >1000 kJ/mol of monomer. "Heavy" by-products from these initial reactions then react to form the resulting carbon microstructure, which consists of graphitic-type planes. Using the reactions listed above, Geiszler assumed that the overall heat of reaction is endothermic. To test this hypothesis, decomposition was

investigated in the current study using DSC. The TGA and DSC spectrum for 6FDA:BPDA(1:1)-DAM decomposition can be found in Figure C.1.

Surprisingly, the DSC spectrum shows that the decomposition of 6FDA:BPDA(1:1)-DAM is exothermic. The initial decomposition at around 500 ^{o}C is endothermic followed by a large exotherm during the remainder of the reaction. Unfortunately, the temperature limit of the available DSC is 800 ^{o}C, and the decomposition reaction is still occurring at that temperature, therefore quantification of the heat of reaction was not possible. When calculating the heat of reaction, Geiszler assumed that most of the reactions were endothermic cleavage reactions which occur during the initial stage of decomposition, and therefore the overall heat of the initial reaction was estimated to be endothermic. The endothermic cleavage reactions are accompanied by the formation of the carbon structure. Since the eventual resulting structure is aromatic, there are a considerable number of formation reactions occurring which result in an overall exothermic reaction. Though the quantitative heat of the reaction is unknown, the key point to this study is that the reaction is exothermic. Appendix D presents sample calculations supporting this experimental observation.

One of the drawbacks of this analysis was that the baseline did not return to a steady state due to the limitations of the instrument. Therefore, a second analysis was performed at higher temperature using a calculated DTA curve from TGA. The maximum operating temperature of the TGA is 1500 ^{o}C, so a higher temperature analysis was performed. Calculated DTA is only useful for qualitative analyses. The point of this experiment was to verify that the reaction is exothermic, therefore, this method is simply used in support to DSC. Figure C.2 shows that the results are similar to DSC. The

overall heat of reaction is exothermic. These results will be considered in later in this analysis.

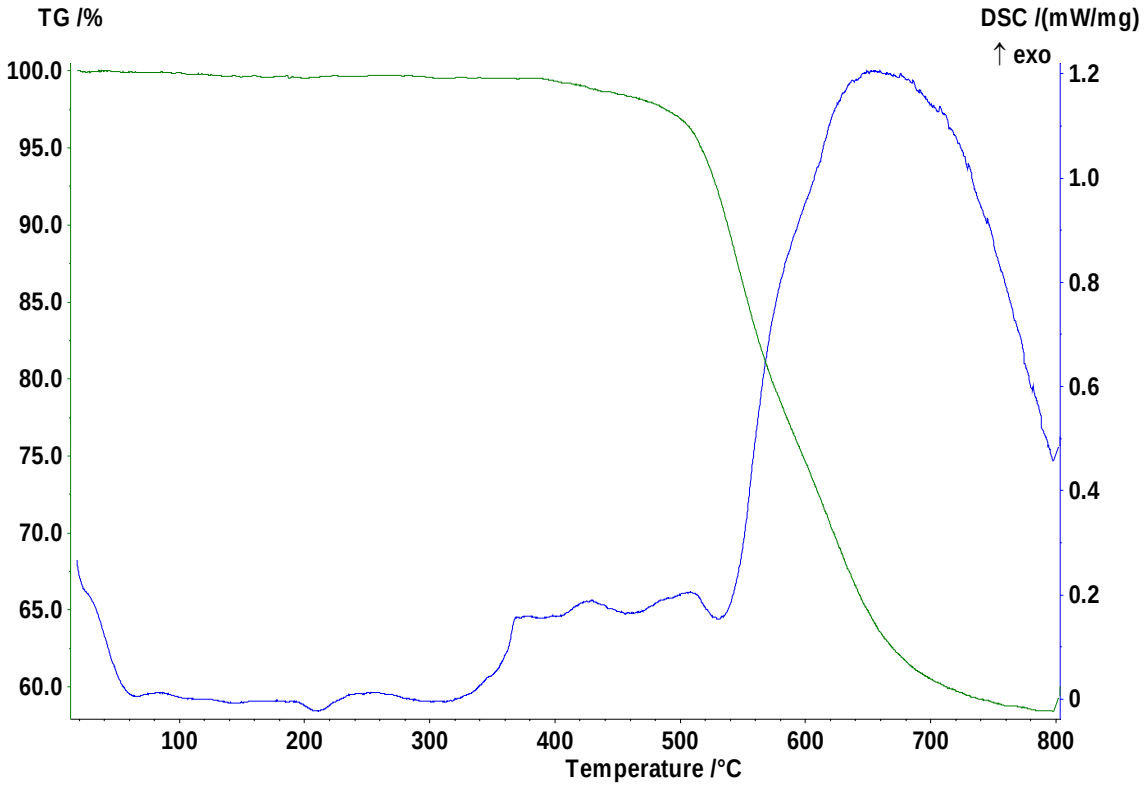

Figure C.1 TGA/DSC spectra for the decomposition of 6FDA:BPDA(1:1)-DAM. The heating rate for the test was 10 K/mol with a sample size of ~ 10 mg.

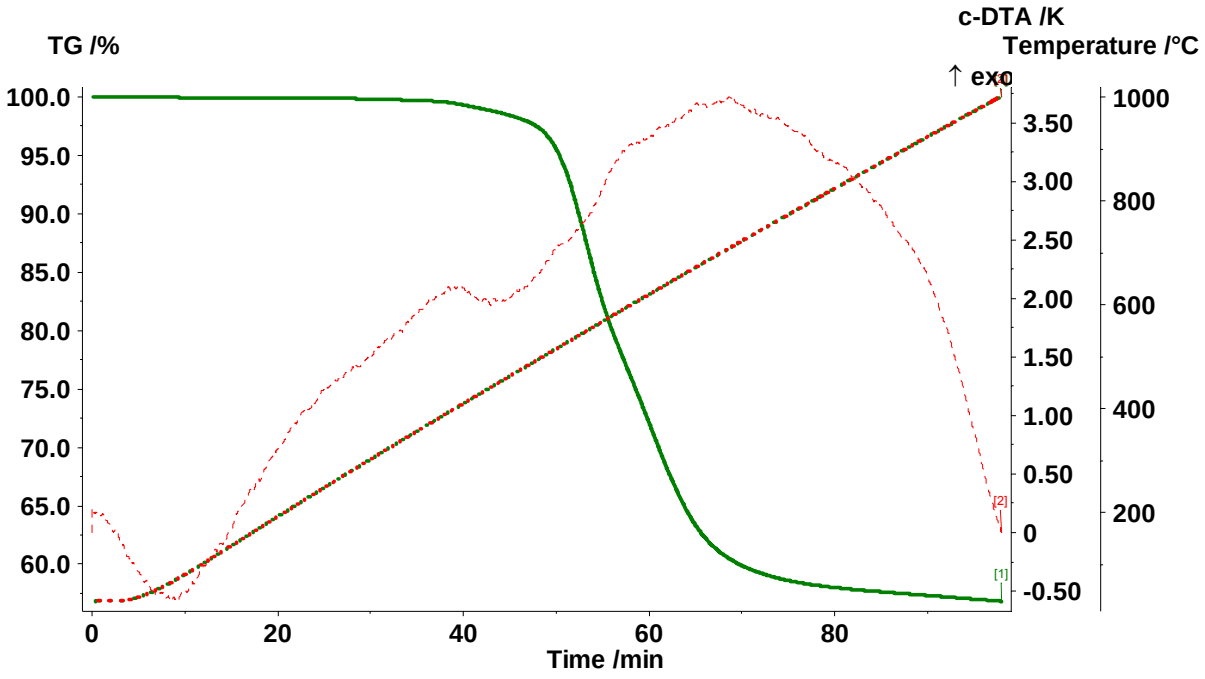

Figure C.2 TGA/DTA spectra for the decomposition of 6FDA:BPDA(1:1)-DAM. The heating rate for the test was 10 K/mol with a sample size of ~ 50 mg.

The heat transfer coefficient for each of the systems investigated was calculated analogous to the mass transfer coefficient. For laminar flow across a flat plate, the average heat transfer coefficient can be determined from Equation C.7.

$$h^*_{avg} = \frac{0.664}{L}\lambda\left(\frac{L\nu\rho}{\mu}\right)^{1/2}\left(\frac{C_p\mu}{\lambda}\right)^{1/3} \qquad (C.7)$$

h^*_{avg}: average heat transfer coefficient over the plate (J/cm-K)

λ: thermal conductivity of the inert gas (J/s-cm-K)

C_p: heat capacity of the inert gas (cal/mol-K)

The heat capacity of the gases was estimated from [9]. The thermal conductivity was estimated by simple kinetic theory using Equation C.8 [4].

$$\lambda = 1.9891 \cdot 10^{-4} \frac{\sqrt{T/M}}{\sigma^2} \qquad \text{(C.8)}$$

Table C.3 lists the thermal conductivities and heat transfer coefficients for each of the pyrolysis conditions. The heat transfer coefficients vary considerably from system to system. In general, the heat transfer coefficients can be divided into three categories. The highest heat transfer coefficients (~10^{-4} J/s-K) are found in purge systems using helium, followed by systems containing argon (~10^{-5} J/s-K). The lowest heat transfer coefficient was found in the vacuum system (~10^{-7} J/s-K). These results suggest that convective heat transfer plays a significant role in inert purge systems as compared to the vacuum system. These results can be used to describe the permeabilities of membranes formed under different pyrolysis environments. It has been shown that increasing the pyrolysis temperature lowers the permeability of carbon membranes produced from 6FDA:BPDA-DAM(1:1) [8]. This is likely to due to sintering of the ultramicropores. During decomposition, heat is given off because the reaction is exothermic. In purge systems, heat is transferred more efficiently away from the membrane by convective heat transfer. Therefore, the "effective" pyrolysis temperature in systems with a flowing inert purge is lower and the permeability of CMS membranes produced in such systems is expected to be higher than those produced utilizing vacuum pyrolysis, which has limited convective heat transfer away from the CMS membrane.

Table C.3 Thermal conductivity and heat transfer coefficients for the various pyrolysis environments

Purge gas	Pressure (torr)	Flow rate (cc/min)	λ (J/s-cm-K))	h_{avg} (J/s-K)
Argon	760	50	2.9E-04	1.40E-05
Argon	3	46	2.9E-04	1.34E-05
Argon	760	200	2.9E-04	2.79E-05
Argon	8	270	2.9E-04	3.24E-05
Helium	760	50	2.6E-03	4.14E-05
Helium	3	46	2.6E-03	3.97E-05
Helium	760	200	2.6E-03	8.28E-05
Helium	8	270	2.6E-03	9.62E-05
Air (Nitrogen)	0.005	0.00086	7.9E-05	6.14E-08
Air (Nitrogen)	0.042	0.028	7.9E-05	1.48E-07

C.4 DECONVOLUTION OF THE EFFECTS OF PYROLYSIS ATMOSPHERE ON SEPARATION PERFORMANCE

The results in this study have shown that the pyrolysis (and post-pyrolysis "cool down") atmosphere plays a major role in the separation performance of CMS membranes. Experimental results show that three environmental factors may contribute to the separation performance of CMS membranes: (1) the concentration of oxygen in the pyrolysis environment, (2) enhanced mass transfer due to convection, and (3) enhanced heat transfer due to convection. These three factors can be used to describe differences in the separation performance for membranes produced using the same thermal decomposition profile. The net result of these three factors is as follows: (1) Increasing the total oxygen exposure increases the level of oxidation of the ultramicropores in the CMS membrane which results in a reduction of permeability and enhanced selectivity.

There is likely a limit to the amount of oxygen than can be used, though, since in the presence of too much oxygen, the structure will be oxidized to the point that defects will likely occur in the membrane. For example, oxidation of a CMS membrane in high temperature air at atmospheric pressure will result in a 100% weight loss and formation of CO and CO_2. (2) Adding a convective flow across the surface of CMS membranes will increase convective heat transfer and the effective pyrolysis temperature will be lower, resulting in higher permeability. (3) In addition, convective mass transfer may enhance the evolution of large by-products away from the membrane surface. Large by-products are expected to re-react with the carbon structure and lower the effective pore size, therefore increasing convective mass transfer may also increase the average pore size of the membrane. It is more likely that heat transfer effects are more significant than mass transfer effects, though and based on estimates of the energetics of reactions occurring in the final stages of structure formation (Appendix D), convective heat transfer could reduce the temperature at the membrane surface in this critical phase relative to vacuum pyrolysis protocols. This provides slightly less consolidation and hence produces a more "open" and slightly less selective medium. Therefore these tools can be used to tailor the separation performance of CMS membrane. Though the effects from heat and transfer are likely secondary to those from oxidation, they are important factors to consider when designing pyrolysis systems for CMS production.

C.5 REFERENCES

1. Geiszler, V.C. and Koros, W.J., *Effects of Polyimide Pyrolysis Conditions on Carbon Molecular Sieve Membrane Properties.* Industrial and Engineering Chemistry Research, 1996. **35**: p. 2999-3003.

2. Geiszler, V., *Polyimide Precursors for Carbon Molecular Sieve Membranes*. 1997, University of Texas, Austin: Austin.

3. McCabe, W.L., Smith, J.C., and Harriot, P., *Unit Operations of Chemical Engineering*. Vol. Fifth Edition. 1993, New York: McGraw-Hill Inc.

4. Hirschfelder, J., Curtiss, C., and Bird, R.B., *Molecular Theory of Gases and Liquids*. 1954: John Wiley and Sons.

5. Cussler, E.L., *Diffusion, Mass Transfer in Fluid Systems*. Second ed. 1997, Cambridge. UK: Cambridge University Press.

6. Hines, A.L. and Maddox, R.N., *Mass Transfer Fundamentals and Applications*. 1985, Englewood Cliffs, New Jersey: Prentice-Hall.

7. Steel, K.M., *Carbon membranes for challenging separations*, in *Department of Chemical Engineering*. 2000, University of Texas - Austin: Austin, TX.

8. Singh, A., *Membrane materials with enhanced selectivity; an entropic interpretation.* Ph. D. Dissertation, The University of Texas at Austin, 1997.

9. Felder, R.M. and Rousseau, R.W., *Elementary Principles of Chemical Processes*. 1986, New York: John Wiley and Sons.

APPENDIX D

CALCULATION OF HEATS OF REACTION FOR MODEL REACTIONS OCCURING DURING CMS FORMATION

In this appendix, the heats of formation are calculated for two "model" compounds which are likely formed during the formation of CMS membranes, benzene and naphthalene. Though these are small molecules, they are likely the initial compounds formed during CMS formation, since CMS membranes consist of sheets of sp^2 hybridized carbon. The heats of reaction are calculated here to support the hypothesis that in the later stages of CMS formation, the reactions which form CMS membranes are exothermic. These calculations support the experimental observations given in Appendix C using DSC and DTA.

D.1 HEAT OF FORMATION OF BENZENE

The heats of formation were calculated using the heats of combustion of each of the reactants as described in Equation D.1 [1].

$$\Delta\hat{H}_r^o = \sum_{reactants} |\nu_i| \left(\Delta\hat{H}_c^o\right)_i - \sum_{products} |\nu_i| \left(\Delta\hat{H}_c^o\right)_i \qquad (D.1)$$

$\Delta\hat{H}_r^o$ = standard heat of the reaction (kJ/mol)

$\Delta\hat{H}_f^o$ = standard heat of combustion of the ith species in the reaction (kJ/mol)

$|\nu_i|$ = absolute value of the stoichiometric coefficient of the ith species in the reaction

The formation of benzene from ethylene follows the reaction given below in Figure D.1. The heats of formation of each of the reactants were obtained from [1] and are listed in Table D.1.

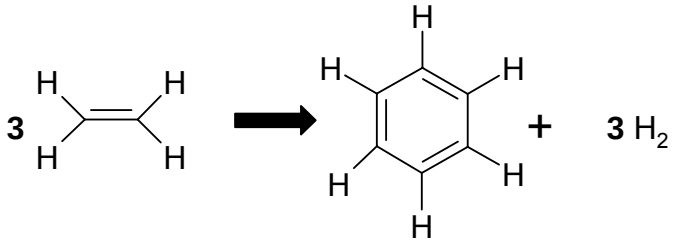

Figure D.1 Reaction mechanism used for the formation of benzene from ethylene

Table D.1 Heats of formation for components in the formation of benzene from ethylene [1]

Reactant	$\Delta\hat{H}_c^o$ **(kJ/mol)**
Benzene	-3301.5
Hydrogen	-285.84
Ethylene	-1410.99

Applying equation D.1, the heat of formation of benzene was calculated as in equation D.2.

$$\Delta\hat{H}_r^o = 3(-1410.99) - (-3301.5) - 3(-285.84) - = -73.95(\text{kJ}/\text{mol}) \qquad \text{(D.2)}$$

These results show that the formation of benzene from ethylene is **exothermic** which is consistent with the results obtained from DSC.

D.2 HEAT OF FORMATION OF NAPTHALENE

As a second model reaction, the conversion of benzene to naphthalene was also investigated. This reaction was chosen because it could follow the formation of benzene and be an intermediate reaction during the formation of carbon sheets in CMS membranes. The formation of naphthalene from benzene follows the reaction shown in Figure D.2 and the heats of formation of each of the components are listed in Table D.2

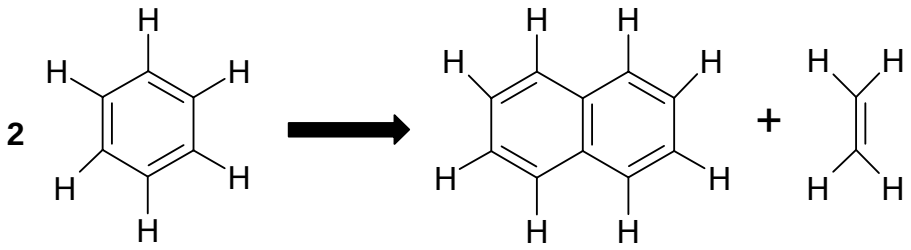

Figure D.2 Reaction mechanism for the formation of naphthalene from benzene

Table D.2 Heats of combustion for each component in the formation of naphthalene from benzene [1]

Reactant	$\Delta\hat{H}_c^o$ **(kJ/mol)**
Benzene	-3301.5
Naphthalene	-5157
Ethylene	-1410.99

The heat of reaction for the formation of naphthalene was calculated using equation D.3.

$$\Delta\hat{H}_r^o = 2(-3301.5) - (-5157) - (-1410.99) = -35.01(\text{kJ/mol}) \qquad \text{(D.3)}$$

Therefore, the formation of naphthalene from benzene is also **exothermic**. Both of these model reactions illustrate that in the later stages of CMS formation, the reactions are likely exothermic.

D.3 REFERENCES

1. Felder, R.M. and Rousseau, R.W., *Elementary Principles of Chemical Processes*. 1986, New York: John Wiley and Sons.

VITA

PAUL JASON WILLIAMS

Jason Williams was born to Paul J. Williams Jr. and Wanda Williams on August 12, 1977 in Chattanooga, TN. He attended elementary and middle school at The Senter School in Chattanooga, Tennessee and graduated from Notre Dame High School. Jason then attended Tennessee Technological University and received his Bachelors of Science in Chemical Engineering in May 1999 and a Master of Science degree in Chemical Engineering in August 2001. In 2001, he began his pursuit of a Doctor of Philosophy in Chemical Engineering from the Georgia Institute of Technology. In April 2005, Jason married Melissa Ann Zubris of North Tonawanda, NY. After graduation, Jason plans to join Shell in Houston, TX.